UNITED STATES
DEPARTMENT OF COMMERCE
NATIONAL INSTITUTE OF STANDARDS
AND TECHNOLOGY

NIST Technical Note 1351

Standard Spherical Dipole Source

G. Koepke
L. D. Driver
K. Cavcey
K. Masterson
R. Johnk
M. Kanda

Standard Spherical Dipole Source

G. Koepke
L. D. Driver
K. Cavcey Kenneth H.
K. Masterson
R. Johnk
M. Kanda

Electromagnetic Fields Division
Electronics and Electrical Engineering Laboratory
National Institute of Standards and Technology
Boulder, Colorado 80303-3328

U.S. DEPARTMENT OF COMMERCE, Robert A. Mosbacher, Secretary
NATIONAL INSTITUTE OF STANDARDS AND TECHNOLOGY, John W. Lyons, Director
Issued December 1991

National Institute of Standards and Technology Technical Note
Natl. Inst. Stand. Technol., Tech. Note 1351, pages (132)
CODEN:NTNOEF

U.S. GOVERNMENT PRINTING OFFICE
WASHINGTON: 1991

For sale by the Superintendent of Documents, U.S. Government Printing Office, Washington, DC 20402-9325

Contents

Standard Spherical Dipole Source

G. Koepke, L. D. Driver, K. Cavcey
K. Masterson, R. Johnk, and M. Kanda

National Institute of Standards and Technology
Electromagnetic Fields Division
Boulder, Colorado 80303

A spherical dipole was developed to provide a source that can be characterized both by theory and experiment and integrated into modern automated test systems. The frequency and amplitude of the radiated electromagnetic field are established remotely using a signal generator. This signal and all other control features are transmitted to and from the sphere using fiber optic cable. The field measurements show good agreement with predictions over much of the frequency band.

Key words: electromagnetic fields; electronic circuits; fiber optic; remote control; spherical dipole; standard radiator.

1. INTRODUCTION

The spherical dipole rf antenna developed at the National Institute of Standards and Technology and documented in this report is designed to be a standard (known and repeatable) electromagnetic (em) source. The ability to predict and monitor the em fields produced by the standard source will provide an effective means to determine the accuracy of emissions measurement systems. These measurement systems must quantify the unintentional emissions of a wide variety of electronic devices. These devices are not designed as em sources yet the internal electronic systems may produce interfering signals with unknown radiation characteristics. A predictable standard source would permit meaningful comparisons of different facilities or techniques and be a useful instrument for further improvements in emissions metrology.

We examined several possible geometries which could be used for a standard source antenna. The short monopole over a box containing a power source has been used successfully as a control standard to monitor the repeatability of various measurements. This geometry is difficult to model accurately due to the variable (usually small) ground plane size which depends on the proximity of a ground reference. The monopole is a good solution when the source is characterized by experiment alone. Another geometry that merits consideration is the fat cylindrical dipole. However, the cylindrical dipole and other more complicated geometries were abandoned in favor of a simple sphere with a small gap on the equator.

The sphere provides a desirable symmetry and avoids sharp edges which complicate the theoretical model. The idea for using a small spherical dipole as a control standard radiator or as a receiving antenna has been explored by several researchers [1 through 9] with good success. The volume provided by a spherical shape allows the antenna to be self-contained. All the necessary circuitry and power sources can be internal, thereby eliminating interconnecting lines which disrupt the radiated field. Previous radiators have employed internal oscillators with rich harmonic content to provide radiating signals; however, there was no remote control over amplitude or frequency. A spherical low frequency probe [7 through 9] and a recent effort by Murakawa, et al., [6] with a spherical radiator have demonstrated the use of a fiber optic transmission line to communicate with the spherical antenna. The use of fiber optic components for microwave frequencies has been made possible due to recent advances in physical size, power consumption, and modulation bandwidth. The spherical radiator described in this report also uses optical fiber to control the frequency and amplitude of the radiated signal. The communication between the operator and the sphere is further enhanced by provisions for monitoring internal functions of the radiator. These functions include the drive rf voltage applied to the equatorial gap, the ambient temperature within the sphere, and a standby mode to maximize battery life.

This report is written to provide the theoretical formulations used to predict electromagnetic fields radiated from a spherical dipole in free space (section 2), to detail the experimental comparison with these predictions (section 3), and to provide complete design and construction details of the standard spherical dipole (sections

4 and 5). Section 6 draws conclusions and section 7 acknowledges contributions by other individuals.

2. RADIATED FIELDS FROM A SPHERICAL DIPOLE

2.1 Derivation of the Electric and Magnetic Fields for the Standard Spherical Radiator

In this section, expressions are derived for the electric and magnetic fields of the standard spherical radiator of figure 1. As can be seen in figure 1, the spherical radiator consists of two perfectly conducting hemispheres that are separated by an infinitesimally small gap at the equator ($\theta = \pi/2$). An infinitesimal gap has a width that is immeasurably or incalculably small. Thus, for analysis, the gap width is assumed to be arbitrarily close to 0. Because of the geometry of this structure, the spherical coordinates (r, θ, ϕ) are used to describe the field behavior in the region external to the surface of the sphere. In order to create the electric and magnetic fields, a complex, time-harmonic voltage V is applied across the gap; this, in turn, sets up time-harmonic electric and magnetic fields in the region external to the sphere. The assumption of a time-harmonic source means that a sinusoidal voltage of amplitude $|V|$ is applied between the two hemispheres for an infinitely long time so that field transients are allowed to decay away. As a careful study of figure 1 reveals, the assumed gap does not correspond to the actual gap of the standard radiator because the actual gap has a small but measurable width. However, in all practical situations, the assumption of an infinitesimal gap will have virtually no effect on the values of the computed fields. Because of the spherical symmetry of this antenna, the gap voltage generates an electric field E that is θ-directed and a magnetic field H that is ϕ-directed.

The spherical symmetry of this structure allows us to obtain a closed-form solution for the electric and magnetic fields. The ϕ-

directed magnetic field can be expanded in a series of spherical harmonics as follows [10]:

$$H_\phi(r,\theta) = \sum_{n=1}^{\infty} A_n r^{-1/2} P_n^1(\cos\theta) H_{n+1/2}^{(2)}(k_0 r) . \tag{1}$$

The θ-directed electric field can be found by applying eq (1) to the Maxwell curl relation:

$$\overline{E} = \frac{1}{j\omega\epsilon} \nabla\times\overline{H}. \tag{2}$$

The result of this process is

$$E_\theta(r,\theta) = \sum_{n=1}^{\infty} \frac{jA_n}{\omega\epsilon} r^{-3/2} P_n^1(\cos\theta) \left[k_0 r H_{n-1/2}^{(2)}(k_0 r) - n H_{n+1/2}^{(2)}(k_0 r)\right] . \tag{3}$$

In eqs (1) and (3), A_n is a yet to be determined coefficient; $P_n^1(\cos\theta)$ is an associated Legendre function of the first kind of order n and degree 1; and $H_{n\pm1/2}^{(2)}(k_0 r)$ are second Hankel functions with the fractional indices $n \pm 1/2$. Also, $k_0 = 2\pi f/c$ (f = frequency; c = 3.0×10^8 m/s) is the free-space wave number and r is the distance from the center of the sphere to the point at which the fields are being calculated. This series has been selected since the fractional-order Hankel functions and the associated Legendre functions arise naturally in the solution of electromagnetic structures with a spherical symmetry. Since the terms of the series of eqs (1) and (3) are a function of the spherical coordinates (r, θ, ϕ), the application of boundary conditions to this solution is a straightforward process. It should be noted that eqs (1) and (3) are not dependent on ϕ. This lack of a dependence on ϕ is due to the fact that the gap is being excited uniformly with a voltage V around the circumference of the spherical radiator.

From the standpoint of numerically evaluating the series of eq (1), the presence of the Hankel and the Legendre functions seems, at first, intimidating and perhaps puzzling. As it turns out, the special functions can be replaced by much simpler trigonometric and algebraic functions. In order to illustrate this point, the Hankel and associated Legendre functions are given below for n = 1, 2, 3.

The first three Hankel functions are given by [11]:

$$H_{1/2}^{(2)}(x) = \sqrt{\frac{2}{\pi x}}\,[\sin x + j\cos x]\,, \tag{4}$$

$$H_{3/2}^{(2)}(x) = \sqrt{\frac{2}{\pi x}}\,[(\frac{\sin x}{x}-\cos x)+j(\sin x+\frac{\cos x}{x})]\,, \tag{5}$$

and

$$H_{5/2}^{(2)}(x) = \sqrt{\frac{2}{\pi x}}\,[(\{\frac{3}{x^2}-1\}\sin x-\frac{3}{x}\cos x)+j(\frac{3}{x}\sin x+\{\frac{3}{x^2}-1\}\cos x)]\,. \tag{6}$$

The first four associated Legendre functions are given by [11]:

$$P_0^1(\cos\theta) = 0, \tag{7}$$

$$P_1^1(\cos\theta) = \sin\theta, \tag{8}$$

$$P_2^1(\cos\theta) = 3\sin\theta\cos\theta, \tag{9}$$

and

$$P_3^1(\cos\theta) = \frac{3}{2}\sin\theta(5\cos^2\theta-1)\,. \tag{10}$$

As an inspection of eqs (4) through (10) indicates, the evaluation of the first few spherical Hankel functions and associated Legendre functions is a straightforward process. In order to evaluate functions with higher indices, we could, in principle, utilize expressions similar to those of eqs (4) through (10). However, as the index n becomes larger, the resulting expressions become more and more complex and cumbersome. An alternative approach to finding the value of these functions for a given argument x and an arbitrary index n (n > 3) is to use eqs (4) through (10) to evaluate the functions at the first several indices, and then to find the value of the function at a higher index by using a recurrence relation. The recurrence relation for the associated Legendre functions is

$$(n-1)P_n^1(x) = x(2n-1)P_{n-1}^1(x) - nP_{n-2}^1(x) \,. \tag{11}$$

The fractional-index Hankel functions can be expressed in terms of the spherical Hankel functions as

$$h_n^{(2)}(x) = \sqrt{\frac{\pi}{2x}}\, H_{n+1/2}^{(2)}(x) \,. \tag{12}$$

The recurrence relation for the spherical Hankel function is

$$h_{n-1}^{(2)}(x) + h_{n+1}^{(2)}(x) = \left(\frac{2n+1}{x}\right) h_n^{(2)}(x) \,. \tag{13}$$

Equations (12) and (13) constitute the recurrence relation for the fractional-order Hankel functions. As an inspection of eqs (11) through (13) indicates, for a given argument x, the value of either of the Legendre function or the Hankel functions can be found for an arbitrary index n, provided that two initial starting values are given. For instance, if the values of the functions are known at x for n = 1, 2 the functions can be evaluated for n ≥ 3 for the same argument. Recurrence relations are particularly suitable when the functions are being programmed on a computer. We must be careful, however, when the recurrence relations are used to evaluate either the associated Legendre functions or the Hankel function for a large index n. A large index n requires the repeated use of a recurrence relation, which can generate potentially inaccurate results due to numerical instabilities. The existence of numerical instabilities depends on the form of a given recurrence relation. Some recurrence relations are inherently stable and can be used for large indices, while others cannot be used for a large index due to instabilities that can be introduced by a given recurrence relation. For the parameters of this problem, the recurrence relations of eqs (11) and (13) are stable up to an index of about 40. Fortunately, such a large index is never encountered in this problem since the series of eqs (1) and (3) converge rapidly and require only a few terms (for the case of the 10 cm diameter spherical radiator) in order to generate an accurate result. Thus the recurrence relations will have to be used at most for a few repeated iterations.

Up to this point, the coefficient A_n in eqs (1) and (3) has not yet been evaluated. In order to determine this coefficient, boundary conditions must be invoked. For this case the boundary condition of a vanishing electric field at the surface of the sphere (except at the gap) is sufficient to determine uniquely this coefficient. At the surface of the sphere (r = a), the expression for the electric field is given by:

$$\begin{aligned} E_\theta(a,\theta) &= V\delta(\theta-\pi/2) \\ &= \sum_{n=1}^{\infty} \frac{jA_n}{\omega\epsilon} a^{-3/2} P_n^1(\cos\theta)\,[k_0 r H_{n-1/2}^{(2)}(k_0 a) - nH_{n+1/2}^{(2)}(k_0 a)]\,, \end{aligned} \tag{14}$$

where the term $\delta(\theta - \pi/2)$ is the Dirac delta function. This function is 0 for every angle except for $\theta = \pi/2$ where it becomes infinite. The electric field, therefore, is 0 everywhere on the surface of the sphere except at the gap, where it becomes infinite. The fact that the field becomes infinite at the gap location is due to the assumption of an infinitesimally small gap width. For the actual spherical radiator, the gap is small and has a finite width. Thus the field is finite for the actual radiator, although it is still large in the gap region. In order to evaluate the coefficient A_n, both sides of eq (14) are multiplied by $P_m^1(\cos\theta)$ $\sin\theta$ and integrated with respect to the angle θ from 0 to π. This process is written as

$$\begin{aligned} & V\int_0^\pi \sin\theta \; P_m^1(\cos\theta)\,\delta(\theta-\pi/2)\; d\theta \\ & = \sum_{n=1}^{\infty} \frac{jA_n}{\omega\epsilon} a^{-3/2}\,[k_0 r H_{n-1/2}^{(2)}(k_0 a) - nH_{n+1/2}^{(2)}(k_0 a)] \\ & \times \left[\int_0^\pi P_m^1(\cos\theta)\,P_n^1(\cos\theta)\sin\theta d\theta\right]. \end{aligned} \tag{15}$$

The integrals on both sides of eq (15) can be evaluated readily by using the basic properties of the Dirac delta function and the orthogonal properties of the associated Legendre function. A well-behaved function that is multiplied by a Dirac delta function and integrated over some range yields

$$\int_a^c f(x)\,\delta(x-b)\,dx = f(b) \quad (a<b<c), \qquad \mathbf{(16)}$$
$$= 0 \quad (otherwise).$$

The orthogonal property of the associated Legendre function is given by

$$\int_0^\pi P_m^1(\cos\theta)\,P_n^1(\cos\theta)\sin\theta\; d\theta = \frac{2n(n+1)}{(2n+1)} \quad (m=n), \qquad \mathbf{(17)}$$
$$= 0 \quad (m\neq n).$$

Applying eqs (16) and (17) to eq (15) yields the coefficient A_n:

$$A_n = \frac{\omega\epsilon V a^{3/2}(2n+1)\,P_n^1(0)}{j2n(n+1)\,a\left[k_0 a H_{n-1/2}^{(2)}(k_0 a) - nH_{n+1/2}^{(2)}(k_0 a)\right]}. \qquad \mathbf{(18)}$$

Equation (18) in conjunction with eqs (1) and (3) are the final desired expressions for the electric and magnetic fields.

2.2 Expressions for the Radiated Power Density and the Total Radiated Power

The radiated power density of a given antenna structure has the dimension of W/m^2, and it is a measure of power per unit area for any point external to the radiator. The radiated power density is defined in terms of the electric and magnetic fields by taking the vector cross product of the electric field and the complex conjugate of the magnetic field:

$$\overline{P}_d = \frac{1}{2} Re\,\{\overline{E}\times\overline{H}^*\}, \qquad \mathbf{(19)}$$

where the symbol (*) denotes the complex conjugate of the time-harmonic magnetic field. In order to find the radiated power density, the solutions of the standard spherical radiator given by eqs (1), (3), and (18) must be applied to eq (19).

$$\begin{aligned}\overline{P}_d &= \frac{1}{2} Re\,\{\overline{E}\times\overline{H}^*\} \\ &= \overline{a}_r \frac{1}{2} Re\left\{\sum_{m=1}^{\infty}\sum_{n=1}^{\infty}\frac{jA_nA_m^*}{\omega\varepsilon r^2}P_m^1(\cos\theta)\,P_n^1(\cos\theta)\right. \\ &\quad\left.\times\left[k_0 r H_{m-1/2}^{(2)}(k_0 r) - mH_{m+1/2}^{(2)}(k_0 r)\right]H_{n+1/2}^{(2)*}(k_0 r)\right\}.\end{aligned} \tag{20}$$

Equation (20) is the expression for the radiated power density. The radiated power density is a function of the location of the field observation point (r, θ). The double series form of eq (20) looks formidable and computationally involved; however, in the case of the spherical radiator, relatively few terms are required for the series to converge. This issue is treated in the next section.

The expression for the total radiated power can be readily derived from a Poynting integration in conjunction with the expressions for the electric and magnetic fields that have already been developed. In this case, the Poynting integral corresponds to the following surface integration of the power density:

$$P_{rad} = \frac{1}{2} Re\left\{\oint_S [\overline{E}\times\overline{H}^*]\cdot\overline{a}_n\; dS\right\}. \tag{21}$$

Although the surface over which the integration is carried out is arbitrary, it is mathematically convenient to integrate over the surface of a sphere of radius R (R > a) whose center is coincident with the center of the spherical antenna. For a spherical surface, eq (21) becomes

$$P_{rad} = \frac{1}{2} Re\left\{\int_0^{2\pi}\int_0^{\pi}[\overline{E}\times\overline{H}^*]\cdot[\overline{a}_r]\, r^2\sin\theta\;\, d\theta d\phi\}\,\Big|_{r=R}\right\}. \tag{22}$$

From eqs (1), (3), and (18), the vector cross product of the electric field and the complex conjugate of the magnetic field is given by

$$\overline{E}\times\overline{H}^* = \overline{a}_r \sum_{m=1}^{\infty}\sum_{n=1}^{\infty} \frac{jA_nA_m^*}{\omega\epsilon R^2} \times \left[k_0RH_{m-1/2}^{(2)}(k_0R) - mH_{m+1/2}^{(2)}(k_0R)\right]H_{n+1/2}^{(2)*}(k_0R) \times \left[P_m^1(\cos\theta)P_n^1(\cos\theta)\right]. \tag{23}$$

Applying eq (23) to (22) and performing the ϕ integration yields the following expression for the total radiated power:

$$P_{rad} = \pi\ Re\left\{\sum_{m=1}^{\infty}\sum_{n=1}^{\infty}\frac{jA_nA_m^*}{\omega\epsilon} \times \left[k_0RH_{m-1/2}^{(2)}(k_0R) - mH_{m+1/2}^{(2)}(k_0R)\right]H_{n+1/2}^{(2)*}(k_0R) \times \int_0^{\pi} P_m^1(\cos\theta)P_n^1(\cos\theta)\sin\theta\ d\theta\right\}. \tag{24}$$

Applying the orthogonality relation of eq (17) to eq (24) yields the following single-series expression for the total radiated power:

$$P_{rad} = \pi\ Re\left\{\sum_{n=1}^{\infty}\frac{j|A_n|^2}{\omega\epsilon}\frac{2n(n+1)}{(2n+1)} \times \left[k_0RH_{n-1/2}^{(2)}(k_0R) - nH_{n+1/2}^{(2)}(k_0R)\right]H_{n+1/2}^{(2)*}(k_0R)\right\}. \tag{25}$$

Equation (25) is the final expression for the total amount of radiated power out of a spherical antenna of radius a. The total radiated power is completely independent of the selected radius of integration R. This fact is not readily apparent in eq (25) for general values of R. Independence from R, however, can be demonstrated as R → +∞ by utilizing appropriate large argument expansions for the spherical Hankel functions [11]. As is the case with the series expressions for the fields and the radiated power densities, only a few terms of the series of eq (25) are necessary in order to generate accurate results for the standard spherical radiator. This issue is dealt with in more detail in the next section.

2.3 Convergence of the Field and Power Expressions for the Standard Spherical Radiator

Table 1 depicts the complex electric field for the standard spherical radiator with a gap voltage of 1 V. This has been computed from eq (3) as a function of frequency and the number of terms in the series using [12] and the program listed in appendix A. The observation angle has been chosen as $\theta = \pi/2$ since this corresponds to the electric (and magnetic) field maxima. Also, the rates of series convergence are similar to those obtained at other values of θ. As a careful study of the table indicates, summing five terms in the series is more than sufficient to ensure four-place accuracy. Up to an operating frequency of 900 MHz three terms are sufficient to yield four-place accuracy. Since only a few terms are required in order to obtain accurate results, the series of eq (3) is convenient to use.

Table 2 depicts the complex magnetic field results as a function of frequency and the number of terms of eq (1). The results are similar to those of the electric field in that five terms ensure four-place accuracy, and three terms are sufficient to obtain four-place accuracy up to 800 MHz. The ratio of E_θ in table 1 to H_ϕ in table 2 is also close to the free space value of 120π.

Results for the total radiated power as a function of frequency and the number of series terms computed from eq (25) are depicted in table 3. As an inspection of this table indicates, only three terms of the series need to be summed in order to ensure four-place accuracy up to 1000 MHz. Thus the series for the radiated power converges more rapidly than the corresponding series expressions for the electric and magnetic fields.

Table 1. The magnitude (V/m) and phase (degrees) of the complex electric field evaluated for a gap voltage V = 1 at an observation distance of R = 10 m and $\theta = \pi/2$ as a function of frequency and the number of series terms N.

freq (MHz)	N = 1	N = 3	N = 5	N = 10
100	8.260×10^{-4} at 57.22°	8.259×10^{-4} at 57.22°	8.258×10^{-4} at 57.22°	8.258×10^{-4} at 57.22°
200	3.360×10^{-3} at -61.72°	3.357×10^{-3} at -61.72°	3.357×10^{-3} at -61.72°	3.357×10^{-3} at -61.72°
300	7.754×10^{-3} at 177.87°	7.740×10^{-3} at 177.88°	7.740×10^{-3} at 177.88°	7.740×10^{-3} at 177.88°
400	1.423×10^{-2} at 56.38°	1.418×10^{-2} at 56.39°	1.418×10^{-2} at 56.39°	1.418×10^{-2} at 56.39°
500	2.297×10^{-2} at -66.35°	2.286×10^{-2} at -66.37°	2.286×10^{-2} at -66.37°	2.286×10^{-2} at -66.37°
600	3.394×10^{-2} at 169.47°	3.372×10^{-2} at 169.42°	3.372×10^{-2} at 169.42°	3.372×10^{-2} at 169.42°
700	4.649×10^{-2} at 43.87°	4.609×10^{-2} at 43.75°	4.609×10^{-2} at 43.75°	4.609×10^{-2} at 43.75°
800	5.919×10^{-2} at -82.75°	5.854×10^{-2} at -82.99°	5.854×10^{-2} at -82.99°	5.854×10^{-2} at -82.99°
900	7.019×10^{-2} at 150.46°	6.921×10^{-2} at 150.03°	6.921×10^{-2} at 150.03°	6.921×10^{-2} at 150.03°
1000	7.821×10^{-2} at 24.46°	7.680×10^{-2} at 23.75°	7.682×10^{-2} at 23.76°	7.682×10^{-2} at 23.76°

Table 2. The magnitude (A/m) and phase (degrees) of the complex magnetic field evaluated for a gap voltage V = 1 at an observation distance of R = 10 m and $\theta = \pi/2$ as a function of frequency and the number of series terms N.

freq (MHz)	N = 1	N = 3	N = 5	N = 10
100	2.198×10^{-6} at 57.22°	2.198×10^{-6} at 57.22°	2.198×10^{-6} at 57.23°	2.198×10^{-6} at 57.23°
200	8.926×10^{-6} at -61.72°	8.919×10^{-6} at -61.72°	8.919×10^{-6} at -61.72°	8.919×10^{-6} at -61.72°
300	2.059×10^{-5} at 177.87°	2.056×10^{-5} at 177.88°	2.056×10^{-5} at 177.88°	2.056×10^{-5} at 177.88°
400	3.778×10^{-5} at 56.38°	3.776×10^{-5} at 56.39°	3.776×10^{-5} at 56.39°	3.776×10^{-5} at 56.39°
500	6.011×10^{-5} at -66.35°	6.071×10^{-5} at -66.37°	6.071×10^{-5} at -66.37°	6.071×10^{-5} at -66.37°
600	9.011×10^{-5} at 169.47°	8.952×10^{-5} at 169.42°	8.952×10^{-5} at 169.42°	8.952×10^{-5} at 169.42°
700	1.234×10^{-4} at 43.87°	1.224×10^{-4} at 43.75°	1.224×10^{-4} at 43.75°	1.224×10^{-4} at 43.75°
800	1.572×10^{-4} at -82.75°	1.554×10^{-4} at -82.99°	1.554×10^{-4} at -82.99°	1.554×10^{-4} at -82.99°
900	1.864×10^{-4} at 150.46°	1.837×10^{-4} at 150.03°	1.838×10^{-4} at 150.03°	1.838×10^{-4} at 150.03°
1000	2.076×10^{-4} at 24.45°	2.039×10^{-4} at 23.75°	2.040×10^{-4} at 23.76°	2.040×10^{-4} at 23.76°

Table 3. The total radiated power (W) evaluated for a gap voltage V = 1 at an observation distance of R = 10 m and $\theta = \pi/2$ as a function of frequency and the number of series terms N.

freq (MHz)	N = 1	N = 3	N = 5	N = 10
100	7.606×10^{-7}	7.606×10^{-7}	7.606×10^{-7}	7.606×10^{-7}
200	1.257×10^{-5}	1.256×10^{-5}	1.256×10^{-5}	1.256×10^{-5}
300	6.689×10^{-5}	6.689×10^{-5}	6.689×10^{-5}	6.689×10^{-5}
400	2.252×10^{-4}	2.252×10^{-4}	2.252×10^{-4}	2.252×10^{-4}
500	5.870×10^{-4}	5.870×10^{-4}	5.870×10^{-4}	5.870×10^{-4}
600	1.281×10^{-3}	1.281×10^{-3}	1.281×10^{-3}	1.281×10^{-3}
800	2.403×10^{-3}	2.403×10^{-3}	2.403×10^{-3}	2.404×10^{-3}
800	3.898×10^{-3}	3.898×10^{-3}	3.898×10^{-3}	3.898×10^{-3}
900	5.480×10^{-3}	5.481×10^{-3}	5.481×10^{-3}	5.480×10^{-3}
1000	6.802×10^{-3}	6.806×10^{-3}	6.806×10^{-3}	6.806×10^{-3}

3. EXPERIMENTAL EVALUATION OF THE SPHERICAL RADIATOR

The spherical radiator circuits were first tested individually to evaluate the performance of the major components. This evaluation was performed concurrently with the final circuit design to verify that operation and performance specifications were realized. The alignment and setup procedures outlined in section 4 were developed during this time. These preliminary measurements also examined the overall quality and stability of the rf optical link and general system performance. The data shown in figures 2, 3, and 4 demonstrate the signal purity attained by the laser transmitter-reciever link. The input signal from a signal generator (left graphs of figures 2 and 3) which modulates the laser and the resulting output signal (right graphs) after being demodulated by the optical receiver and amplified by the MMIC amplifier inside the sphere are shown in figures 2 and 3. The data show no spurious signals being generated by the rf optical link even at this maximum signal level. The data clearly show that when the input contains harmonic signals, these signals will be present in the output. Special care should be exercised when using broadband devices to detect the signal from such a source. The gap voltage detector is such a broadband device and will give an indication of the total contribution from all signals present. There is no correction applied for the simple 50 Ω coax probe used to pick off the signal at the amplifier output and this may account for some of the amplitude variations seen in these figures. Figure 4 shows the frequency response attained by the rf optical link with a constant input to the laser. The frequency is swept from 50 to 1300 MHz. Again there is no correction for the coax probe, but the data clearly indicate a usable bandwidth beyond the 1000 MHz set as a design goal.

The second part of the experimental evaluation examined the spherical radiator transmitting in several environments over a frequency range of 10 MHz to 1000 MHz. The facilities used for radiated field measurements included the TEM cell, anechoic chamber, and open area test site (OATS). The measurements were designed to determine the free-space radiation pattern, power output, and gap voltage indicator transfer function. The radiation pattern and radiated power are necessary to determine how closely the sphere acts as a dipole antenna given all the added material inside the sphere and also the fiber optic control lines which exit the sphere at the equator and connect to the control unit. The closer the measured data follows the predicted data for a perfect spherical dipole, the more accurately radiated fields can be calculated using the theory of section 2. The ability to monitor the rf voltage at the radiating gap around the sphere's equator provides the information necessary to make this calculation and also provides a reference point for repeating a radiating condition. The diode detector, which is described in section 4, has complicated circuitry involved in transmitting the detected voltage to the front panel indicator on the control unit. This circuitry includes an amplifier, voltage-to-frequency converter, optical transmitter/receiver, frequency-to-voltage converter, and additional amplifiers. While the dc components can be aligned and well characterized, the overall rf-to-dc conversion must be calibrated by measurement of the radiated signal. Any direct contact probing of the rf signal in the vicinity of the dipole gap resulted in adverse loading on the final rf amplifier. Direct probing also ignores the actual impedance of the balun and radiating sphere because the hemispheres must be removed to access the rf circuits. The calibration for the gap voltage indicator is then a comparison between the predicted and measured field strength. This scale factor is shown on each radiation pattern figure. The scale factor is the actual gap voltage, determined by calculations, which would produce the measured field. All measurements were performed with a gap voltage indicator reading of 1.0 V.

The small size of this radiator made it compatible with using a TEM cell as a tool for evaluation at frequencies of 100 MHz and below. The radiator was positioned inside the TEM cell at six unique orientations while maintaining a constant output power and frequency. The sum and difference power and relative phase angle were measured at each position as prescribed by the TEM cell emissions technique [13, 14]. The source, in this case the spherical radiator, is modeled by orthogonal electric and magnetic dipoles. These equivalent source components are then determined by measurements of power and phase from the two TEM cell ports through a 0° - 180° hybrid junction. These measurements provide sufficient data to calculate the radiation pattern and power radiated from the sphere.

Figures 5 through 10 show the results of radiating a signal in a TEM cell with a cross section of 1.2 x 1.2 m, processing the data as described, and comparing the pattern information with predicted free-space values. The predicted pattern is scaled as noted on each figure to match the maximum values of the measurement based data. The solid lines are calculated using the theory of section 2 and the dotted lines represent two patterns calculated from measurement data at $\phi = 0^\circ$ and 90°. These data show that the sphere acts very much like the ideal spherical antenna at these frequencies. The scale factor shown on the graphs can be used along with the gap voltage indication and the theory of section 2 to predict the free-space fields from the spherical radiator.

The open area test site (OATS) with a 30 m x 60 m flat ground screen was used to measure radiated field strength from the spherical radiator. The reflected wave from the ground plane was compensated for by correcting the received signal by the amount contributed by such a reflected signal. The value for the correction was determined by accurately positioning the radiating sphere and the calibrated receiving antenna as in figure 11, assuming a perfectly conducting ground reflection and then calculating the contribution using [15]

$$
\begin{aligned}
\frac{|E_{total}|}{|E_{dir}|} &= \frac{|E_{dir} + E_{rfl}|}{|E_{dir}|} \\
&= \frac{\left|\dfrac{e^{-j\beta d}}{d} + \Gamma \dfrac{e^{-j\beta r}}{r}\right|}{\left|\dfrac{e^{-j\beta d}}{d}\right|} \\
&= \sqrt{1 + \left(\frac{\Gamma d}{r}\right)^2 + \left(\frac{2\Gamma d}{r}\right)\cos\phi}\,,
\end{aligned}
\tag{26}
$$

where

$$
\begin{aligned}
d &= \sqrt{D^2 + (h_T - h_R)^2} \quad m \\
r &= \sqrt{D^2 + (h_T + h_R)^2} \quad m \\
\Gamma &= \begin{cases} -1, & horizontal \\ +1, & vertical \end{cases} \\
\phi &= 1.2\, F\,(r - d) \quad degrees \\
F &= frequency,\ MHz.
\end{aligned}
\tag{27}
$$

The data shown in figures 12 through 23 were taken at a separation distance of D = 10 m, transmitter height of h_T = 2 m, and a receiving antenna height adjusted for maximum response.

The radiation pattern begins to show degradation from a perfect dipole at 700 MHz and improves again near 1000 MHz. There is also minor deviation at some lower frequencies (400 to 600 MHz) which are likely to be caused by misalignment and measurement problems. However, the pattern characteristics in the 700 to 900 MHz range show extensive distortion and reduced output level.

The root cause for this distortion in the pattern must lie with the non-uniformity of the feed voltage around the equator (gap). The theory described in section 2 assumes a uniform gap feed voltage and, if that condition is satisfied, a 10 cm sphere does not show an irregular pattern shape at frequencies below 1000 MHz. In fact the dipole pattern is predicted to remain intact well above 3000 MHz. The pattern irregularity must then be caused by internal conditions related to the ability to apply a uniform voltage to the entire gap area. The character of the pattern distortion is consistent with possible internal resonances which distort the gap feed and absorb power. An analysis of the internal volume of the sphere including all the circuitry, batteries, and the dipole feed system has not yet been attempted. A cursory look at spherical modes and resonances in a perfect spherical volume enclosed within a perfectly conducting surface [16] also indicates that the lowest frequency for this to occur is well above the problem area. Additional work is needed to model the complex internal structure and redesign the feed to reduce the distortion. The pattern irregularities should not diminish the utility of the spherical dipole for its intended use as an intercomparison or transfer standard device, but they make it more difficult to theoretically predict the radiated field strength at these higher frequencies.

Antenna pattern measurements taken in an anechoic chamber from 200 to 1000 MHz show the same character as that seen on the open field site. Figures 24 through 32 compare the electric field calculated using the theory in section 2 and adjusted by the listed scale factor to the measured electric field. These data were taken with a 3 m separation distance between sphere and receiving antenna due to the limited space inside the anechoic chamber. The measured pattern amplitude was then extrapolated to 10 m distance for comparison to the open area test site. There were two patterns measured at each frequency, $\phi = 0$ and $\pi/2$, and both are presented on these graphs. As the overall pattern begins to distort at the higher frequencies these orthogonal measurements show less resemblance to each other.

These measurements have provided a partial picture of the spherical dipole character from 10 to 1000 MHz. Figure 33 is a summary of the scale factors for all the data presented in figures 5 through 10 and 12 through 32. The scale factor must be determined at frequencies not represented in these measurements if field strength predictions are to be made based upon gap voltage indications. The radiator and the gap voltage detector demonstrated good repeatability and would be useful for relative measurements without extensive scale factor calibration.

4. DESIGN CONSIDERATIONS

The spherical dipole radiator system was designed to expand the capabilities of earlier devices which used fixed-frequency comb-type oscillators to generate the radiating signal. This system was intended to provide advanced features that will allow it to be incorporated into a modern automated test system and permit the automated test system to control and monitor the frequency and amplitude of the radiated signal. General design goals for the new radiator system were established to take advantage of recent developments in the areas of optical communication, wide bandwidth MMIC amplifiers, and new integrated circuits. The new system was intended to

(1) have continuous frequency coverage from 10 MHz to 1.0 GHz and be suitable for swept frequency, modulated cw, and other automated measurements,

(2) provide at least 40 dB of amplitude dynamic range,

(3) have the rf signal derived from an external signal generator (in keeping with an automated system),

(4) provide a direct indication on the control unit of the gap rf voltage and the ambient temperature inside the sphere,

(5) have all circuitry within the sphere operate on battery supplies and be designed for maximum operating time plus have a provision for remote (at the control unit) on/off,

(6) provide audio and visual alarms for malfunctions or low battery, and

(7) make use of optical cable for all control and signal lines connecting to the sphere.

A block diagram of the complete radiator system is shown in figure 34. The radiator system consists of the spherical radiator with a 10 cm outside diameter and a control unit to interface to the operator and signal source. The two parts are connected by a fully dielectric optical fiber cable. This optical fiber cable is used to carry all the necessary signals between the control unit and sphere. Specific design criteria and rationale for each part of the radiator system are described below.

4.1 Spherical Radiator

As was discussed in the introduction, the geometry for the radiator was chosen to be a spherical dipole. This shape allows some flexibility in packaging components within the sphere. Another concern was the diameter. A large sphere would provide much space for components and reduce the effort necessary for packaging plus it would provide more signal strength at lower frequencies. On the other hand, a large sphere would not be as useful in evaluating small enclosures where the smallest possible source is desired. A small sphere will extend the upper usable frequency and provide a compact source which more closely appears as a point source, but with a loss of output at the lower frequency range. Previous spherical radiators were on the order of 10 to 12 cm and these were quite successful. After examining the space requirements, a 10 cm diameter sphere was selected.

The sphere is divided into two hemispheres by a threaded dielectric spacer. This spacer also provides a mounting surface for the circuit board and the optical cable strain relief. The battery packs are then mounted to the circuit board and extend into both hemispheres. Figure 35 is a cross section of the spherical dipole and details this design. Additional details relating to the circuit design can be found in section 5.

4.2 Control Unit

The control unit had no specific tradeoff considerations as did the sphere. This unit is basically there to house the laser transmitter, other optical components used to control the sphere, displays and output ports, battery charging circuits, and power supplies. These components fit compactly within a 7.6 x 48.3 cm (3 in x 19 in) rack mountable case. The circuit details can be found in section 5.

4.3 Optical Components and Cable

The use of a fiber optic link to the radiating spherical dipole provides complete electrical isolation of the unit. It also gives freedom from electromagnetic interference and distortion of the radiating field that is normally found with conducting leads. In addition, it allows the radiation of a field at a selectable frequency and amplitude. This is in contrast to previous radiating spherical dipoles that use comb generators to radiate fields in several narrow frequency bands simultaneously and have amplitudes that vary according to battery charge. The added control that is available by using the optical link allows the unit to be used for accurate swept frequency measurements with programmable spectral profiles. In order for the sphere to perform its primary function in a reliable and well characterized way, there is a need to monitor its output and to minimize battery drain by having some control over its on-off status. These functions are also admirably performed through fiber optic links.

Clearly it would be cumbersome to have four individual optical cables to route every time the sphere was to be relocated. We thus procured custom built composite optical cable which consisted of two single mode fibers for 1300 nm operation and four multimode fibers (one spare of each type). The cable is a ruggedized design intended for field use and incorporates two layers of Kevlar fibers and plastic coatings. Also included between the layers are some stiffening members to help prevent kinking of the fibers.

The system uses two lengths of the optical cable. A shorter (10 m) length was specially prepared and one end permanently attached to the sphere. This was due to the fusion splice used on the single mode rf link and the space restrictions of the sphere. The other end was fitted with precision optical connectors. A longer (50 m) length with connectors at both ends is used to provide the bulk of the cable length between the control unit and the sphere. A plastic junction box which houses the optical barrel connectors and protects the ends of the fibers is used to connect the two cables.

4.4 Analog rf Link

An analog rf fiber optic link was chosen to give maximum signal fidelity, very low noise, and a high degree of control over the amplitude and frequency of the radiating field. It was desirable to purchase commercial products when available and then design the rest of the system around these components.

Several commercially available analog components and systems were evaluated in-house. The space and power available in the sphere plus the analog signal requirements limited the choices for the optical receiver. The unit chosen proved to be substantially superior to other units considered because of very low power requirements (45 mA at 9 V and 5 mA at -5 V), a very flat frequency response up to above 1 GHz, excellent dynamic range, and was available in a small 14 pin surface mount package. The receiver itself was marginally capable of providing the desired 0 dBm of power to the dipole gap when driven at maximum power. The bias current requirement is increased and the linearity becomes degraded at maximum power so it is better not to operate in that region. A solution to this involved adding an wideband MMIC amplifier following the receiver and lowering the optical carrier power and modulation depth into the reciever. A nominal value of -12 dBm optical power was found to be a minimum setting which provided sufficient drive to the MMIC amplifier to reach the 0 dBm of rf power desired at the dipole gap. This allowed the receiver to operate well below the maximum signal to insure its linearity and stability. The bias current savings into the receiver are consummed by the additional amplifier circuit and the amplifier must be carefully shielded and isolated from the receiver to prevent oscillations, but the overall analog signal performance improvements are worth the effort.

The analog microwave fiber optic transmitter (laser) used in this system proved to be an excellent low noise companion to the receiver. The unit is designed for direct modulation of the laser with an external analog signal. Since it produces about -3 dBm of optical power out of the fiber pigtail, it was necessary to add about 7 dB of optical attenuation (above connector and fiber losses of about 2 dB) in the link to bring the carrier to the desired -12 dBm level. The optical attenuator is housed in the control unit. This system used an adjustable attenuator and by using an optical power meter was set to the correct value.

In order to preserve the low noise characteristics of the optical transmitter it is necessary to reduce the reflections from all fiber connections to the lowest reasonably obtainable values. This is because light reflected back into the laser causes instabilities in the mode structures and is also detected in the photodiode monitoring and feedback control circuitry. The best way to reduce reflections is to use fusion splices for all the fiber connections. Although we did use a fusion splice between the fiber on the receiver and the 10 m pigtail attached to the sphere, it was necessary, because of handling and cable routing during use, to be able to disconnect the sphere and optional 50 m cable link. For this reason, high quality connectors which have low reflection (high return loss) were selected for the cable links. The high return loss is accomplished by polishing the end of the fiber and ferrule at a slight slant, so that reflected light does not couple back into the fiber core.

4.5 Voltage and Temperature Monitoring Links

A primary element in the design concept for the spherical dipole radiator was the ability to accurately monitor the voltage across the dipole's gap in order to calibrate the amplitude of the radiation field, and control it by feedback. Also since the required monitoring circuits are expected to show some sensitivity to the large temperature variations anticipated in field use, we thought it was also important to monitor the unit's temperature and characterize the temperature dependence of its output. This would also enable the user to remove or protect the unit if it appears to overheat from solar absorption.

It was also desirable for the monitoring links to be both reliable and relatively inexpensive. In terms of reliability, it is important that the signals from the monitoring circuits should be independent of the optical power in the link. This is important since the optical power varies both with the temperature of the transmitter and with the cleanliness and quality of the optical connections.

To meet these goals we chose a multimode fiber link with 850 nm LED sources in ST style receptacles inside the sphere. The components are readily available from a number of manufacturers and suppliers. The connectors between the fiber sections and at the control unit are a different style. Since we chose special slant polish connectors from one supplier for the singlencided to use multimode connectors on the cables and PIN photodiode receptacles from the same supplier. This was done primarily as a convenience and to save time by getting all the connectors installed on the patch cords by a single supplier. In retrospect, it appears more desirable to use ST style connectors and receptacles throughout the monitoring links.

To free the response of the monitor links from dependence on optical power level, we converted the measured voltages to frequencies for the LEDs and then reconverted from frequency back to voltage in the base electronics unit. To keep power drain low the voltage-to-frequency converters were operated at 100 kHz and below with a fixed pulse duration set for a 50 percent duty cycle at the highest frequency.

4.6 Power Control Link

Power requirements for the electronics in the sphere limit the operation time between battery recharges to about two hours. However, much of the time a unit is in the field or in a test chamber is actually spent in setup and preparation rather than actual measurements. There are three small switches located inside the sphere for turning battery power on and off, but it is not always convenient to disturb the measurement and access these switches. We, therefore, chose to use an additional optical link to switch the sphere electronics on and off remotely from the base control unit. Thus the sphere is fully powered only during relatively brief periods when actual measurements are being made. With this addition, the useful life of a single battery charge can be preserved much beyond the two hour limit for continuous operation. The optical link that is used for this purpose is very similar to those for the voltage and temperature monitors. In this case an 850 nm LED in the base control unit is coupled through a multimode fiber to a photo-Darlington transistor in the sphere.

5. CIRCUIT OPERATIONS AND CONSTRUCTION DETAILS

In this section we will present an operation and design overview for each circuit in the radiator system. The schematic diagrams begin with figure 36. The reader is urged to refer to the system block diagram (figure 34) and the base control unit block diagram (figure 43) to reference these individual circuits to their location in the system.

5.1 Spherical Radiator Functions

The sphere halves function as the radiating surfaces of the dipole. The volume inside the sphere contains the following system functions:

(1) Battery supplies and related control circuits and voltage or current regulation networks for the various circuits of the sphere.

(2) Fiber optic up and down links that carry rf excitation, rf level, and temperature information.

(3) Fiber optic PINFET receiver (rf excitation mentioned in item 2) and MMIC amplifier that constitutes the rf source which excites the hemispheres.

(4) Individual circuits that realize the functions of 1, 2, and 3 described above.

The base control unit interfaces between the sphere and rf signal source. This unit aids the operator by monitoring several of the system parameters. The following are specific base unit functions:

(1) Charging the sphere batteries through the use of built in constant current sources.

(2) Continuous monitoring of the laser and sphere power status with operator alarms.

(3) Switching sphere battery power off and on by a light carrier on one of the fiber optic links.

(4) Modulating a laser driven fiber optic uplink by the operators' rf signal source.

(5) Monitoring the operating temperature of the sphere and the rf level of the sphere's gap voltage with fiber optic downlink subsystems.

5.2 Sphere Circuitry

A description of the sphere starts with figure 36. This is a block diagram of the various circuits which distribute dc supply power to the various circuits found inside.

The sphere's batteries are connected to the internal circuits through three miniature switches mounted on the circuit board, one for each battery pack. Power status is verified by viewing three miniature LEDs (light emitting diodes) adjacent to the switches on the printed circuit board. At the time these three switches are closed and the battery voltages are applied to the circuits, the regulators IC3 and IC4 of figure 37 are latched in the "off" state. Transistors Q100 and Q102 are conducting, but Q101 is off. When the base control unit sphere power switch (S1 of figure 38) is activated, the current through the light emitting diode (D53) immediately increases to 60 mA and D53 illuminates the fiber-optic line which in turn switches the photo-Darlington transistor Q103 of figure 37 to the conductive state. This turns on transistor Q101 and turns off Q100 and Q102. Voltage regulators IC3 and IC4 are activated and supply +9 and +5 V regulated voltages to the sphere circuitry. These regulators are "smart" regulators which regulate the output, monitor the supply battery voltage and disconnect the supply from the load should the battery voltage drop too low. The first supply battery to become discharged under normal conditions is the 12 V battery supplying the regulator IC3 (9 V output). As the 12 V battery discharges, IC3 maintains a regulated output until that output level drops to 5 percent below the set value or 8.55 V. At this point, pin 5 of IC3 is forced to ground (0 V) which turns on Q100 (latching transistor). This activates shutdown pins (pin 3) on IC3 and IC4 which disconnect the supply batteries from their associated loads. In this latched off or shutdown condition the regulators remain off even though the supply voltages rise after the load is removed. Also, when shutdown, IC3 and IC4 will draw less than 100 μA. The negative voltage regulator, IC5, is used under low current conditions and does not require special protection.

The temperature of the sphere is determined from an AD590 silicon temperature transducer IC12. The device is biased so that it produces a 1 mV/K linear voltage output. Figure 39 shows the transducer connected to an AD654JR (IC8) voltage to frequency converter. Resistor R147 is adjusted to provide a 1 mA full scale current with enough trim range to accommodate the AD654JR's 10 percent FS error and components' tolerances. The transfer function of this circuit is a 100 kHz square wave 50 percent duty cycle pulse train at 1.0 V of input. A monostable retriggerable multivibrator (IC7) was used to maintain a fixed pulse width while the repetition rate is decreased to clock frequencies below 100 kHz. This results in a very short duty cycle at lower repetition rates (frequencies) corresponding to input voltages less than 1 V. The duty cycle rises to 50 percent only when the input voltage reaches 1 V. This scheme was used to greatly reduce battery drain. The pulse train is then converted to optical energy using Q106 which drives the HFBR-1404 LED fiber optic transmitter D108.

Figure 40 shows how the rf gap voltage is detected. A dual matched JFET, Q104, provides a pair of constant current sources for Schottky diodes D105 and D106. The resistors and capacitors in this bridge circuit are used for ac filtering purposes. The reason for using this kind of balanced detector circuit is to minimize the effects of temperature on the sensitive rf detector diode D105. The rectified and filtered voltage from D105 is then amplified by the differential amplifier IC11. This amplified dc voltage drives the AD654JR (IC6) voltage-to-frequency converter shown in figure 41. This circuit functions exactly like that of figure 39 with the same transfer function.

The most important function of the sphere is to radiate electromagnetic energy at the frequency of the modulated laser light sent by the fiber optic uplink. Figure 42 shows a GaAs IC PINFET fiber optic receiver which is used to drive a MMIC phase linear amplifier. This circuitry excites the sphere through the impedance matching transformer TP-103 loaded with R106. This circuit amplifies the rf signal to a maximum 0 dBm over the frequency range of 10 MHz to at least 1 GHz. The PINFET and MMIC circuit appear to be straightforward in design. In reality its function is the most difficult to fabricate due to electromagnetic compatibility considerations. Stray circulating rf fields can and have created problems in other circuitry with prototypes. Most of the problems have been solved by careful parts layout and shielding. The amplifier, balun, and dipole feed structure are contained within a small shielded printed circuit board which is mounted as a unit onto the main board. The output of the receiver is transfered to the amplifier through a short section of miniature coaxial cable.

5.3 Base Control Unit Circuitry

Figure 43 shows the various circuits of the base control unit. A circuit in the base control unit monitors the status of the laser temperature, laser output power, and sphere batteries. In figure 38, three comparators sense these functions. In normal operation D109 and D111, which are green LEDs, signal the operator that the laser is within acceptable operational limits. If the laser should experience difficulty, D110 and or D112 will light red and the audio alarm will sound at one tone.

Control of the sphere's power is invoked by closing switch S1a and exciting D53 of figure 38. Light from this LED is fed by fiber to Q103 of figure 37 and the sphere remains powered up until the regulated +9 V supply circuit drops below 8.55 V. If this occurs, D114 of figure 38 will signal red and the audio alarm will sound with another tone frequency.

The largest demand of current from the sphere battery power supplies is the +12 V system which is regulated at +9 V. It is for this reason that this battery system is monitored. When batteries need recharging, the sphere is opened, the internal power switches are turned off, and the appropriate connector is attached to the base unit's charging circuit which is shown in figure 44. Constant current sources made from JFET devices are used to supply the required charging rates. These current sources can be adjusted to provide the recommended current values by changing the value of the associated feedback resistor in the source to gate loop for each charging line. These resistors are R70, R71, R75, R78, R79, and R80. The JFETs Q54, Q55, and Q56 on the quick charge group may have to be preselected to provide sufficient drain to source current I_{dss} to reach the recommended levels. The following table shows the applicable parameters.

Table 4. Current limits for the battery charging circuits.

Battery System	Normal Charge	Quick Charge
+12.2 V	10.0 mA	30.0 mA
+7.2 V	7.0 mA	21.0 mA
-7.2 V	-7.0 mA	-21.0 mA

Each charging circuit is fused at 0.125 A.

The sphere data downlink receiving circuits shown in figures 45 and 46 are used for both the temperature and rf level. These two downlinks share identical circuit design throughout and while the temperature link (figure 39) and the rf level (figure 41) transmitting circuits in the sphere are shown explicitly, the two receiving circuits in the control unit are shown with a single set of schematics (figures 45 and 46). Due to relatively large tolerances associated with several components in the receiving circuit (e.g., IC1 and IC2), the circuit boards are preselected such that the one which calibrates over the largest range (0 to 1.0 V dc) with the best accuracy is used for the rf level. Since the other channel relates to temperature in Kelvin, a unit accurate in the range of 250 to 350 mV is adequate. These are practical guidelines and in actual practice both receiving channels usually operate adequately over the entire range.

The NE5212 in figure 45 is a transimpedance amplifier designed for the recovery of fiber optic signals in applications where very low signals are obtained from high impedance sources such as D1. The recovered pulse train is amplified by IC14 (OP-37) and converted back to a dc voltage by the frequency-to-voltage converter IC2 (AD650JN). Because the rms (root-mean-square) value of the measurement is desired, an AD637JQ average dc-to-rms convertor is used as shown in figure 46. Further adjustment of the transfer function including offset is accomplished with a final operational amplifier IC15. This amplifier also drives a digital panel meter.

The following alignment procedure for a receiver card should be followed if a card is to be replaced or if measurements indicate a faulty transfer function:

(1) Power up the receiver board while monitoring the currents with suitable meters. The +15 and -15 V lines will draw around 16 mA each and the +5 V line will draw about 24 mA.

(2) Without an input signal applied to the frequency-to-voltage convertor (IC1), adjust R9 of figure 45 to produce 0 V dc at TP17 (test point 17).

(3) Remove J2 of figure 46 and ground pin 3 of IC15. Adjust R32 for 0 V dc at TP19. Replace J2 after this is completed.

(4) Pull J1 of figure 46 and ground pin 13 of the dc-to-rms convertor (IC2). Adjust R17 for 0 V dc at TP18.

(5) Apply 1.0 V dc from an external source between ground and pin 13 of IC2. Adjust R23 for an output of 1.0 V dc at TP18. Also, adjust R25 for 1.0 V dc at TP19.

(6) Adjust R22 fully clockwise for maximum smoothing of any ripple that might appear on the waveform.

(7) Replace jumper J1.

(8) Power up the fiber optic transmitter.

(9) Connect a fiber optic link between the transmitter and the receiver.

(10) At TP8 of figure 41, set the input to the voltage-to-frequency convertor (IC6) at pin 4 for 1.0 V.

(11) At this voltage adjust the output frequency using R142, as seen at pin 1, for 100.0 kHz. The duty cycle here will appear to be around 50 percent.

(12) With the 1.0 V setting and the fiber optic line in place, adjust R7 on the receiver card (figure 45) to produce a 1.5 V peak pulse reading at TP15.

CAUTION: If R7 of figure 45 is set too low, no signal will be present at TP16. If the setting is too high, the frequency output at TP16 will be doubled because the comparator in IC1 is double triggering.

(13) Adjust the input voltage to be 200 mV and check to see that R22 is set for minimum ripple at TP18.

(14) Next, vary the input voltage Vin between 20 mV and 1.2 V dc and observe the transfer function by recording Vin, Vf/v, Vrms, and Vout.

(15) If the error (Vin - Vout) x 100/Vin (in percent) is greater than 1 percent at Vin = 500 mV or > 4 percent with Vin = 100 mV, change the frequency by four or five percent and repeat the measurements. If the tracking error is within 1 percent proceed to step 19.

(16) If the tolerances in step 15 can not be accomplished, return the frequency to 100 kHz at 1 V and adjust Vin to be 300 mV dc.

(17) Adjust R13 of figure 45 to produce 300 mV dc at TP19 of figure 46.

(18) Vary Vin between 250 and 350 mV dc and check the output tracking. The maximum error over this range should not exceed ± 0.5 percent.

(19) A receiver card that tracks within the tolerance of step 15 is suitable for gap voltage use and a card that can only function as described in step 18 is adequate for temperature measurements. Improvements to the internal circuits within the integrated circuits may be necessary to reduce the tracking errors seen in this system.

This completes the alignment procedure for the receiver circuitry.

The remaining figures (47 through 51) are provided as a guide to locate the parts referenced in the text. These assembly drawings show the physical location on the circuit boards for all components listed in Appendix B (parts list). Figure 47 also details the connections for all components in the base control unit chassis.

6. CONCLUSIONS

This effort to design and realize a standard radiator for electromagnetic signals with a wide bandwidth and large dynamic range which could be incorporated into modern automated test systems has been successful. While this paper deals primarily with the design and construction details for this standard radiator, the real value of this device will be determined by the possible insight to be gained from measurements performed with this standard. The use of such a characterized radiator as an intercomparison standard by electromagnetic interference testing laboratories will assist the continuing efforts to improve these measurements.

There is much more work to be done to formalize the standard operating practice related to this radiator. The design allows for a wide range of possiblilies and only experience in the field will provide the information needed to bring these devices into service as intercomparison or reference standards.

7. ACKNOWLEDGEMENTS

The authors acknowledge the high level of cooperative support and enduring patience for this work from the Naval Air Systems Command (Robert Haislmaier), Digital Equipment Corporation (Bruce Archambeault), and the management of the NIST Electromagnetic Fields Division (Ramon Baird, Chief).

The authors also acknowledge the consistent support from all the members of the Fields and Interference Metrology Group, NIST, who assisted in the design, construction, testing, documentation, and innumerable other tasks which were critical to the success of this project.

8. REFERENCES

1. Crawford, M. L.; Workman, J. L. Spherical dipole for radiating standard fields. Proceedings CPEM; June 23-27, 1980.

2. Crawford, M. L.; Workman, J. L. Predicting free-space radiated emissions for electronic equipment using TEM cell and open-field site measurements. IEEE International Symposium on EMC (Baltimore); October 7-9, 1980.

3. Mantovani, J. C. Spherical dipole emissions source. Final Report, Project A-3310, Georgia Institute of Technology, Engineering Experiment Station, Atlanta, Georgia; August, 1983.

4. Mantovani, J. C.; Heirman, D. N. A spherical dipole source for use as a transfer standard between radiated emission test sites. IEEE International Symposium on EMC, pp 583-588; 1984.

5. Heirman, D. N.; Investigating open area test site measurement differences. 7th International Zurich Symposium and Technical Exhibition on EMC: 335-338; March 3-5, 1987.

6. Murakawa, K.; Kuwabara, N.; Amemiya, F. Radiation properties of a spherical dipole antenna. IEEE International Symposium on EMC, EMC '89, Nagoya, Japan, p 573; 1989.

7. Valentino, A. R. A small ELF electric field probe. IEEE International EMC Symposium Record, Arlington Heights, IL, pp 265-270; July 18-20, 1972.

8. Spiegel, R. J.; Cooper, E. H.; Bronaugh, E. L.; Kerns, D. R. An improved optically isolated ELF electric field sensor. IEEE International Symposium on EMC, San Diego, CA, pp 429-434; October 9-11, 1979.

9. Gorakpurwalla, H. D.; Cooper, E. H.; Johnson, M. J. A spherical dipole probe system (SPDPS) for the measurement of electric fields from 30 Hz - 1 MHz," IEEE National Symposium on EMC, San Antonio, TX, pp 171-179; April 24-26, 1984.

10. Ramo, S.; Whinnery, J. R.; Van Duzer, T. Fields and Waves in Communication Electronics. John Wiley & Sons, New York, NY, pp 640-645; 1984.

11. Abramowitz, M.; Stegun, I. NBS Handbook of Mathematical Functions. Applied Mathematics Series, vol. 55, Washington, D.C.; 1964.

12. Press, W. H.; Flannery, B. P.; Teukolsky, S. A.; Vetterling, W. T. Numerical Recipes. Cambridge University Press, Cambridge, Great Britain, pp 180-183; 1989.

13. Ma, M. T.; Koepke, G. H. A Method to Quantify the Radiation Characteristics of an Unknown Interference Source. National Bureau of Standards (U.S.) Technical Note 1059; October 1982.

14. Koepke, G. H.; Ma, M. T.; Bensema, W. D. Theory and Measurements of Radiated Emissions Using a TEM Cell. National Institute of Standards and Technology (U.S.) Technical Note 1326; January 1989.

15. Larsen, E. B.; Ehret, R. L.; Camell, D. G.; Koepke, G. H. Calibration of Antenna Factor at a Ground Screen Field Site Using an Automatic Network Analyzer. IEEE EMC Symposium, Denver CO; August 1989.

16. Harrington, R. F. Time-Harmonic Electromagnetic Fields. McGraw-Hill, New York, NY, chapter 6; 1961.

Appendix A

FORTRAN and BASIC Programs

Calculate Electromagnetic Fields from a Spherical Source

FORTRAN program listing

Calculate the electric and magnetic fields and radiated power from a sphere with small gap excited by a uniform voltage.

```
      COMPLEX EFIELD,HFIELD,MAGEFD,MAGHFD,HFCJ,J,SUMPWR1
      REAL PI,K,PWR,PWR1
      INTEGER N
      OPEN(UNIT=6,FILE='SPHDAT',STATUS='UNKNOWN')
      PRINT*,'ENTER THE FREQUENCY IN MHZ'
      READ(5,*) FREQ
      WRITE(6,*) 'THE FREQUENCY IN MHZ'
      WRITE(6,*) FREQ
      FREQ=FREQ*1.0E+06
      PRINT*,'ENTER THE GAP VOLTAGE'
      READ(5,*) V
      WRITE(6,*) 'THE GAP VOLTAGE'
      WRITE(6,*) V
      PRINT*,'ENTER THE RADIUS OF THE SPHERE IN METERS'
      READ(5,*) A
      WRITE(6,*) 'THE RADIUS OF THE SPHERE M'
      WRITE(6,*) A
      PRINT*,'ENTER THE NUMBER OF SPHERICAL MODES TO BE SUMMED'
      READ(5,*) NM
      WRITE(6,*) 'THE NUMBER OF MODES'
      WRITE(6,*) NM
      PRINT*,'ENTER THE FIELD OBSERVATION DISTANCE IN M'
      READ(5,*) R
      WRITE(6,*) 'THE FIELD OBSERVATION DISTANCE M'
      WRITE(6,*) R
      PRINT*,'ENTER THE NUMBER OF ANGULAR STEPS'
      READ(5,*) NSTEPS
      WRITE(6,*) '# OF ANGULAR STEPS'
      WRITE(6,*) NSTEPS

      NSTEPS1=NSTEPS+1
      PI=4.0*ATAN(1.0)
      J=(0.0,1.0)
      ANG=0.0
      DO 100 I=1,NSTEPS1
      THETA=PI/180.0*ANG
      K=2.0*PI*FREQ/3.0E+08
      CALL FIELD(A,R,THETA,FREQ,NM,EFIELD,HFIELD,SUMPWR1)
      CALL POLR(EFIELD,MAGEFD)
      CALL POLR(HFIELD,MAGHFD)
      HFCJ=REAL(HFIELD)-J*AIMAG(HFIELD)
```

```
      PWR=0.5*V*V*REAL(EFIELD*HFCJ)
      PWR1=V*V*ABS(EFIELD)*ABS(EFIELD)/(2.0*377.0)
      SUMPWR1=V*V*SUMPWR1


      WRITE(5,*) 'ANGLE, E-FIELD MAG & PHASE (DEG)'
      WRITE(6,*) 'ANGLE, E-FIELD MAG & PHASE (DEG)'
      WRITE(5,*) 'H-FIELD MAG & PHASE'
      WRITE(6,*) 'H-FIELD MAG & PHASE'
      WRITE(5,*) 'POWER DENSITY-W/M^2 & THE COMPLEX POWER'
      WRITE(6,*) 'POWER DENSITY-W/M^2 & THE COMPLEX POWER'
      WRITE(5,*) ANG,MAGEFD
      WRITE(6,*) ANG,MAGEFD
      WRITE(5,*) MAGHFD
      WRITE(6,*) MAGHFD
      WRITE(5,*) PWR
      WRITE(6,*) PWR
      WRITE(5,*) PWR1
      WRITE(6,*) PWR1
      WRITE(5,*) SUMPWR1
      WRITE(6,*) SUMPWR1

      ANG=ANG+90.0/NSTEPS
100   CONTINUE
      END



      FUNCTION PLGNDR(L,M,X)
      INTEGER L,M
      REAL X
      IF(M.LT.0.OR.M.GT.L.OR.ABS(X).GT.1.0) PAUSE
&     'IMPROPER ARGUMENTS'
      PMM=1.0
      IF(M.GT.0) THEN
      SOMX2=SQRT((1.0-X)*(1.0+X))
      FACT=1.0
      DO 11 I=1,M
      PMM=-PMM*FACT*SOMX2
      FACT=FACT+2.0
11    CONTINUE
      ENDIF
      IF(L.EQ.M) THEN
      PLGNDR=PMM
      ELSE
      PMMP1=X*(2.0*M+1.0)*PMM
      IF (L.EQ.M+1) THEN
      PLGNDR=PMMP1
      ELSE
      DO 12 LL=M+2,L
      PLL=(X*(2*LL-1)*PMMP1-(LL+M-1)*PMM)/(LL-M)
      PMM=PMMP1
      PMMP1=PLL
12    CONTINUE
      PLGNDR=PLL
```

```
      ENDIF
      ENDIF
      RETURN
      END



      SUBROUTINE SPHRBSF(X,N,H1,H2)
      COMPLEX J,H1,H2
      REAL PI,X,BSJ(50),BSY(50)
      INTEGER N
      PI=4.0*ATAN(1.0)
      J=(0.0,1.0)
      BSJ(1)=SIN(X)/X
      BSJ(2)=SIN(X)/(X*X)-COS(X)/X
      BSJ(3)=(3.0/(X*X*X)-1.0/X)*SIN(X)-3.0/(X*X)*COS(X)
      BSY(1)=-COS(X)/X
      BSY(2)=-COS(X)/(X*X)-SIN(X)/X
      BSY(3)=(-3.0/(X*X*X)+1.0/X)*COS(X)-3.0/(X*X)*SIN(X)
      IF (N.EQ.0) THEN
      H1=BSJ(1)+J*BSY(1)
      H2=BSJ(1)-J*BSY(1)
      H1=H1*SQRT(X/(PI/2.0))
      H2=H2*SQRT(X/(PI/2.0))
      RETURN
      ENDIF
      IF(N.EQ.1) THEN
      H1=BSJ(2)+J*BSY(2)
      H2=BSJ(2)-J*BSY(2)
      H1=H1*SQRT(X/(PI/2.0))
      H2=H2*SQRT(X/(PI/2.0))
      RETURN
      ENDIF
      IF(N.EQ.2) THEN
      H1=BSJ(3)+J*BSY(3)
      H2=BSJ(3)-J*BSY(3)
      H1=H1*SQRT(X/(PI/2.0))
      H2=H2*SQRT(X/(PI/2.0))
      ENDIF
      IF(N.GE.3) THEN
      DO 11 I=3,N
      A=I
      BSJ(I+1)=(2.0*I-1.0)/X*BSJ(I)-BSJ(I-1)
      BSY(I+1)=(2.0*I-1.0)/X*BSY(I)-BSY(I-1)
11    CONTINUE
      H1=BSJ(N+1)+J*BSY(N+1)
      H2=BSJ(N+1)-J*BSY(N+1)
      H1=H1*SQRT(X/(PI/2.0))
      H2=H2*SQRT(X/(PI/2.0))
      ENDIF
      RETURN
      END
```

```
      SUBROUTINE FIELD(SRAD,DIST,ANGLE,FR,NTERMS,ELFLD,HLFLD,SUMPWR)
      COMPLEX ELFLD,HF1,HF2,SUM,J,TEMP1,TEMP2,AN,SN,HLFLD
      COMPLEX SUM1,SN1,HLFLD,CPWR,SUMPWR,TEMP3,TEMP4
      REAL FREQ,SRAD,DIST,ANGLE,OMEGA,EPS,KA,KR,BN
      INTEGER NTERMS,I,I1
      J=(0.0,1.0)
      PI=4.0*ATAN(1.0)
      SUM=(0.0,0.0)
      SUM1=(0.0,0.0)
      SUMPWR=(0.0,0.0)
      OMEGA=2.0*PI*FR
      EPS=8.85E-12
      KA=2.0*PI*FR/3.0E+08*SRAD
      KR=2.0*PI*FR/3.0E+08*DIST
      DO 100 I=1,NTERMS
C   COMPUTE THE COEFFICIENT B(N)
      BN=(2.0*I+1.0)*(-PLGNDR(I,1,0.0))/(2.0*I*(I+1)*SRAD)
C   COMPUTE THE COEFFICIENT A(N)
      I1=I-1
      CALL SPHRBSF(KA,I1,HF1,HF2)
      TEMP1=HF2
      CALL SPHRBSF(KA,I,HF1,HF2)
      TEMP2=HF2
      AN=OMEGA*EPS*((SRAD)**(1.5))*BN/(J*(KA*TEMP1-I*TEMP2))
      CALL SPHRBSF(KR,I1,HF1,HF2)
      TEMP1=HF2
      CALL SPHRBSF(KR,I,HF1,HF2)
      TEMP2=HF2
      TEMP3=REAL(AN)-J*AIMAG(AN)
      TEMP4=REAL(TEMP2)-J*AIMAG(TEMP2)
      CPWR=PI*(J*AN/(OMEGA*EPS)*(KR*TEMP1-I*TEMP2))*
&     TEMP3*TEMP4*2.0*I*(I+1.0)/(2.0*I+1.0)
      SUMPWR=SUMPWR+CPWR
      A=COS(ANGLE)
      SN=J*AN/(OMEGA*EPS)/((DIST)**(1.5))*(-PLGNDR(I,1,A)*
&     (KR*TEMP1-I*TEMP2)
      SN1=AN/SQRT(DIST)*(-PLGNDR(I,1,A))*TEMP2
      SUM=SUM+SN
      SUM1=SUM1+SN1
100   CONTINUE
      ELFLD=SUM
      HLFLD=SUM1
      RETURN
      END



      SUBROUTINE POLR(ZR,RM)
      COMPLEX ZR,RM,J
      REAL MAG,PHASE,PI,XR,YR
      PI=4.0*ATAN(1.0)
      J=(0.0,1,0)
      MAG=ABS(ZR)
      XR=REAL(ZR)
```

```
YR=AIMAG(ZR)
IF (MAG.EG.0.0) THEN
RM=(0.0,0.0)
RETURN
ENDIF
IF (XR.GT.0.0) THEN
PHASE=ATAN(YR/XR)
PHASE=180.0/PI*PHASE
ENDIF
IF (XR.LT.0.0.AND.YR.GE.0.0) THEN
PHASE=PI-ATAN(ABS(YR)/ABS(XR))
PHASE=180.0/PI*PHASE
ENDIF
IF (XR.LT.0.0.AND.YR.LT.0.0) THEN
PHASE=-PI+ATAN(ABS(YR)/ABS(XR))
PHASE=180.0/PI*PHASE
ENDIF
RM=MAG+J*PHASE
RETURN
END
```

Rocky Mountain BASIC (HP) Program to Calculate the Radiated Fields from a Spherical Antenna

NOTE: This program will calculate the radiated electric and magnetic fields, the radiated power and the total power radiated. It also will format and save the results of these calculations on a mass storage medium. The source code for this program is available from the authors.

```
100!   RE-STORE "SPHERE_PWR"
102   !
104   ! This routine will calculate the radiated power and total power
106   ! radiated from a spherical dipole source antenna with a uniform
108   ! gap (equator) excitation voltage.
110   !
112   ! Original: 03 Jul 1990, g. Koepke translated from FORTRAN program
114   !                        derived and written by Bob Johnk.
116   ! Revision: 30 Aug 1990:  1400 hours
118   !
120    OPTION BASE 1
122    RAD
124    GOSUB Declare_vars
126    GOSUB Init_values
128 Repeat_calcs:OFF KEY
130    GOSUB Enter_specs
132    GOSUB Allocate_arrays
134    Timein=TIMEDATE
136    GOSUB Calculate_fld
138    Timedone=TIMEDATE
140    PRINTER IS CRT
142    GOSUB Save_results
144    GOSUB Deallocate_arys
146    DISP "CALCULATIONS COMPLETE... ";DROUND((Timedone-Timein),4);" second
148    BEEP
150    ON KEY 0 LABEL "Repeat",Local_prty GOTO Repeat_calcs
152    ON KEY 1 LABEL "END",Local_prty GOTO End_prog
154 Spin:GOTO Spin
156 End_prog:OFF KEY
158    MASS STORAGE IS Msi_id$
160    IF Sys_id$[1,4]="S300" THEN       ! reset to S300 keys and crt
162        CONTROL KBD,15;0
164        CONTROL CRT,12;2
166    END IF
168    LOAD KEY
170    DISP "PROGRAM FINISHED ... RUN TO RESTART."
172    BEEP
174    STOP
176    !
178    ! ////////////////////////////////////////////////////////////
180    !
182 Declare_vars:!
```

```
184    COMPLEX Efield,Hfield,Magefd,Maghfd,Hfcj,J,Sumpwr1
186    REAL K,Pwr,Pwr1
188    REAL Ang,Theta
190    REAL Timein,Timedone
192    INTEGER N,I,I1,Title_print,Local_prty
194    INTEGER Filesize,Datacount
196    DIM Id$[40],Test$[160]
198    COM /Setup/ REAL Freq,V,A,R,INTEGER Nm,Nsteps
200    COM /Sys_msi/ Msi_id$[20]
202    COM /Sys/ Sys_id$[10]
204    COM /Interrupts/ INTEGER Intr_prty
206    COM /Files/ Diskdrive$[20],Filename$[10]
208    RETURN
210    !
212    ! ////////////////////////////////////////////////////////////
214    !
216 Init_values:!
218    Local_prty=5
220    Msi_id$=SYSTEM$("MSI")
222    Sys_id$=SYSTEM$("SYSTEM ID")
224    ! IF Sys_id$[1,4]="S300" THEN CALL Compat_200
226    OUTPUT KBD USING "K,#";"SCRATCH KEY E"
228    DISP CHR$(129)
230    RETURN
232    !
234    ! ////////////////////////////////////////////////////////////
236    !
238 Enter_specs:!
240    PRINTER IS CRT
242    CLEAR SCREEN
244    IF Freq>0 THEN OUTPUT KBD USING "#,K,K";Freq/1.0E+6,"H"
246    INPUT "ENTER the FREQUENCY in MHz. ",Freq
248    PRINT "Frequency (MHz) = ";Freq
250    IF Freq<1.0E-10 THEN Enter_specs
252    Freq=Freq*1.0E+6
254    !
256 Gap_v:!
258    IF V>0 THEN OUTPUT KBD USING "#,K,K";V,"H"
260    INPUT "ENTER the GAP VOLTAGE (volts). ",V
262    PRINT "GAP volts = ";V
264    IF V<0 THEN Gap_v
266    !
268 Sphere_rad:!
270    IF A>0 THEN OUTPUT KBD USING "#,K,K";A,"H"
272    INPUT "ENTER the RADIUS of the SPHERE (meters). ",A
274    PRINT "Sphere RADIUS (m) = ";A
276    IF A<1.0E-20 THEN Sphere_rad
278    !
280 Modesum:!
282    IF Nm>0 THEN OUTPUT KBD USING "#,K,K";Nm,"H"
284    INPUT "ENTER the number of SPHERICAL MODES to be summed. ",Nm
286    PRINT "The number of MODES summed = ";Nm
288    IF Nm<1 THEN Modesum
290    !
292 Observ: !
```

```
294    IF R>0 THEN OUTPUT KBD USING "#,K,K";R,"H"
296    INPUT "ENTER the FIELD OBSERVATION DISTANCE (meters). ",R
298    PRINT "FIELD OBSERVATION DISTANCE (meters) = ";R
300    IF R<A THEN Observ
302    !
304 Num_steps:!
306    IF Nsteps>0 THEN OUTPUT KBD USING "#,K,K";Nsteps,"H"
308    INPUT "ENTER the number of ANGULAR STEPS. ",Nsteps
310    PRINT "Angular STEPS = ";Nsteps
312    IF Nsteps<1 THEN Num_steps
314    !
316    RETURN
318    !
320    ! ////////////////////////////////////////////////////////////
322    !
324 Allocate_arrays:! Setup all data files for saving/graphing
326    IF Nsteps>0 THEN
328        ALLOCATE Pdata(Nsteps*4+1,2),Edata(Nsteps*4+1,2)
330        ALLOCATE Hdata(Nsteps*4+1,2)
332        Filesize=Nsteps*4+1
334    ELSE
336        BEEP
338        DISP "ILLEGAL number of STEPS.    hit RUN ... "
340        CALL Pause_key_on
342    END IF
344    RETURN
346    !
348    ! /////////////////////////////////////////////////////////////
350    !
352 Deallocate_arys:!
354    DEALLOCATE Pdata(*),Edata(*)
356    DEALLOCATE Hdata(*)
358    Filesize=0
360    RETURN
362    !
364    ! ////////////////////////////////////////////////////////////
366    !
368 Calculate_fld:!
370    !
372    Title_print=1
374    J=CMPLX(0.,1.0)
376    FOR I=0 TO Nsteps
378        Ang=I*90.0/Nsteps
380        DISP "Calculating angle ";Ang;" ... "
382        Theta=(PI/180.0)*Ang    !convert to radians
384        K=2.0*PI*Freq/3.0E+8
386        CALL Field(A,R,Theta,Freq,Nm,Efield,Hfield,Sumpwr1)
388        DEG
390        Magefd=CMPLX(ABS(Efield),ARG(Efield))
392        Maghfd=CMPLX(ABS(Hfield),ARG(Hfield))
394        RAD
396        Hfcj=REAL(Hfield)-J*IMAG(Hfield)
398        Pwr=.5*V*V*REAL(Efield*Hfcj)
400        Pwr1=V*V*ABS(Efield)*ABS(Efield)/(2.0*377.0)
402        Sumpwr1=V*V*Sumpwr1
```

```
404         GOSUB List_results
406         !
408         Pdata(I+1,1)=Ang
410         Pdata(I+1,2)=Pwr
412         !
414         Edata(I+1,1)=Ang
416         Edata(I+1,2)=REAL(Magefd)
418         !
420         Hdata(I+1,1)=Ang
422         Hdata(I+1,2)=REAL(Maghfd)
424         !
426     NEXT I
428     DISP CHR$(12)
430     PRINTER IS 701
432     PRINT USING "@"
434     PRINTER IS CRT
436     RETURN
438     !
440     ! ////////////////////////////////////////////////////////////
442     !
444  List_results:!
446     PRINTER IS 701
448     IF Title_print THEN
450         Title_print=0  ! only once
452         PRINT TAB(20);"SPHERICAL DIPOLE FIELDS"
454         PRINT RPT$("_",80)
456         PRINT
458         PRINT "Operating FREQUENCY = ";Freq/1.0E+6;" MHz."
460         PRINT "Gap Drive Voltage = ";V;"volts.       Sphere radius = ";A;"m."
462         PRINT "Spherical MODES = ";Nm;".      Observation distance = ";R;"m."
464         PRINT "Total Radiated POWER = ";REAL(Sumpwr1);" watts."
466         PRINT RPT$("_",80)
468         PRINT TAB(48);"  Power Density (w/m^2)"
470         PRINT "Angle    E (mag ---- phase)  H (mag ---- phase)";
472         PRINT "  REAL (ExH) --- E^2/Z"
474         PRINT RPT$("-",80)
476     END IF
478  Image1:IMAGE M3D.DD,X,MD.4DE,X,M3D.DD,X,MD.4DE,X,M3D.DD,#
480  Image2:IMAGE X,MD.4DE,X,MD.4DE,
482     PRINT USING Image1;Ang,Magefd,Maghfd
484     PRINT USING Image2;Pwr,Pwr1
486     RETURN
488     !
490     ! ////////////////////////////////////////////////////////////
492     !
494  Save_results:!
496     !
498     ! fill in arrays for 0,360 degrees.
500     !
502     I1=Nsteps+1
504     FOR I=Nsteps TO 1 STEP -1
506         Ang=180-Pdata(I,1)
508         I1=I1+1
510         Pdata(I1,1)=Ang
512         Pdata(I1,2)=Pdata(I,2)
```

```
514         Edata(I1,1)=Ang
516         Edata(I1,2)=Edata(I,2)
518         Hdata(I1,1)=Ang
520         Hdata(I1,2)=Hdata(I,2)
522     NEXT I
524     !
526     I1=2*Nsteps+1
528     FOR I=2 TO 2*Nsteps+1
530         Ang=180+Pdata(I,1)
532         I1=I1+1
534         Pdata(I1,1)=Ang
536         Pdata(I1,2)=Pdata(I,2)
538         Edata(I1,1)=Ang
540         Edata(I1,2)=Edata(I,2)
542         Hdata(I1,1)=Ang
544         Hdata(I1,2)=Hdata(I,2)
546     NEXT I
548     Datacount=4*Nsteps+1   ! same as Filesize
550     !
552     ! SAVE THE DATA HERE......
554     !
556     Diskdrive$=""
558     Filename$=""
560     Test$="Power:"&VAL$(PROUND(Freq/1.0E+6,-1))&"gV="&VAL$(V)
562     Test$=Test$&"a"&VAL$(A)&"Nm"&VAL$(Nm)&"z'="&VAL$(R)
564     IF LEN(Test$)>40 THEN
566         Id$=Test$[1,40]
568         BEEP
570         DISP "ID$ is too long ... striping to 40 chrs."
572         WAIT 3
574         DISP CHR$(12)
576     ELSE
578         Id$=Test$[1,LEN(Test$)]
580     END IF
582     IF LEN(Diskdrive$)=0 THEN
584         CLEAR SCREEN
586      !  CALL Select_disk
588     END IF
590     PRINT TABXY(1,18);" ......... SAVING POWER DATA ..........."
592     !  CALL Data_to_disk_r(Pdata(*),Filesize,Datacount,Id$)
594     Filename$=""
596     Id$[1,5]="E-fld"
598     PRINT TABXY(1,18);" ......... SAVING E Field DATA ..........."
600     !  CALL Data_to_disk_r(Edata(*),Filesize,Datacount,Id$)
602     Filename$=""
604     Id$[1,5]="H-fld"
606     PRINT TABXY(1,18);" ......... SAVING H Field DATA ..........."
608     !  CALL Data_to_disk_r(Hdata(*),Filesize,Datacount,Id$)
610     CLEAR SCREEN
612     CLEAR LINE
614     RETURN
616     !
618     ! ///////////////////////////////////////////////////////////
620     !
622     END
```

```
624     !
626     ! ************************************************************
628     !
630     DEF FNPlgndr(INTEGER L,M,REAL X)
632         REAL Pmm,Fact,Somx2,Plgndr,Pmmp1,Pll
634         INTEGER I,Ll
636         IF (M<0. OR M>L OR ABS(X)>1.0) THEN
638             BEEP
640             DISP "IMPROPER ARGUMENTS in FN Plgndr ... "
642             PAUSE
644         END IF
646         Pmm=1.0
648         IF M>0 THEN
650             Somx2=SQRT((1.0-X)*(1.0+X))
652             Fact=1.0
654             FOR I=1 TO M
656                 Pmm=-Pmm*Fact*Somx2
658                 Fact=Fact+2
660             NEXT I
662         END IF
664         !
666         IF L=M THEN
668             Plgndr=Pmm
670         ELSE
672             Pmmp1=X*(2.0*M+1.0)*Pmm
674             IF L=M+1 THEN
676                 Plgndr=Pmmp1
678             ELSE
680                 FOR Ll=M+2 TO L
682                     Pll=(X*(2*Ll-1)*Pmmp1-(Ll+M-1)*Pmm)/(Ll-M)
684                     Pmm=Pmmp1
686                     Pmmp1=Pll
688                 NEXT Ll
690                 Plgndr=Pll
692             END IF
694         END IF
696         RETURN Plgndr
698     FNEND
700     !
702     ! ************************************************************
704     !
706     DEF FNFac(INTEGER N)
708         INTEGER I
710         REAL Fac
712         IF N=0 THEN RETURN (1.0)
714         Fac=1.0
716         FOR I=1 TO N
718             Fac=Fac*I
720         NEXT I
722         RETURN Fac
724     FNEND
726     !
728     ! ************************************************************
730     !
732     SUB Sphrbsf(REAL X,INTEGER N,COMPLEX H1,H2)
```

```
734         ! calculate spherical basis functions.
736         COMPLEX J
738         REAL Bsj(50),Bsy(50)
740         J=CMPLX(0.,1.0)
742         !
744         Bsj(1)=SIN(X)/X
746         Bsj(2)=SIN(X)/(X*X)-COS(X)/X
748         Bsj(3)=(3.0/(X*X*X)-1.0/X)*SIN(X)-3.0/(X*X)*COS(X)
750         !
752         Bsy(1)=-COS(X)/X
754         Bsy(2)=-COS(X)/(X*X)-SIN(X)/X
756         Bsy(3)=(-3.0/(X*X*X)+1.0/X)*COS(X)-3.0/(X*X)*SIN(X)
758         !
760         SELECT N
762         CASE 0
764             H1=Bsj(1)+J*Bsy(1)
766             H2=Bsj(1)-J*Bsy(1)
768             H1=H1*SQRT(X/(PI/2.0))
770             H2=H2*SQRT(X/(PI/2.0))
772         CASE 1
774             H1=Bsj(2)+J*Bsy(2)
776             H2=Bsj(2)-J*Bsy(2)
778             H1=H1*SQRT(X/(PI/2.0))
780             H2=H2*SQRT(X/(PI/2.0))
782         CASE 2
784             H1=Bsj(3)+J*Bsy(3)
786             H2=Bsj(3)-J*Bsy(3)
788             H1=H1*SQRT(X/(PI/2.0))
790             H2=H2*SQRT(X/(PI/2.0))
792         CASE >2
794             FOR I=3 TO N
796                 Bsj(I+1)=(2.0*I-1.0)/X*Bsj(I)-Bsj(I-1)
798                 Bsy(I+1)=(2.0*I-1.0)/X*Bsy(I)-Bsy(I-1)
800             NEXT I
802             H1=Bsj(N+1)+J*Bsy(N+1)
804             H2=Bsj(N+1)-J*Bsy(N+1)
806             H1=H1*SQRT(X/(PI/2.0))
808             H2=H2*SQRT(X/(PI/2.0))
810         END SELECT
812         SUBEXIT
814     SUBEND
816     !
818     ! ***********************************************************
820     !
822      SUB Field(REAL Srad,Dist,Angle,Fr,INTEGER Nterms,COMPLEX Elfld, Hlf
Sumpwr)
824 Field: ! Calculate the field from a spherical dipole.
826         COMPLEX Hf1,Hf2,Sum,Sum1,Sn,Sn1,J,An,Cpwr
828         COMPLEX Temp1,Temp2,Temp3,Temp4
830         REAL Omega,Eps,Ka,Kr,Bn,A
832         INTEGER I,I1
834         !
836         J=CMPLX(0.,1.0)
838         Sum=CMPLX(0.,0.)
840         Sum1=CMPLX(0.,0.)
```

```
842        Sumpwr=CMPLX(0.,0.)
844        Omega=2.0*PI*Fr
846        Eps=8.85E-12
848        Ka=2.0*PI*Fr/3.0E+8*Srad
850        Kr=2.0*PI*Fr/3.0E+8*Dist
852        !   PRINT RPT$("?",20);Fr;" MHz,  Angle = ";Angle
854        !   PRINT "Omega =";Omega;", Ka =";Ka;", Kr =";Kr
856        !
858        FOR I=1 TO Nterms
860            ! calculate the coefficient B(N)
862            Bn=(2.0*I+1.0)*(-FNPlgndr(I,1,0.))/(2.0*I*(I+1.0)*Srad)
864            !       PRINT "*****************"
866            !       PRINT "Index number I =";I
868            !       PRINT "Bn = ";Bn;",  ";
870            ! calculate the coefficient A(N)
872            I1=I-1
874            CALL Sphrbsf(Ka,I1,Hf1,Hf2)
876            Temp1=Hf2
878            CALL Sphrbsf(Ka,I,Hf1,Hf2)
880            Temp2=Hf2
882            An=Omega*Eps*((Srad)^(1.5))*Bn/(J*(Ka*Temp1-I*Temp2))
884    !       PRINT "An = ";An
886            !
888            CALL Sphrbsf(Kr,I1,Hf1,Hf2)
890            Temp1=Hf2
892    !       PRINT "Temp1 =";Temp1
894            CALL Sphrbsf(Kr,I,Hf1,Hf2)
896            Temp2=Hf2
898            !       PRINT "Temp2 =";Temp2
900            Temp3=REAL(An)-J*IMAG(An)
902            Temp4=REAL(Temp2)-J*IMAG(Temp2)
904            !       PRINT "Temp3 =";Temp3
906            !       PRINT "Temp4 =";Temp4
908            Cpwr=PI*(J*An/(Omega*Eps)*(Kr*Temp1-I*Temp2))*Temp3*Temp4
910            Cpwr=Cpwr*2.0*I*(I+1.0)/(2.0*I+1.0)
912            !       PRINT "Cpwr =";Cpwr
914            Sumpwr=Sumpwr+Cpwr
916            !       PRINT "Sumpwr =";Sumpwr
918            A=COS(Angle)
920            Sn=(J*An/((Omega*Eps)*(Dist^1.5)))*(-FNPlgndr(I,1,A))
922            Sn=Sn*(Kr*Temp1-I*Temp2)
924            !       PRINT "Sn = ";Sn
926            Sn1=An/SQRT(Dist)*(-FNPlgndr(I,1,A))*Temp2
928            Sum=Sum+Sn
930            !       PRINT "Sum (E) =";Sum
932            Sum1=Sum1+Sn1
934        NEXT I
936        Elfld=Sum
938        Hlfld=Sum1
940   !    PRINT RPT$("end-",5);" ANGLE";Angle
942        SUBEXIT
944    SUBEND
946    !
948    ! ***************************************************************
```

Appendix B

Parts List

SYMBOL	EQUIVALENT
AC	ALARM CIRCUIT
BD	BIAS DETECTOR
DLR	DOWN-LINK RECEIVER
DLT	DOWN LINK TRANSMITTER
BCC	BATTERY CHARGING CIRCUIT
RFL	R-F LINK
SR	SPHERICAL REGULATOR
ULS	UP-LINK SWITCH

PASSIVE COMPONENTS (resistors and capacitors)

All resistance values are in ohms (Ω) and capacitance values are in Farads (F). Tolerances are ± 10 percent unless otherwise marked. POT is a potentiometer or variable resistor.

RESISTOR	VALUE	LOCATION	CONNECTION	FIGURE
R1	1K	DLR	D1, -15VDC	45
R2	10	DLR	C2, IC 13 PIN 2	45
R3	511	DLR	C4, IC 14 PIN 2	45
R4	511	DLR	C5, GND	45
R5	511	DLR	IC 14 PIN 3, GND	45
R6	10	DLR	+15VDC, IC 14 PIN 7	45
R7	50K POT	DLR	IC 14 PIN 2 and PIN 6	45
R8	10	DLR	IC 14 PIN 4, -15VDC	45
R9	20K POT	DLR	IC 1 PIN 13 and PIN 14	45
R10	270K, 1%	DLR	R9, IC 1 PIN 12	45
R11	10	DLR	+15VDC, IC 1 PIN 12	45
R12	511	DLR	IC 1 PIN 9 and PIN 10	45
R13	20K	DLR	R14, IC 1 PIN 1	45
R14	5.1K	DLR	IC 1 PIN 3, R13	45
R15	10	DLR	IC 1 PIN 5, -15VDC	45
R16	1K	DLR	+15VDC, R17	46
R17	50K POT	DLR	R16, R18	46
R18	1K	DLR	R17, -15VDC	46
R19	1M	DLR	IC 2 PIN 4, R17	46
R20	100	DLR	+15VDC, IC 2 PIN 11	46
R21	1K	DLR	R22, IC 2 PIN 1	46
R22	100K POT	DLR	R21, IC 2 PIN 6	46
R23	1K POT	DLR	IC 2 PIN 6 and PIN 9	46
R24	100	DLR	IC 2 PIN 10, -15VDC	46
R25	5K POT	DLR	IC 2 PIN 14, GND	46
R26	10K, 1%	DLR	IC 15 PIN 2, R27	46
R27	100, 1%	DLR	R26, GND	46
R28	10	DLR	+15VDC, IC 15 PIN 7	46

R29	10K, 1%	DLR	IC 15 PIN 2 and PIN 6	46
R30	10	DLR	-15VDC, IC 15 PIN 4	46
R31	10K,1%	DLR	R27, C26	46
R32	50K POT	DLR	C30, R33	46
R33	1K	DLR	R32, +15VDC	46
R34	20K, 1%	DLR	IC 15 PIN 6, GND	46
R35	10K	DLR	-15VDC, R32	46
R50	1M	AC	IC 16 PIN 2, +15VDC	38
R51	1M	AC	IC 16 PIN 2, GND	38
R52	1.5K,1/4w	AC	IC 16 PIN 3, +15VDC	38
R53	1K,1/4w	AC	IC 16 PIN 6, D109	38
R54	1K POT	AC	IC 16 PIN 6, D110	38
R55	1M	AC	IC 16 PIN 2, +15VDC	38
R56	1M	AC	IC 16 PIN 2, GND	38
R57	1.5K,1/4w	AC	IC 16 PIN 3, +15VDC	38
R58	1K,1/4w	AC	IC 16 PIN 6, D111	38
R59	1K POT	AC	IC 16 PIN 6, D112	38
R60	1M	AC	IC 16 PIN 3, S16	38
R61	270	AC	R62, D113	38
R62	10M	AC	R61, IC 16 PIN 2	38
R63	220K	AC	IC 16 PIN 2, GND	38
R64	10K POT	AC	IC 16 PIN 1 and PIN 5	38
R65	1K POT	AC	IC 16 PIN 6, D114	38
R66	20K	AC	IC 16 PIN 6, D52	38
R67	10K POT	AC	+5VDC, Q50	38
R68	49.9, 1%	ULS	+5VDC, D53	38
R69	20K POT	ULS	Q50, GND	38
R70	500 POT	BCC	D115, Q51	44
R71	500 POT	BCC	D116, Q52	44
R72	100	BCC	D117, Q53	44
R73	200	BCC	Q51, R76	44
R74	100	BCC	Q52, R77	44
R75	500 POT	BCC	Q53, R78	44
R76	50	BCC	R73, Q54	44
R77	50	BCC	R74, Q55	44
R78	100 POT	BCC	R75, Q56	44
R79	100 POT	BCC	Q54, D119	44
R80	100 POT	BCC	Q55, D120	44
R81	50	BCC	Q56, D121	44
R82	1K	BCC	+15VDC,D124	44
R96	560	RFL	+9VDC,Q57	42
R97	18	RFL	IC 9 PIN 15,C138	42
R98	310	RFL	R97,GND	42
R99	310	RFL	R97,GND	42
R100	22	RFL	IC 9 PIN 1, C100	42
R101	22	RFL	+9VDC, C101	42
R102	22	RFL	IC 9 PIN 4, C102	42
R103	22	RFL	IC 9 PIN 6, C106	42
R104	100	RFL	C103, C104	42
R105	150	RFL	+7.2VDC, L100	42
R106	200	RFL	across TP-103	42
R107	499K, 1%	SR	Q100, R108	37
R108	499K, 1%	SR	IC 3 PIN 5, Q100	37
R109	100K, 1%	SR	Q100, D101	37
R110	1M	SR	D104, C108	37

R111	100K	SR	Q101, Q102	37
R112	1K, 1%	SR	D103, Q102	37
R113	1M POT	SR	IC 3 PIN 1 and PIN 7	37
R114	100K, 1%	SR	IC 3 PIN 7, GND	37
R115	1K, 1%	SR	IC 3 PIN 3, IC 4 PIN 3	37
R116	5K POT	SR	IC 4 PIN 8, Q103	37
R117	10K	SR	Q103, GND	37
R118	470, 1%	SR	IC 5 PIN OUT, R119	37
R119	5K POT	SR	R118, GND	37
R120	10K	BD	+12.2VDC, C118	40
R121	100K POT	BD	Q104 PIN 1, R122	40
R122	51.1K, 1%	BD	R121, Q104 PIN 3	40
R123	82.5K, 1%	BD	Q104 PIN 5 and PIN 7	40
R124	681K, 1%	BD	C119, C121	40
R125	681K, 1%	BD	C120, C122	40
R126	500	BD	D105, C123	40
R127	500	BD	D106, C124	40
R128	1M, 1%	BD	IC 11 PIN 10, R129	40
R129	1M, 1%	BD	R128, IC 11 PIN 12	40
R130	20K POT	BD	IC 11 PIN 9 and PIN 13	40
R131	22.1K, 1%	BD	IC 11 PIN 8 and PIN 9	40
R132	22.1K, 1%	BD	IC 11 PIN 13 and PIN 14	40
R133	22.1K, 1%	BD	IC 11 PIN 8 and PIN 2	40
R134	22.1K, 1%	BD	IC 11 PIN 14 and PIN 3	40
R135	22.1K, 1%	BD	IC 11 PIN 1 and PIN 2	40
R136	22.1K, 1%	BD	IC 11 PIN 3, GND	40
R137	100K	BD	IC 11 PIN 1, GND	40
R138	20K	BD	IC 11 PIN 1, C127	40
R139	100K	BD	IC 11 PIN 7, GND	40
R140	10	DLT	+5VDC, IC 6 PIN 8	41
R141	500, 1%	DLT	IC 6 PIN 3, TP3, R142	41
R142	1K POT	DLT	R141, GND	41
R143	1K	DLT	IC 6 PIN 1, +5VDC	41
R144	10K	DLT	IC 7 PIN 2, +5VDC	41
R145	100, 1%	DLT	Q105, GND	41
R146	910, 1%	DLT	IC 8 PIN4, R147	39
R147	200 POT	DLT	R146, GND	39
R148	100	DLT	+5VDC, IC 8 PIN 8	39
R149	500, 1%	DLT	IC 8 PIN 3, TP3, R150	39
R150	1K POT	DLT	R149, TP3, GND	39
R151	1K	DLT	+5VDC, IC 8 PIN 1	39
R152	10K	DLT	+5VDC, IC 7 PIN 14	39
R153	100, 1%	DLT	Q106, GND	39
R154	220K	SR	R155, L102	39
R155	220K	SR	R154, L103	39
R156	270K	SR	R101, R146	39

CAPACITOR	VALUE	LOCATION	CONNECTION	FIGURE
C1	.1μF	DLR	R1, GND	45
C2	.1μF	DLR	+5VDC, GND	45
C3	1.0μF	DLR	IC 13 PIN 2, GND	45
C4	.1μF	DLR	IC 13 PIN 5, R3	45
C5	.1μF	DLR	IC 13 PIN 7, R4	45

C6	.1µF	DLR	+15VDC, GND	45
C7	1.0µF	DLR	IC 14 PIN 7, GND	45
C8	1.0µF	DLR	IC 14 PIN 4, GND	45
C9	.1µF	DLR	R8, GND	45
C10	.1µF	DLR	R11, GND	45
C11	0.001µF	DLR	IC 14 PIN 6, IC 1 PIN 9	45
C12	1µF	DLR	IC 1 PIN 11 and PIN 12	45
C13	.001µF	DLR	IC 1 PIN 1 and PIN 3	45
C14	150pF	DLR	IC 1 PIN 6, GND	45
C15	1µF	DLR	IC 1 PIN 5, GND	45
C16	.1µF	DLR	-15VDC, GND	45
C17	.1µF	DLR	R16, GND	46
C18	.1µF	DLR	R18, GND	46
C19	.1µF	DLR	+15VDC, GND	46
C20	1µF TANT.	DLR	IC 2 PIN 11, GND	46
C21	.01µF,NPO* CHIP CAP	DLR	IC 2 PIN 1, GND	46
C22	1µF TANT	DLR	IC 2 PIN 10, GND	46
C23	.1µF	DLR	-15VDC, GND	46
C24	.1µF	DLR	+15VDC, GND	46
C25	1µF TANT	DLR	IC 15 PIN 7, GND	46
C26	.1µF	DLR	R27, GND	46
C27	1µF TANT	DLR	IC 15 PIN 4, GND	46
C28	.1µF	DLR	R30, GND	46
C29	.1µF	DLR	R31, GND	46
C30	.1µF	DLR	R32, GND	46
C31	.1µF	DLR	R32, GND	46
C50	.1µF	MLS	Q50, GND	38
C100	.1µF	RFL	R100, GND	42
C101	.1µF	RFL	R101, IC#9 PIN 9	42
C102	.1µF	RFL	R102, GND	42
C103	.1µF	RFL	R104, GND	42
C104	.1µF	RFL	R104, GND	42
C105	.1µF	RFL	IC 9 PIN 5, GND	42
C106	.1µF	RFL	R103, GND	42
C107	1000pF	RFL	IC 10 OUTPUT, D100	42
C108	1µF TANT	SR	D104, R110	37
C109	.1µF	SR	IC 3 PIN 8, GND	37
C110	.01µF	SR	IC 3 PIN 1 and PIN 7	37
C111	4.7µF TANT	SR	IC 3 PIN 1, R113	37
C112	1µF TANT	SR	Q102, GND	37
C113	.1µF	SR	IC 4 PIN 8, GND	37
C114	.01µF	SR	IC 4 PIN 2, PIN 6	37
C115	4.7µF TANT	SR	IC 4 PIN 1, GND	37
C116	4.7µF TANT	SR	IC 5 ADJ, GND	37
C117	.1µF	SR	IC 5 IN, GND	37
C118	.1µF	BD	R120, GND	40
C119	.01µF	BD	Q104 PIN 3 and PIN 4	40
C120	.01µF	BD	Q104 PIN 4 and PIN 7	40
C121	.001µF	BD	D105, GND	40
C122	.001µF	BD	D106, GND	40
C123	.001µF	BD	IC 11 PIN 10, GND	40
C124	.001µF	BD	GND, IC 11 PIN 12	40
C125	.01µF	BD	+5VDC, GND	40
C126	.01µF	BD	-5VDC, GND	40

C127	.1μF	BD	R138, GND	40
C128	.1μF	DLT	IC 6 PIN 8, GND	41
C129	1000pF **	DLT	IC 6 PIN 6 and PIN 7	41
C130	270pF	DLT	IC 7 PIN 1 and PIN 2	41
C131	.1μF	DLT	IC 8 PIN 8, GND	39
C132	1000pF **	DLT	IC 8 PIN 6 and PIN 7	39
C133	270 pF	DLT	IC 7 PIN 14 and PIN 15	39
C134	.1μF	SR	+5VDC, GND	37
C135	.1μF	SR	-5VDC, GND	37
C136	1000pF	RFL	+7.2VDC, R105	42
C137	1000pF	RFL	D105, TP2	40,42
C138	1000pF	RFL	R97,IC10 input	42
C139	1.0μF	RFL	Q57,GND	42

NOTE : ** means POLY CARBONATE or POLYSTYRENE
* means CERAMIC
TANT means Tantalum

SYMBOL	EQUIVALENT
AC	ALARM CIRCUIT
BD	BIAS DETECTOR
DLR	DOWN-LINK RECEIVER
DLT	DOWN LINK TRANSMITTER
BCC	BATTERY CHARGING CIRCUIT
RFL	R-F LINK
SR	SPHERICAL REGULATOR
ULS	UP-LINK SWITCH

SEMICONDUCTORS (transistors, diodes, ICs and LEDs)

COMPONENT	TYPE	LOCATION	CONNECTION	FIGURE	MANUFACTURER
IC 1	AD 650JN	DLR	PIN 1 TO C13	45	A.D.
IC 2	AD 637JQ RMS/DC	DLR	PIN 1 TO C21	46	A.D.
IC 3	LP2951CM	SR	PIN 5 TO R108	37	National
IC 4	LP2951CM	SR	PIN 6 TO C114	37	National
IC 5	LM337LZ	SR	ADJ. TO C116	37	Harris
IC 6	AD654JR	DLT	PIN 6 TO C129	41	A.D.
IC 7	HC4538	DLT	PIN 2 TO R144	39	Motorola
IC 8	AD654JR	DLT	PIN 6 TO C132	39	A.D.
IC 9	PDC 2200-24	RFL	PIN 5 TO C105	42	B.T.D.
IC 10	MSA-0635	RFL	OUT TO C107	42	Avantek
IC 11	MC34184D	BD	PIN 2 TO R135	40	Motorola
IC 12	AD590	DLT	R146, +5VDC	39	HP
IC 13	NE5212	DLR	PIN 5 TO C4	45	Signetics
IC 14	OP AMP OP37	DLR	PIN 2 TO R3	45	PMI
IC 15	OP AMP OP37	DLR	PIN 2 TO R26	46	PMI
IC 16	LH0042CH	AC	PIN 3 to Laser pin 9	44	National
IC 17	LH0042CH	AC	PIN 3 to Laser pin 7	44	National
IC 18	LH0042CH	AC	PIN 3 to IC 5 pin 1	44	National
D1 (P31)	710-502-000	DLR	IC 13 PIN 1	45	Radiall
D50	1N270	AC	L53,-OF ALARM	38	generic
D51	1N270	AC	L55,-OF ALARM	38	generic
D52	1N4153	AC	R66, GND	38	Unitrode
D53	MFOE1202	ULS	Q50,R68	38	Motorola
D100	1N5235B, 6.8V	RFL	R96,GND	42	Motorola
D101	1N4153	SR	R109, IC 3 PIN 3	37	Unitrode
D102	1N4153	SR	IC 3 PIN 3,C108	37	Unitrode
D103	1N4153	SR	IC 3 PIN 3,R112	37	Unitrode
D104	1N4153	SR	D102, Q101	37	Unitrode
D105	HP5082-2755	BD	R126,IC 10 out	40,42	HP
D106	HP5082-2755	BD	R127, GND	40	HP
D107	HFBR-1404	DLT	+5VDC, Q105	41	HP
D108	HFBR-1404	DLT	+5VDC, Q106	39	HP

NOTE: The backshells are removed on D107 and D108.

SEMICONDUCTORS (transistors, diodes, ICs and LEDs)

COMPONENT	TYPE	LOCATION	CONNECTION	FIGURE	MANUFACTURER
	* Panel mounted #276-069(green) or #276-068(red)				
D109	GREEN LED*	AC	R53, GND	38	Radio Shack
D110	RED LED*	AC	R54, D50	38	" "
D111	GREEN LED*	AC	R58, GND	38	" "
D112	RED LED*	AC	D50, R59	38	" "
D113	GREEN LED*	AC	R61, GND	38	" "
D114	RED LED*	AC	D51, R65	38	" "
D115	GREEN LED*	BCC	+12.2V, R70	44	" "
D116	GREEN LED*	BCC	+7.2V, R71	44	" "
D117	GREEN LED*	BCC	-7.2V, R72	44	" "
D118	RED LED*	BCC	R79, +12.2V	44	" "
D119	RED LED	BCC	See D118	44	generic (miniature)
D120	RED LED*	BCC	R80, +7.2V	44	Radio Shack
D121	RED LED	BCC	See D120	44	generic (miniature)
D122	RED LED*	BCC	R81,-7.2V	44	Radio Shack
D123	RED LED	BCC	See D122	44	generic (miniature)
D124	GREEN LED*	BCC	R82,GND	44	Radio Shack
D125	LED HLMP-K155	SR	R156, SWITCH	36	HP
D126	LED HLMP-K155	SR	R154, SWITCH	36	HP
D127	LED HLMP-K155	SR	R155, SWITCH	36	HP
L100	2μH Chip Inductor	RFL	R105, C107	42	American Precision Industries, Inc. East Aurora, NY
Q50	2N3904 NPN BJT	ULS	R67, R69	38	Motorola
Q51	J310	BCC	R70, R73	44	Motorola
Q52	J310	BCC	R71, R74	44	Motorola
Q53	J310	BCC	R72, R75	44	Motorola
Q54	J310	BCC	R76, R79	44	Motorola
Q55	J310	BCC	R77, R80	44	Motorola
Q56	J310	BCC	R78, R81	44	Motorola
Q57	2N3904	RFL	R96,C136	42	Motorola
Q100	2N3906 PNP BJT	SR	R108, R107	37	Motorola
Q101	2N3904	SR	R111, R110	37	Motorola
Q102	2N5460 P channel JFET	SR	R112, C112	37	Motorola
Q103	MRD360 Photo Darlington	SR	R117, R116	37	Motorola
Q104	2N5906 **	BD	R121, R123	40	Harris
Q105	2N3904	DLT	R145, D107	41	Motorola
Q106	2N3904	DLT	R153, D108	39	Motorola
	note : ** is dual matched N channel JFET				
T1	TP103	RFL	C107,R106	42	Anzac

Connectors and other miscellaneous parts

BUC = BASE UNIT CONTROL

COMPONENT	TYPE	LOCATION	CONNECTION	FIGURE	MANUFACTURER
P1	Filtered AC Connector with 5A Fuse.	BUC	AC input	47	Corcom
P2	Fuse Holder	BUC	AC input	47	Littelfuse Tracor
P3	Fuse,1/4A	BUC	P2	47	generic
P4	Fuse,1/16A	BCC	-15V,R75,R78	44,48	generic
P5	Fuse,1/16A	BCC	+15V,R74,R77	44,48	generic
P6	Fuse,1/16A	BCC	+24V,R73,R76	44,48	generic
P7	Fuse holders	BCC	P4,P5,P6	48	generic
P8 (R32)	Variable Resistor 10 turn, 50Kohm #536	BUC	R33,C30	47	Spectrol
P9	Switch DPDT MTA 206N	BUC	P1,P3	47	Alco
P10	Switch (AC on/off) 275-676	BUC	P1,P41	47	Radio Shack
P11	Switch DPDT 275-652	BUC	+5V,R62;+5V,R67	47	Radio Shack
P12	Connectors,7 pin TKR-7 (receptacle), TKP-7 (cable plug)	BUC	Normal Batt.Chg.	47	Viking
P13	see P12	BUC	Quick Batt.Chg.	47	Viking
P14	Panel Connector Type N to SMA 3080-2240-00	BUC	rf input,laser	47	Omni-Spectra
P15	Connector SMA to cable, 5285-1	BUC	P20 to P14	47	Connecting Devices
P16	Connector SMA to cable right angle 5850-1CC	BUC	P20 to P35	47	Connecting Devices
P17	Connector BNC Panel UG 1094/U	BUC	IC15 on Temp Downlink Rcvr	47	Amphenol
P18	see P17	BUC	IC15 on Gap Volt Downlink Rcvr	47	Amphenol
P19	Connector,9-Pin-D	BUC	Laser (P35)	47	provided with laser
P20	Semi-rigid coax EZF-141-50,M17/130	BUC	P14,P35	47	EZ Form Cable Corp.
P21	Optical Cable 2-Single Mode 4-Multimode Ruggedized	BUC	BUC to Sphere	47	Siecor
P22	Optical Connectors Multimode line F710-019-000 for Gap Voltage Downlink		see P21,P31	47	Radiall
P23	see P22 for Temp Downlink, P21,P32				
P24	see P22 for Power Switch Uplink, P21,P33				
P25	Optical Connectors Single Mode line-F716-023-000 for rf-laser uplink		see P21,P34	47	Radiall

P26	Optical Connectors		on pigtail of laser		Radiall
	Single Mode line-F716-002-000				
P27	Optical Connectors in Junction box				Radiall
	F710-019-000 (8 ea.)				
P28	see P27, F716-023-000 (4 ea.)				Radiall
P29	F710-700-000 (4 ea.) Barrel Connector				Radiall
P30	F714-704-000 (2 ea.) Barrel Connector				Radiall
P31 (D1)	Optical receiver	BUC	IC13, pin 1	47	Radiall
	with PIN photodiode		(Gap Volts)		
	710-502-000				
P32 (D1)	see P31	BUC	see P31	47	Radiall
			(Temp Downlink)		
P33 (D53)	Optical Transmitter		Q50,R68	47	Radiall
	with LED, 710-456-000				
P34	Optical Variable Attenuator		P25,P26	47	Radiall
	F716-708-000				
P35	Fiber Optic Laser Transmitter			47	Ortel
	OC 3510A-M01				
P36	Audio Alarm	BUC	see Figures 50,38,47		Mallory
	Sonalert SC616WY				

DC Power Supplies:

P37	+/-15 VDC	BUC	Battery Charger	47	Sola Solids
	#84-15-2110				
P38	+24 VDC	BUC	Battery Charger	47	Sola Solids
	#84-24-050				
P39	+/-15 VDC	BUC		47	Acopian
	DB15-50				
P40	+/-5 VDC	BUC		47	Acopian
	5EB200				
P41	+/-5 VDC	BUC		47	Acopian
	5EB100				

3-1/2 Digit Front Panel LED Displays:

P42	DP-3522	BUC	Gap Voltage	47	Acculex
P43	see P42	BUC	Temperature	47	Acculex
P44	Battery Pack	SR	+12 V Supply	36	Shelley-Ragon, Inc.
	Custom made, 10x1.2V cells				
P45	7.2V Ni-Cad Pack	SR	+7.2V Supply	36	generic
	(2) sets		-7.2V Supply		
P46	BUC Enclosure	BUC		47	Tracewell Enclosures
	630-001/R317-12				
P50	Optical Connector	SR	D107,D108,Q103	51	Optical Fiber
	OFTI-STC				Technologies, Inc.
	300-4STC-0001				
P51	Connector SMA	SR	IC10	51	Omni-Spectra
	right angle plug				
	2007-7985-02, 0.085" coax				
P52	Pin Connectors	Not shown, used to connect			ACE R/C, Inc.
	ACE/DEANS 2 PIN	12V battery to circuit board			

	#19K53	in sphere	
P53	Pin Connectors ACE/DEANS 4 PIN #19K50	Not shown, used to connect 7.2V batteries and charger to sphere circuit board	ACE R/C, Inc. Higgensville, MO.
	Spring loaded contact pins connecting the hemispheres to the balun circuit in the sphere Part # S-4-A-7-G		Interconnect Devices,In Kansas City, Kansas

Plus miscellaneous bits and pieces of hardware, some purchased (e.g. nuts and bolts) and some fabricated as needed (e.g. brass sphere parts, power supply and circuit board mounts, etc.).

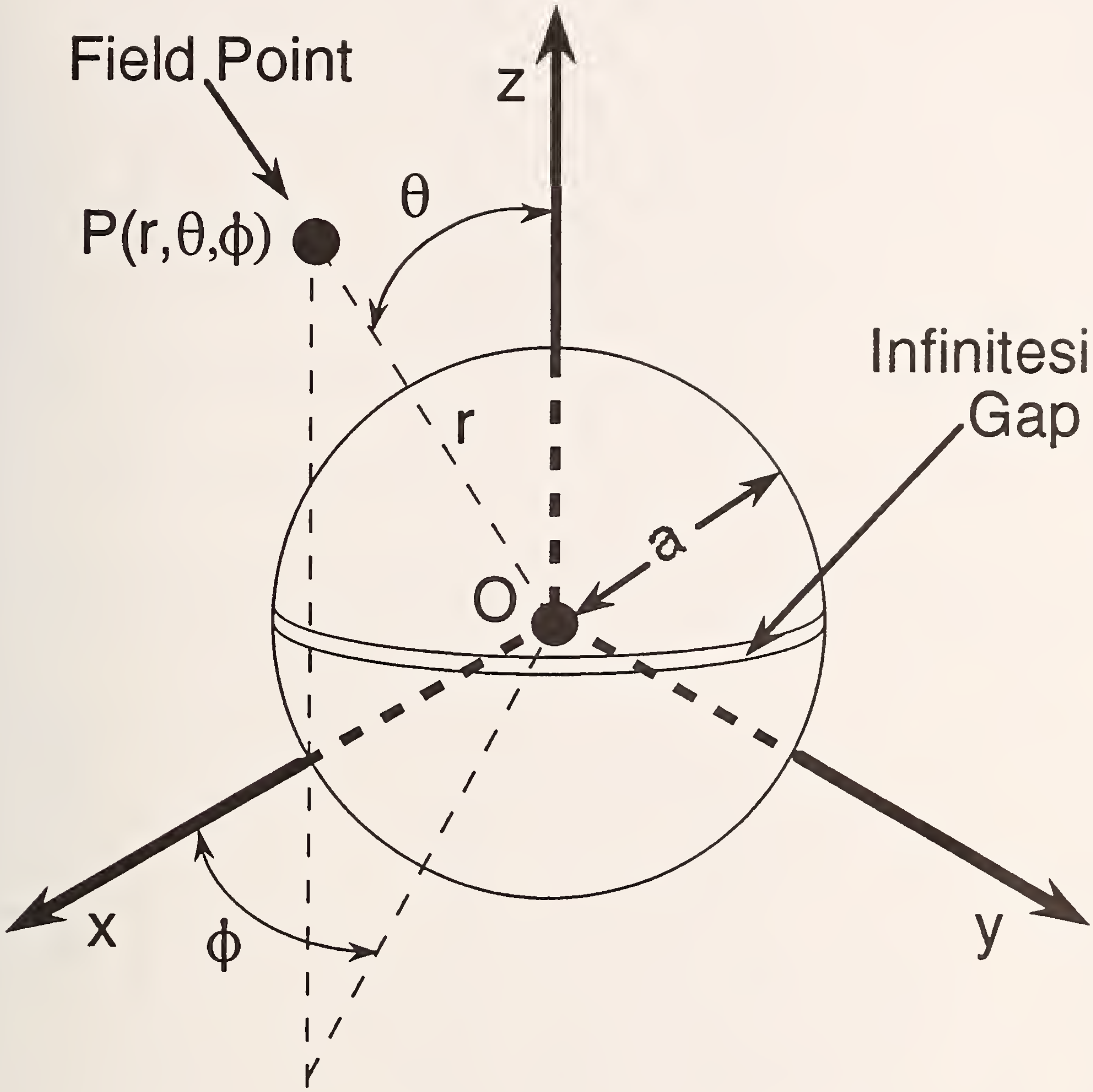

Figure 1. Coordinate system for the spherical dipole. The infinitesimal gap lies in the $\theta=90°$ plane.

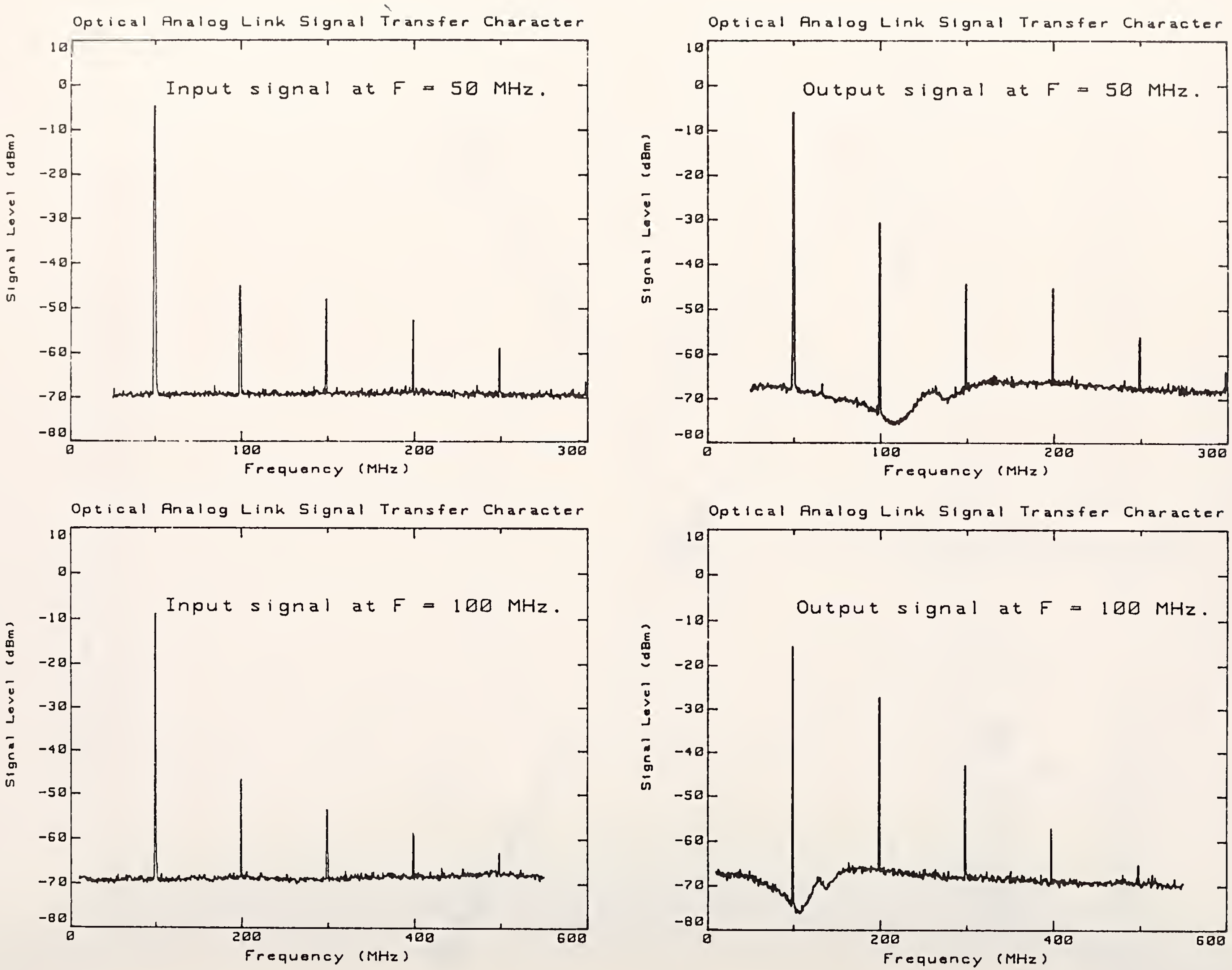

Figure 2. Spectrum plot of the analog rf link for generator frequencies of 50 and 100 MHz. The input is shown on the left and the corresponding output is on the right.

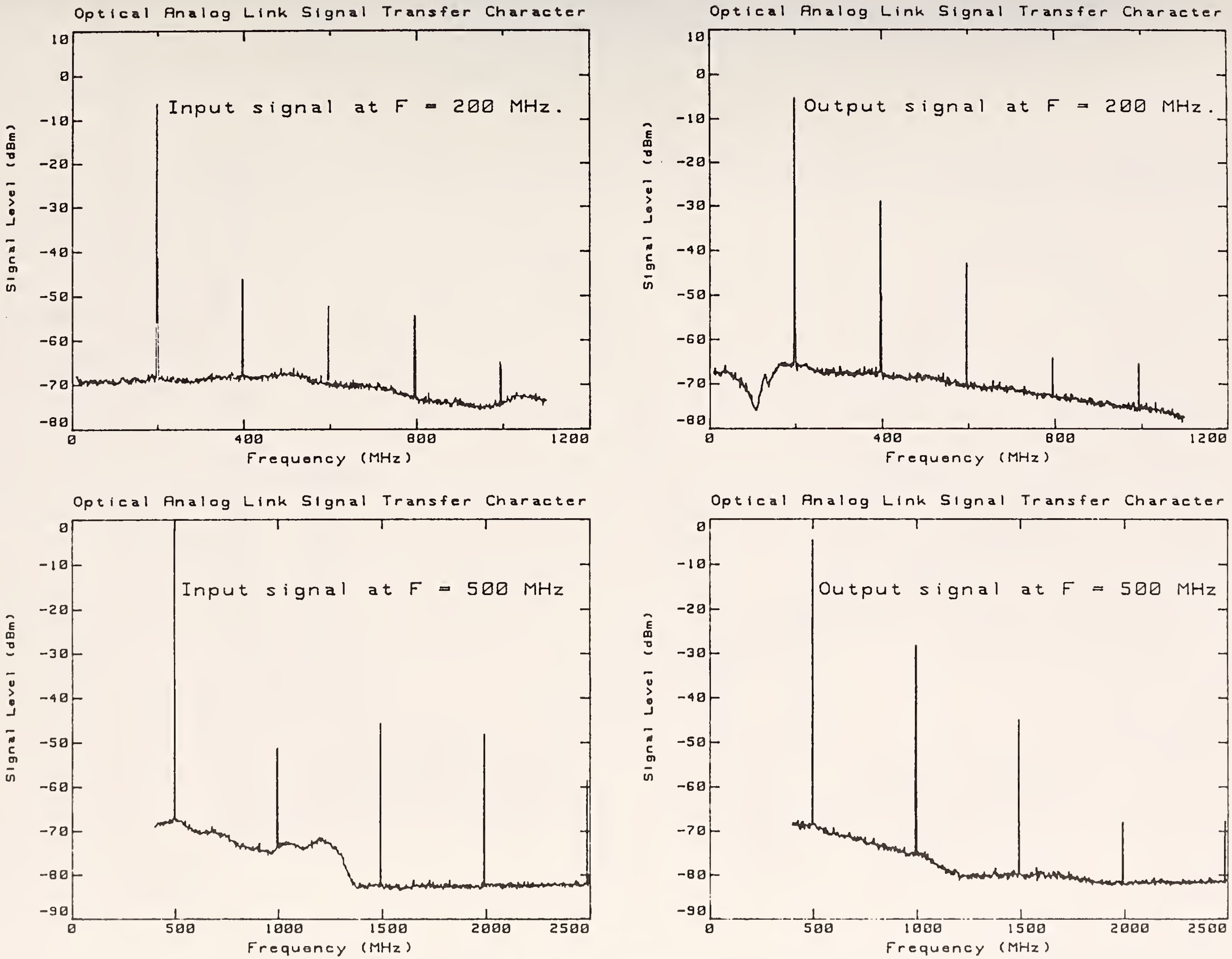

Figure 3. Spectrum plot of the analog rf link for generator frequencies of 200 and 500 MHz. The input is shown on the left and the corresponding output is on the right.

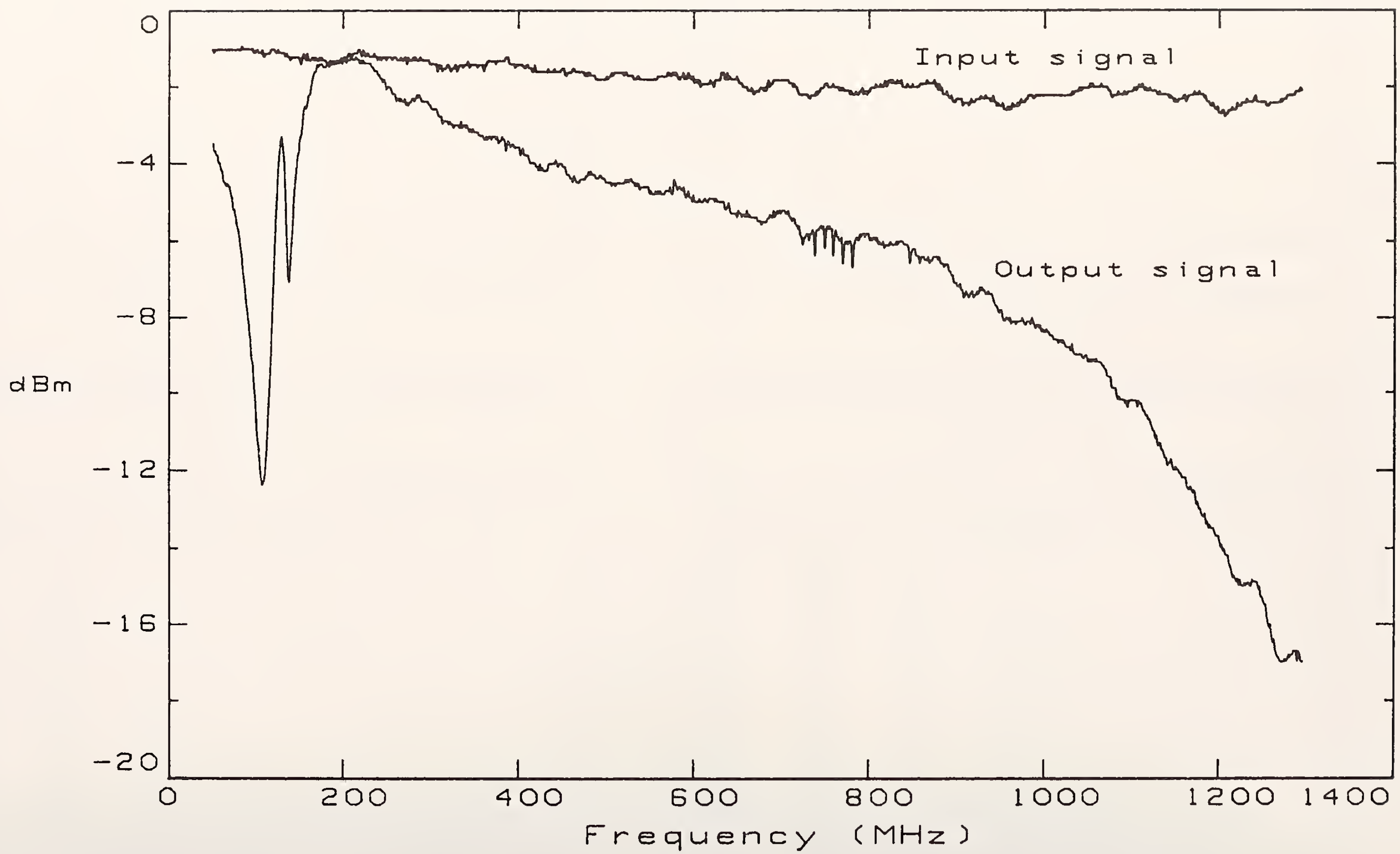

Figure 4. Transfer characteristics of the analog optical link from 50 to 1300 MHz.

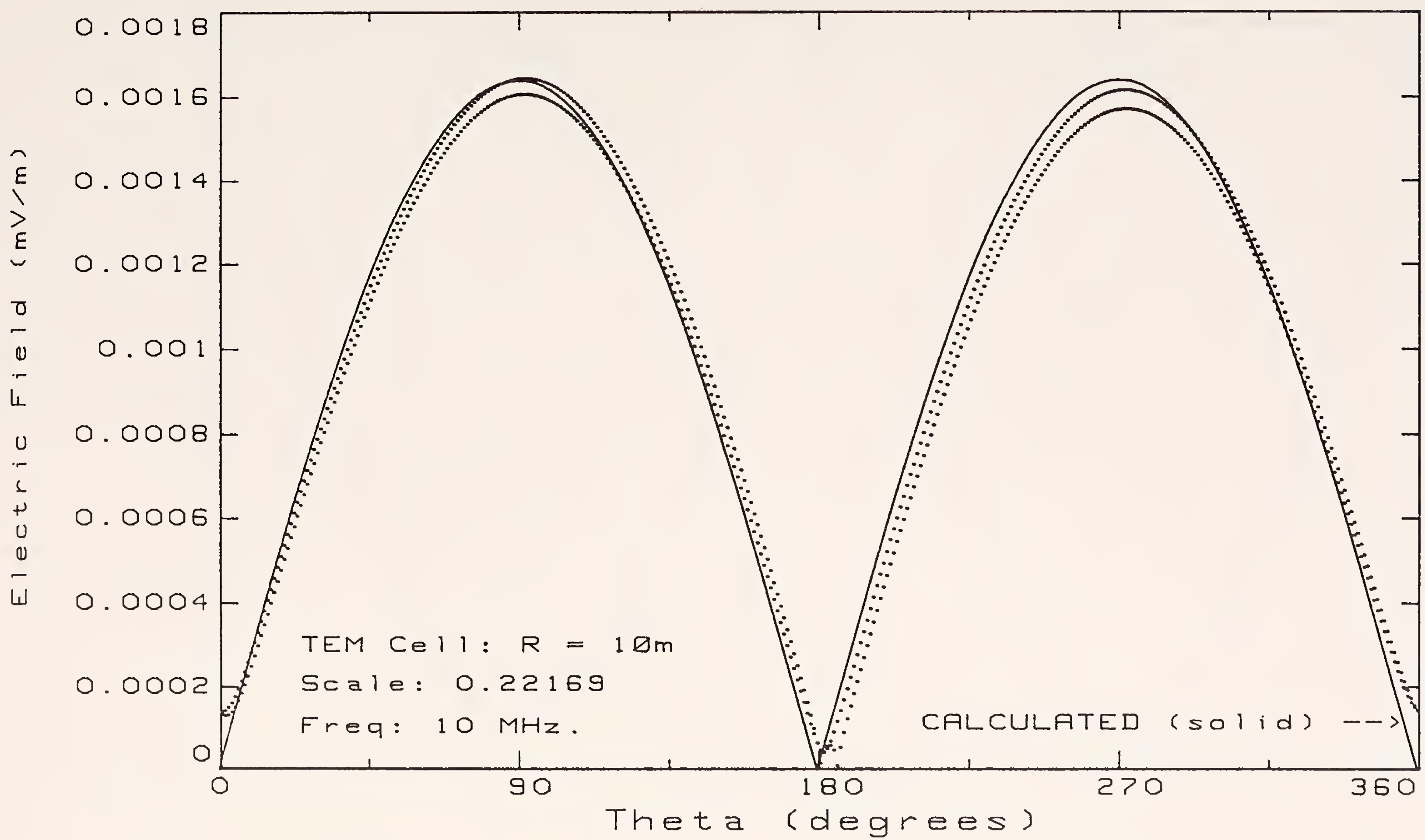

Figure 5. Sphere electric field radiation pattern determined using TEM cell measurements at 10 MHz.

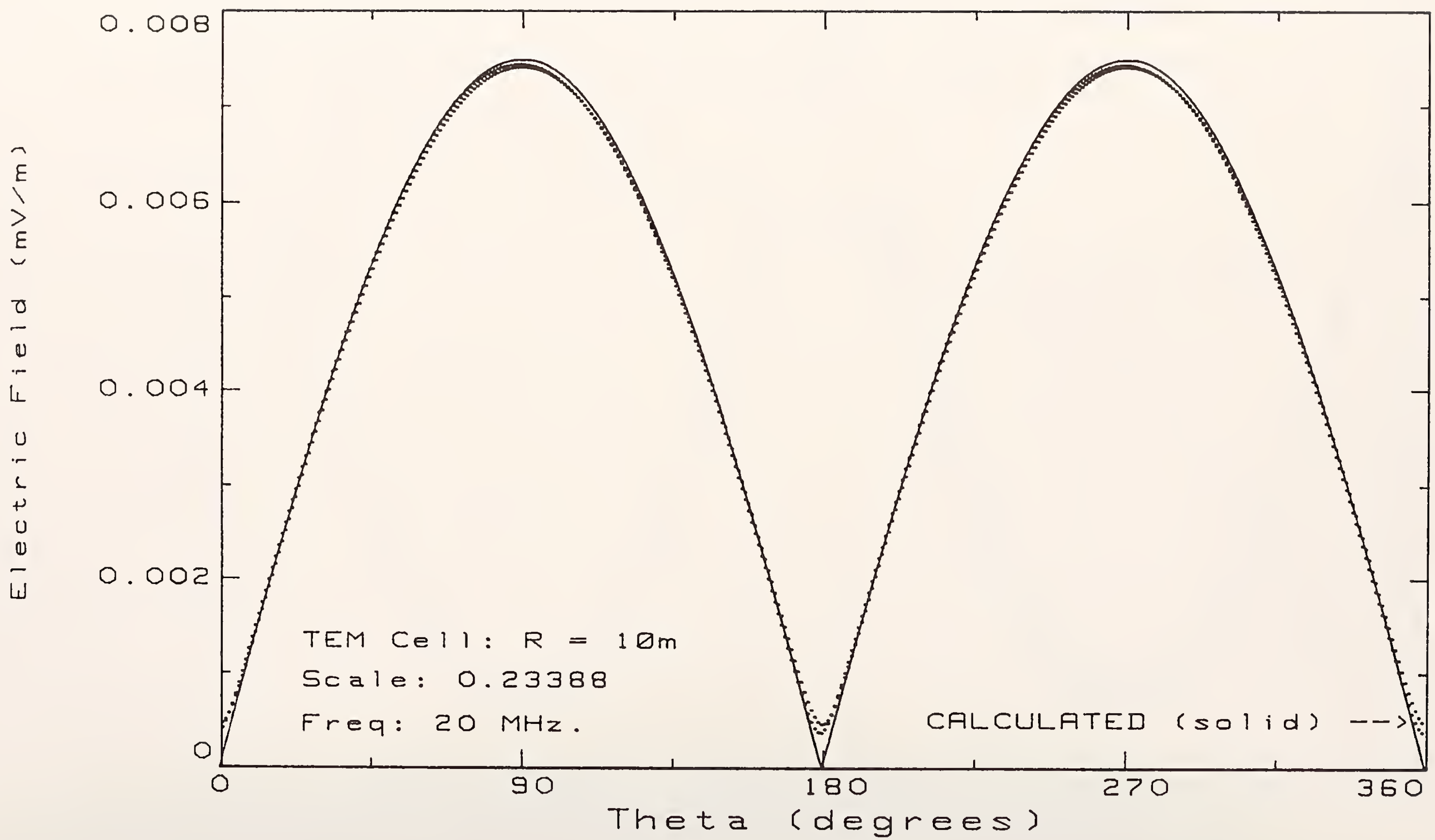

Figure 6. Sphere electric field radiation pattern determined using TEM cell measurements at 20 MHz.

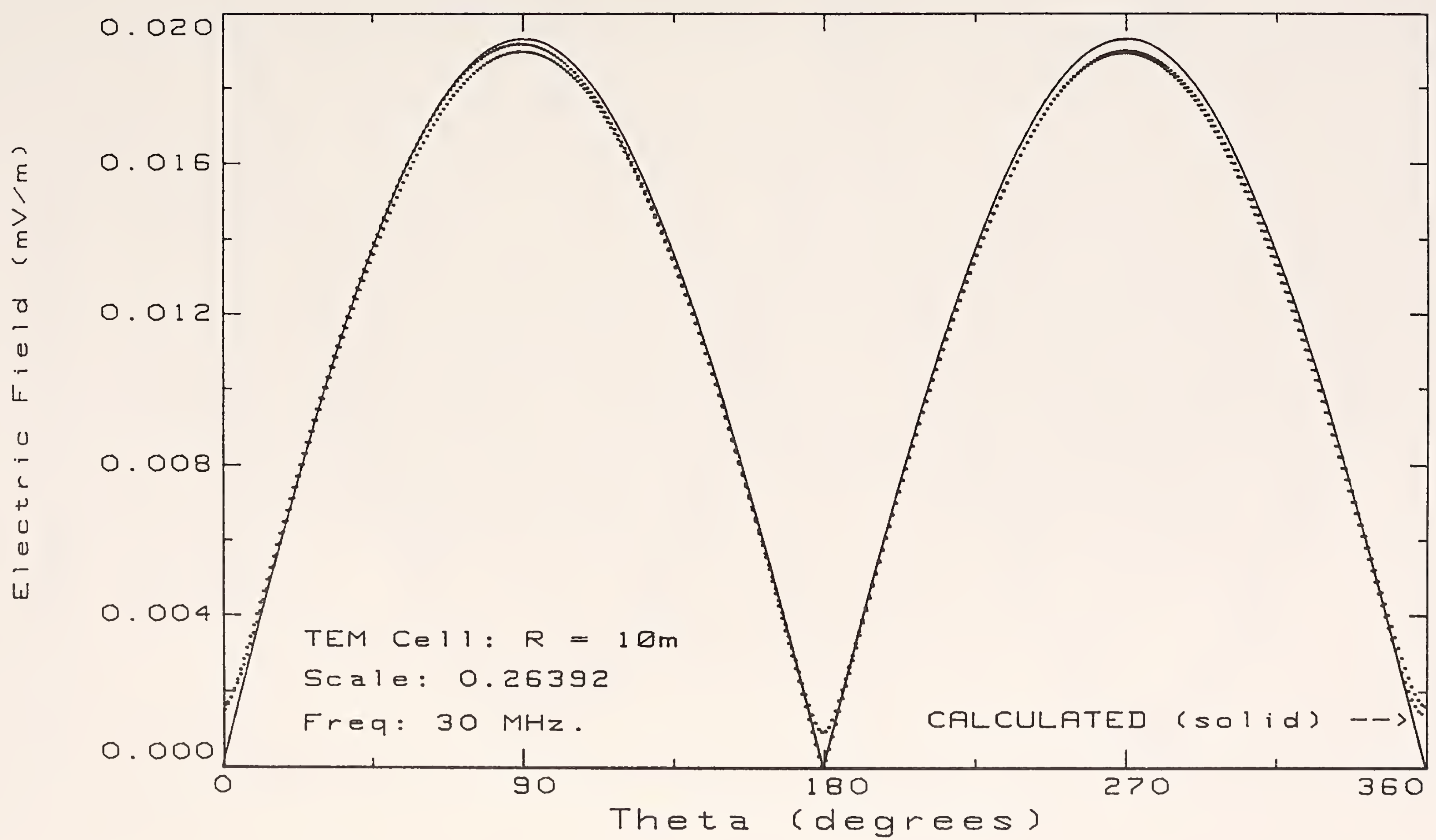

Figure 7. Sphere electric field radiation pattern determined using TEM cell measurements at 30 MHz.

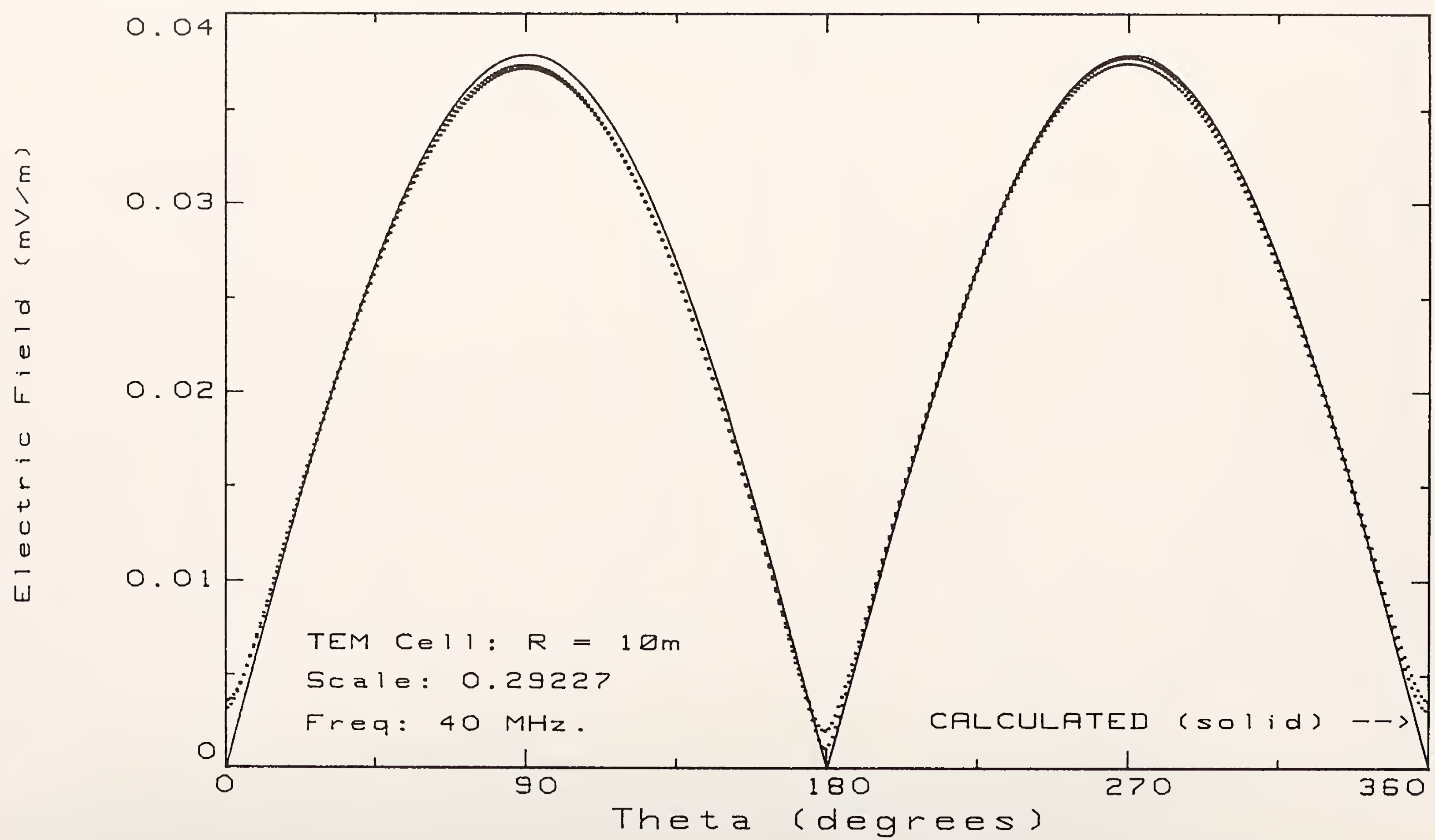

Figure 8. Sphere electric field radiation pattern determined using TEM cell measurements at 40 MHz.

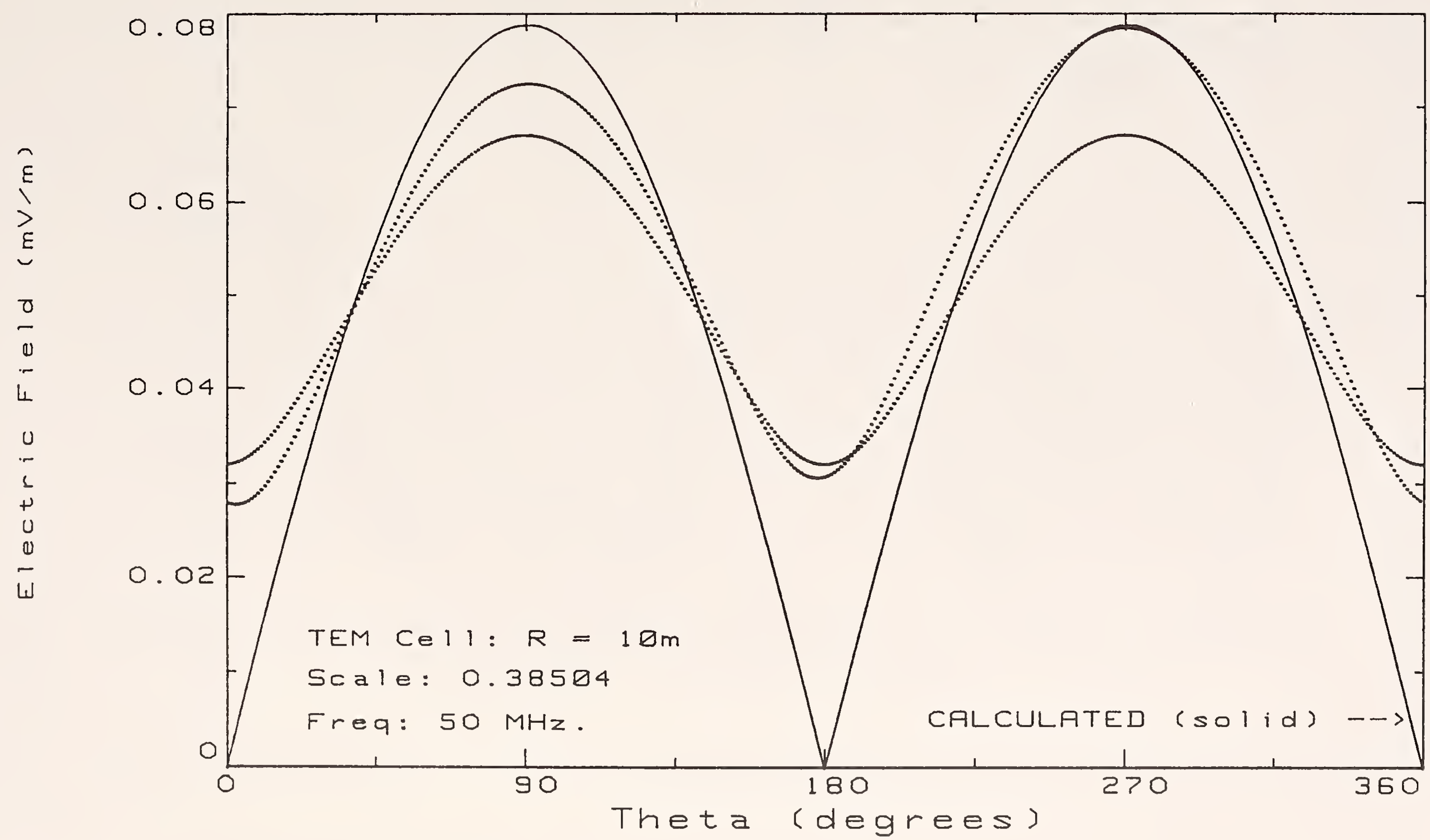

Figure 9. Sphere electric field radiation pattern determined using TEM cell measurements at 50 MHz.

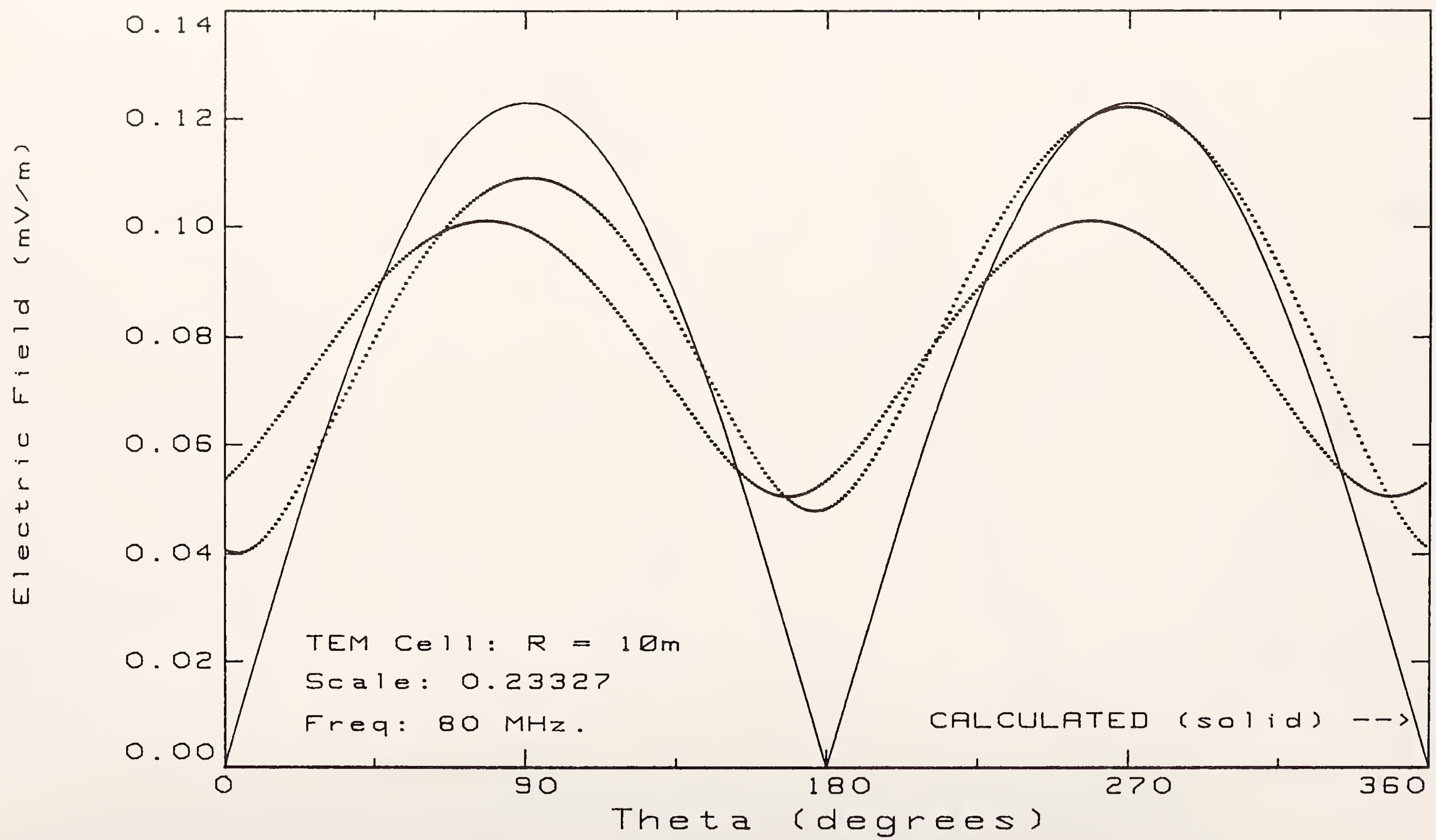

Figure 10. Sphere electric field radiation pattern determined using TEM cell measurements at 80 MHz.

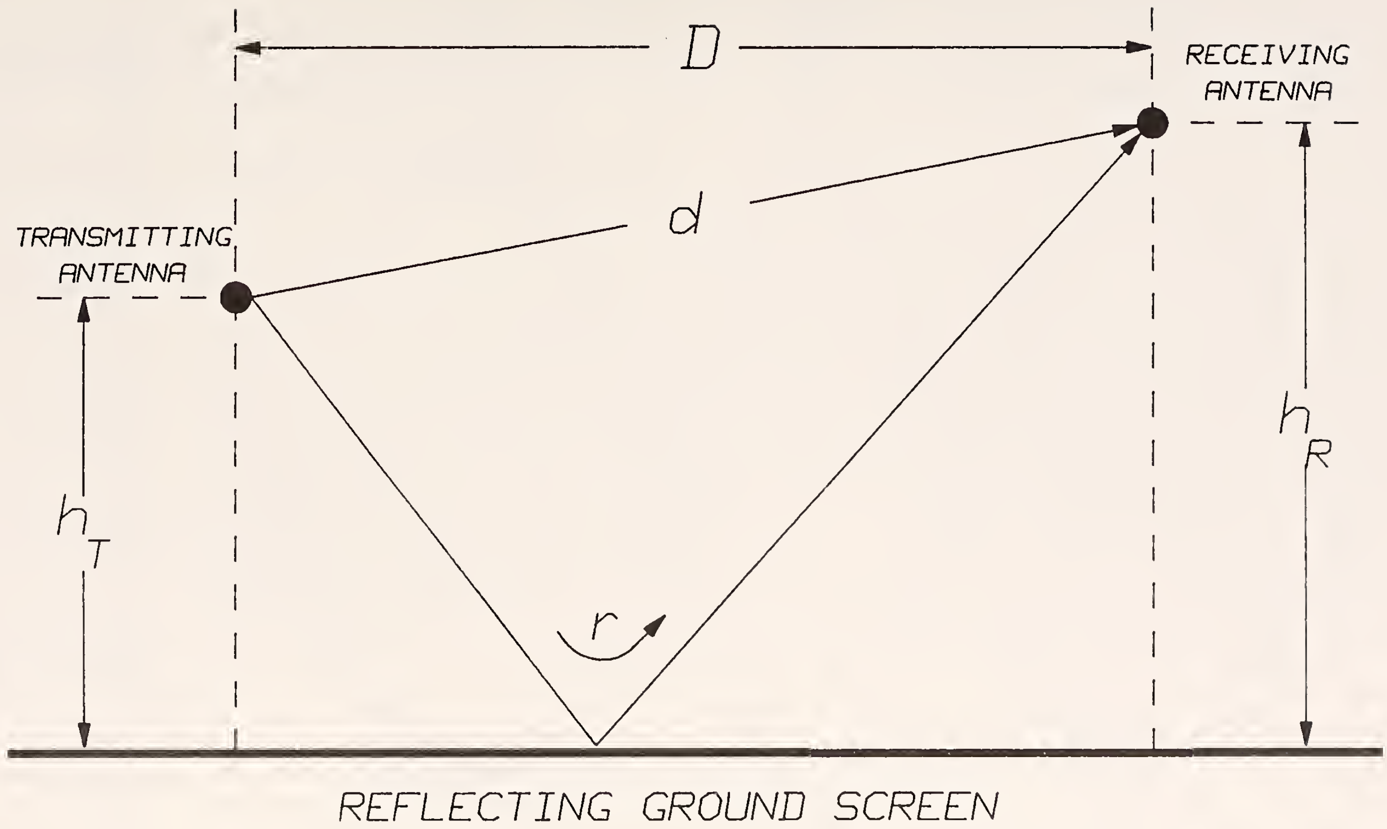

Figure 11. Configuration of open area test site (OATS).

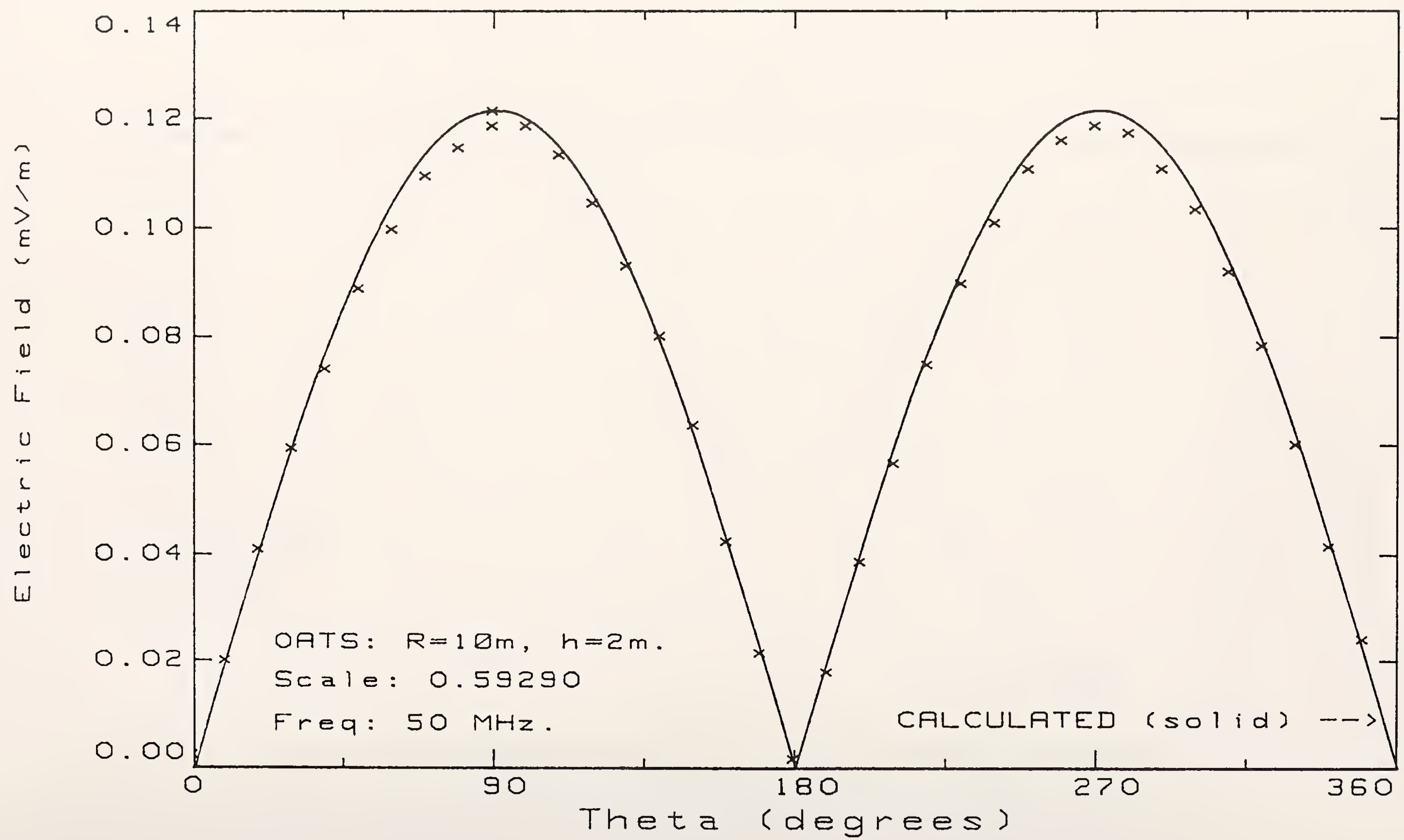

Figure 12. Sphere electric field radiation pattern determined using open area test site (OATS) measurements at 50 MHz.

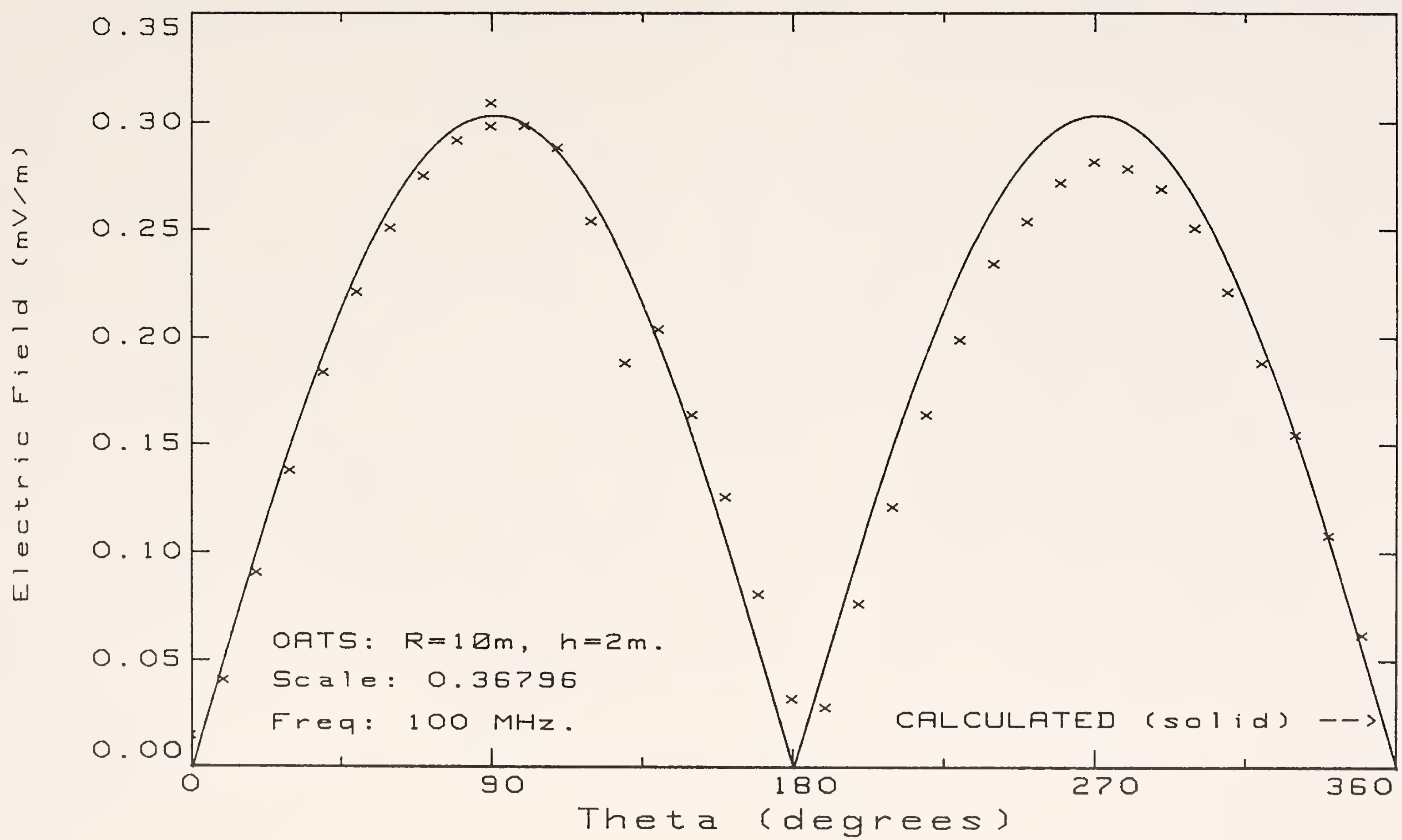

Figure 13. Sphere electric field radiation pattern determined using OATS measurements at 100 MHz.

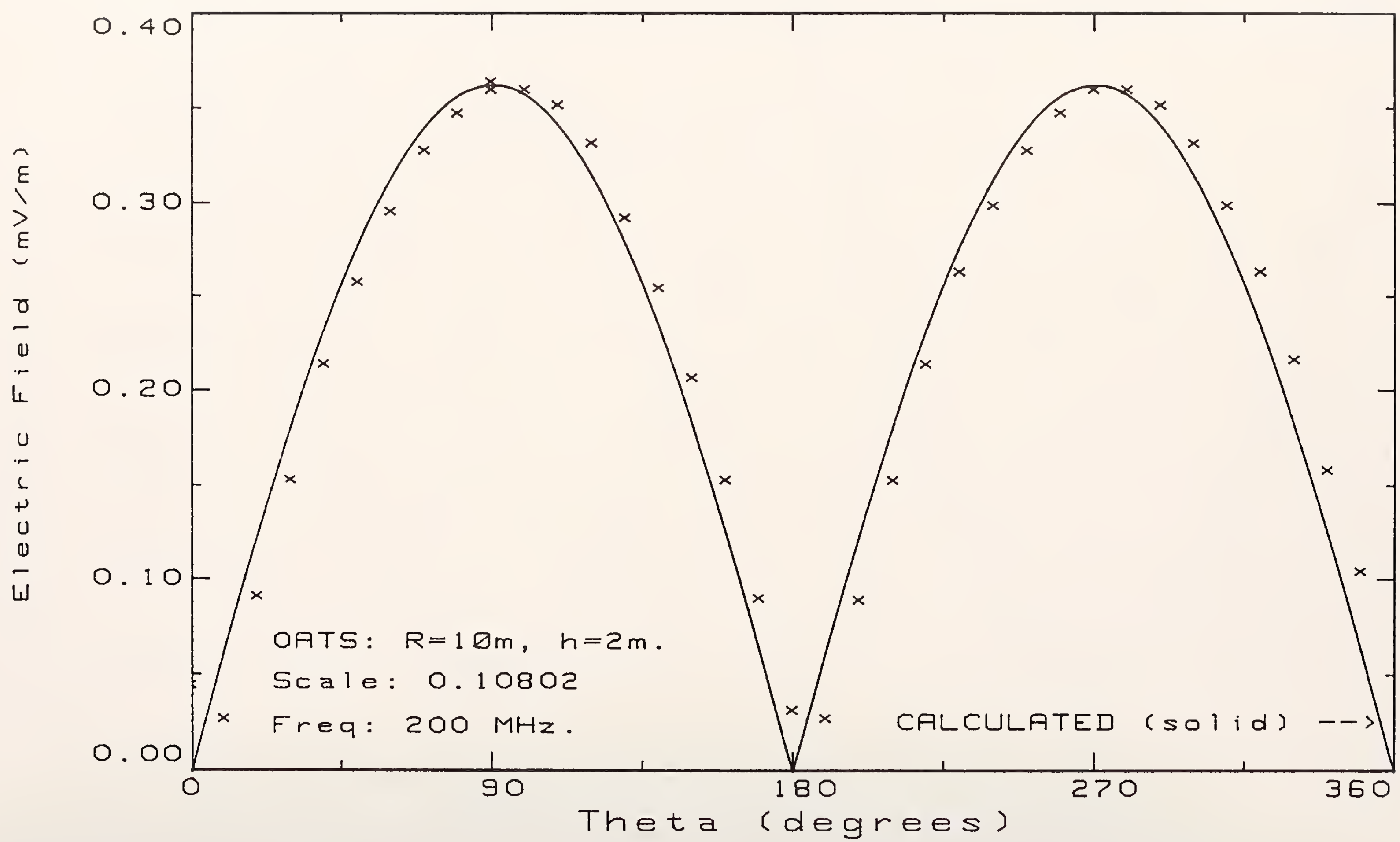

Figure 14. Sphere electric field radiation pattern determined using OATS measurements at 200 MHz.

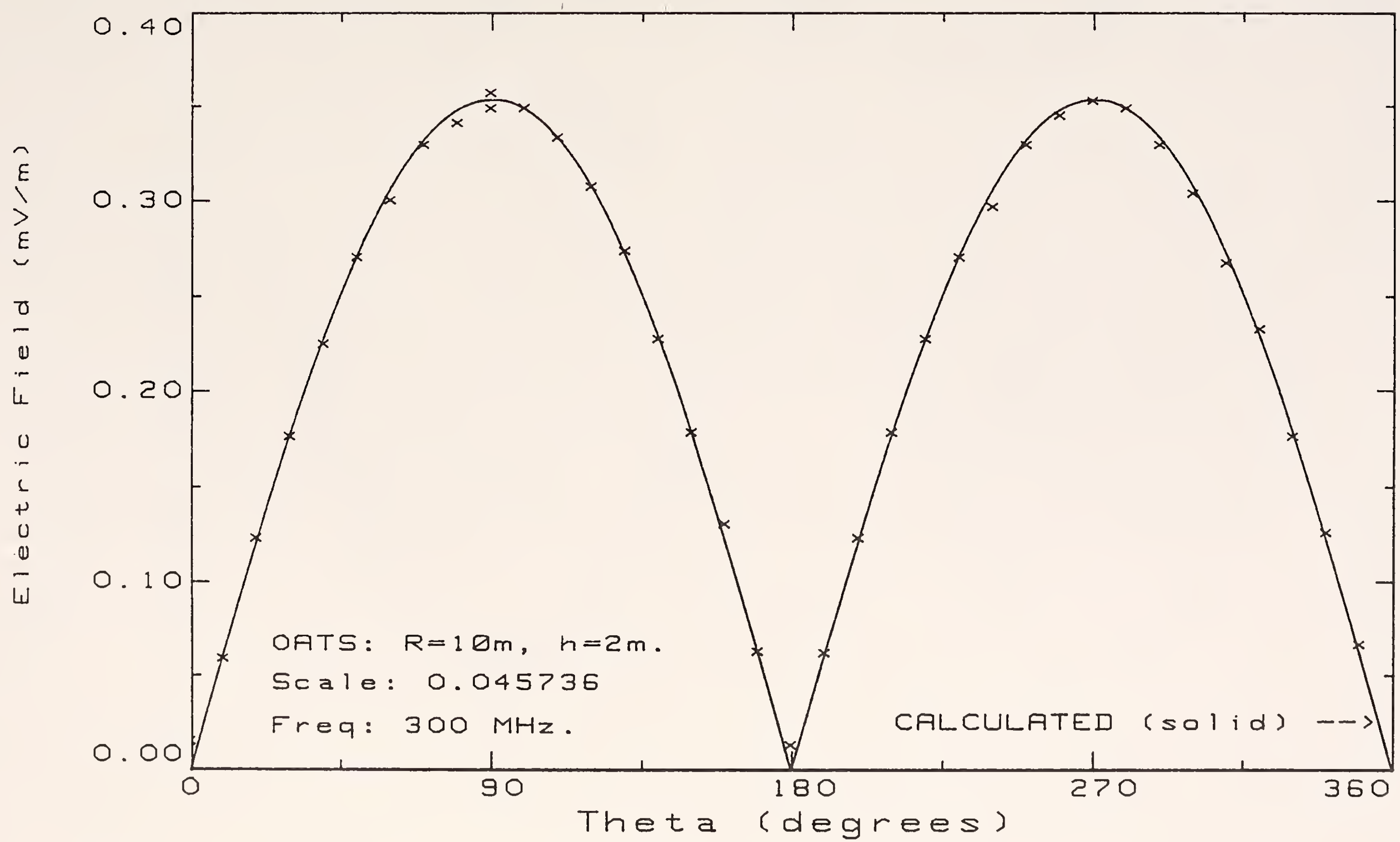

Figure 15. Sphere electric field radiation pattern determined using OATS measurements at 300 MHz.

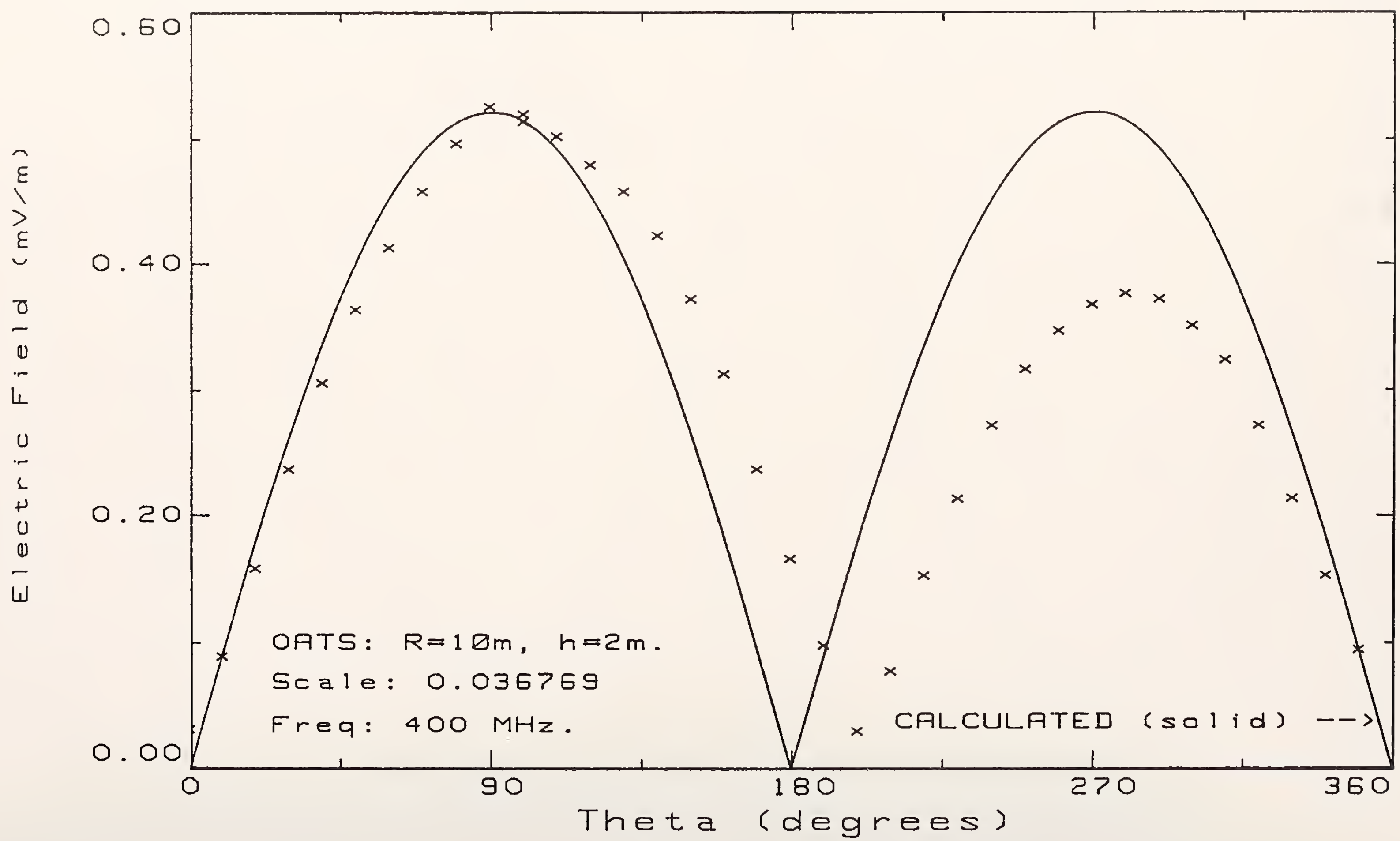

Figure 16. Sphere electric field radiation pattern determined using OATS measurements at 400 MHz.

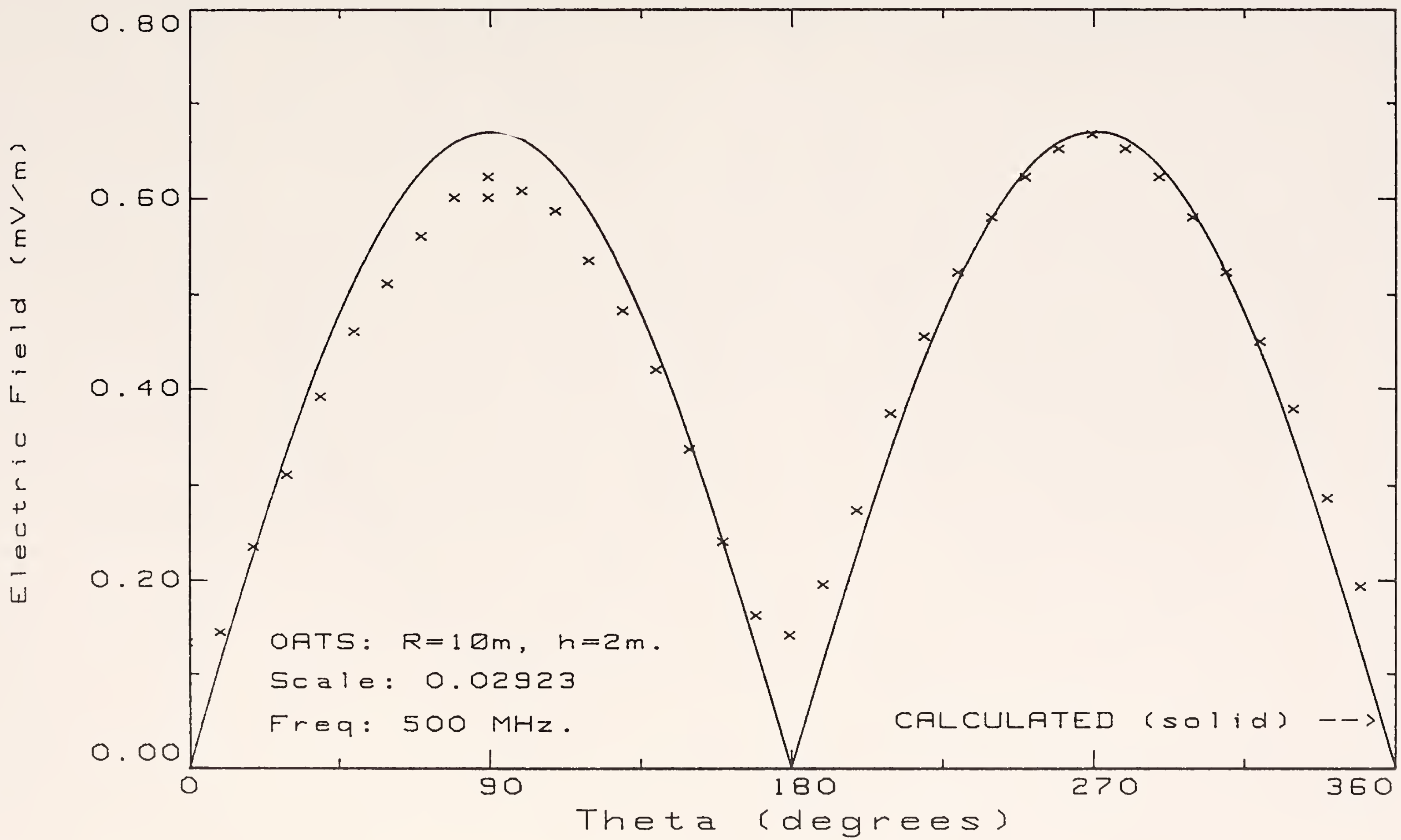

Figure 17. Sphere electric field radiation pattern determined using OATS measurements at 500 MHz.

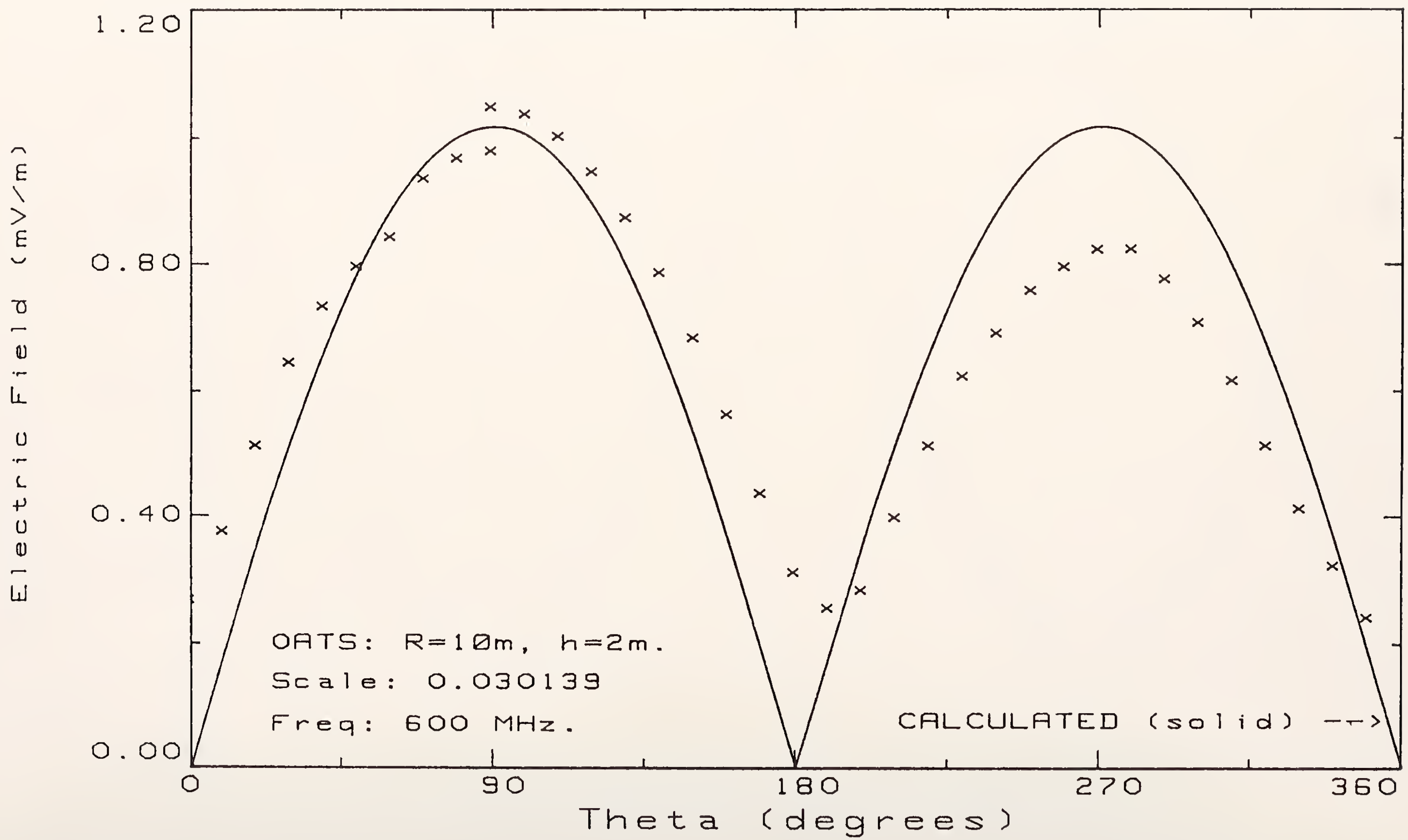

Figure 18. Sphere electric field radiation pattern determined using OATS measurements at 600 MHz.

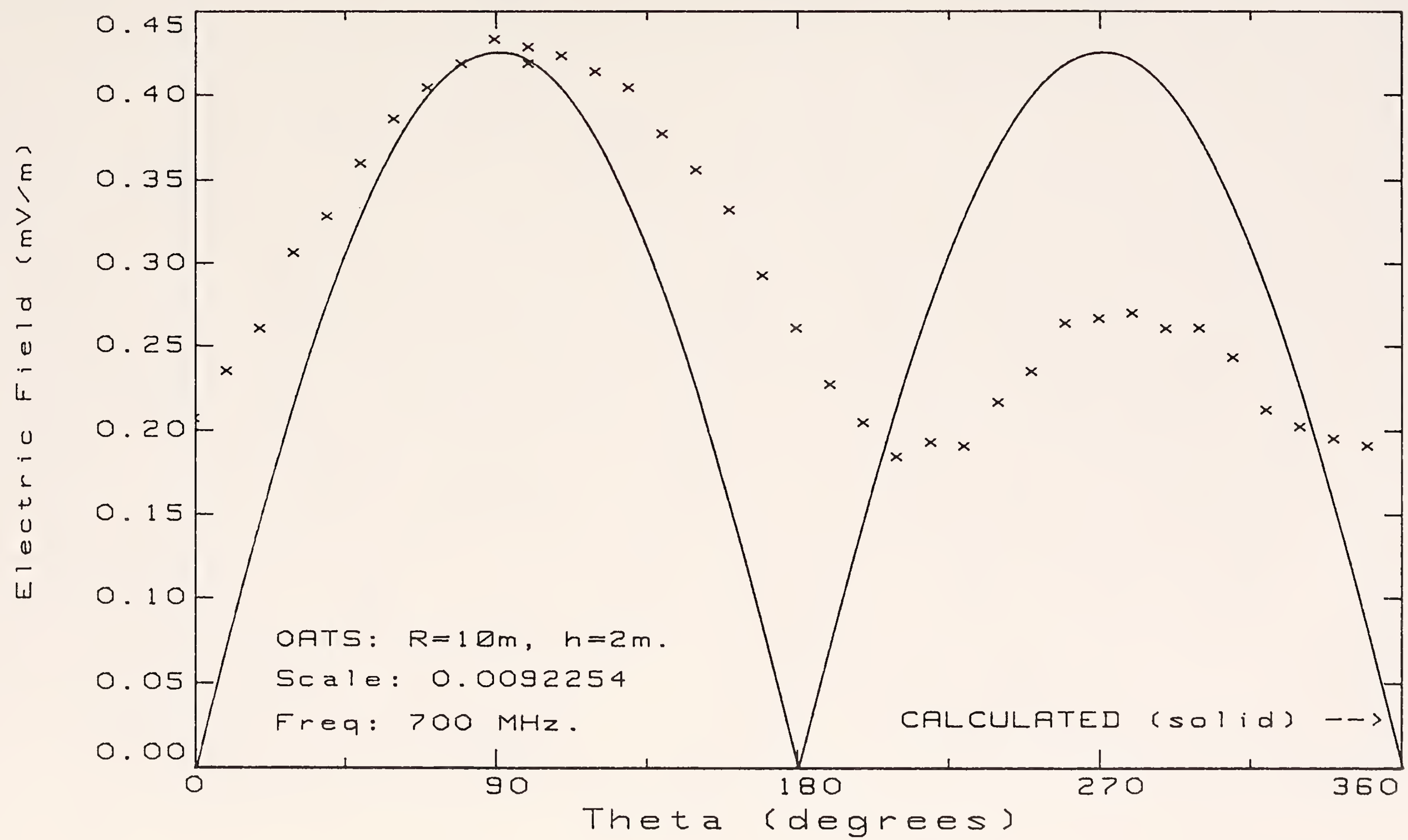

Figure 19. Sphere electric field radiation pattern determined using OATS measurements at 700 MHz.

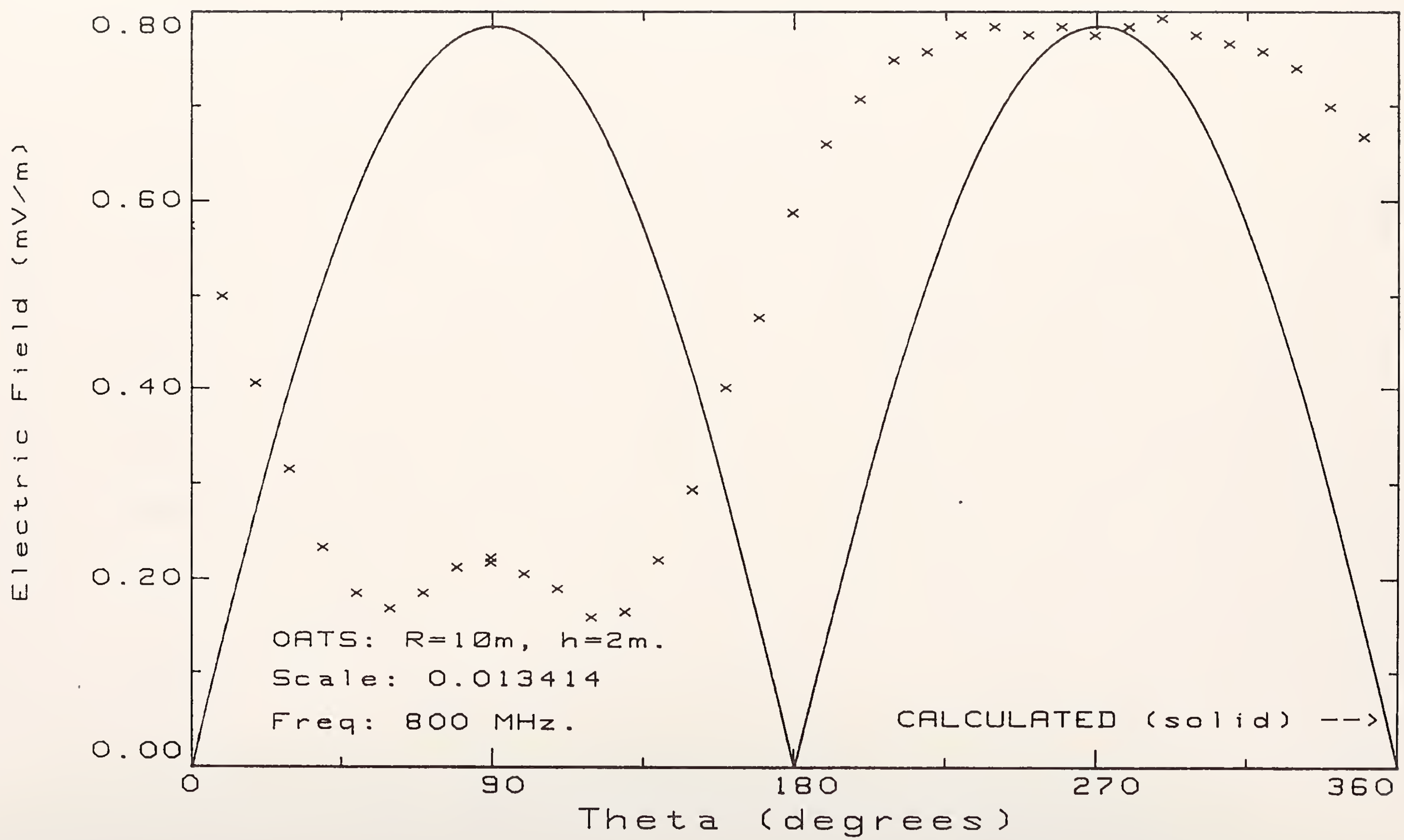

Figure 20. Sphere electric field radiation pattern determined using OATS measurements at 800 MHz.

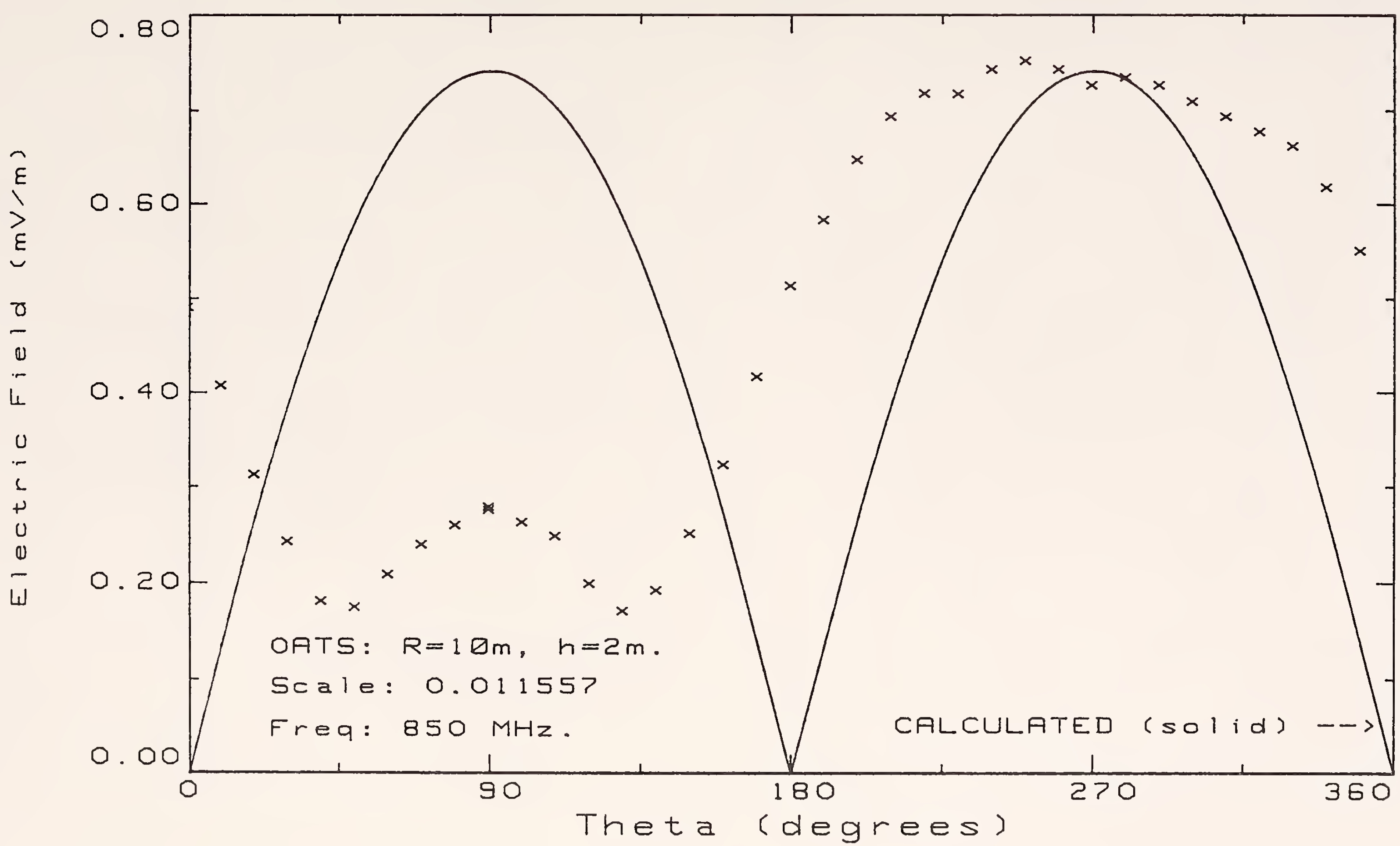

Figure 21. Sphere electric field radiation pattern determined using OATS measurements at 850 MHz.

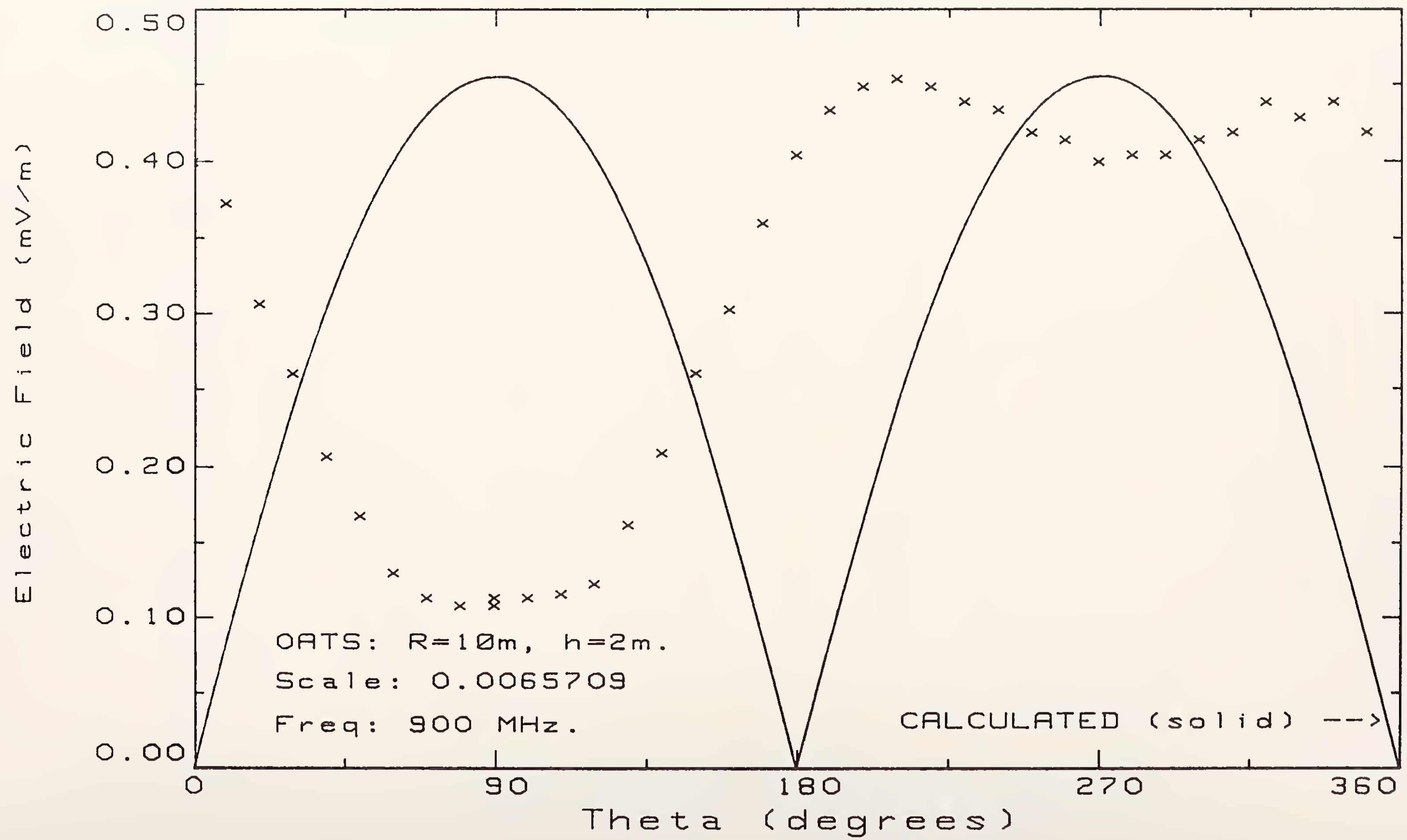

Figure 22. Sphere electric field radiation pattern determined using OATS measurements at 900 MHz.

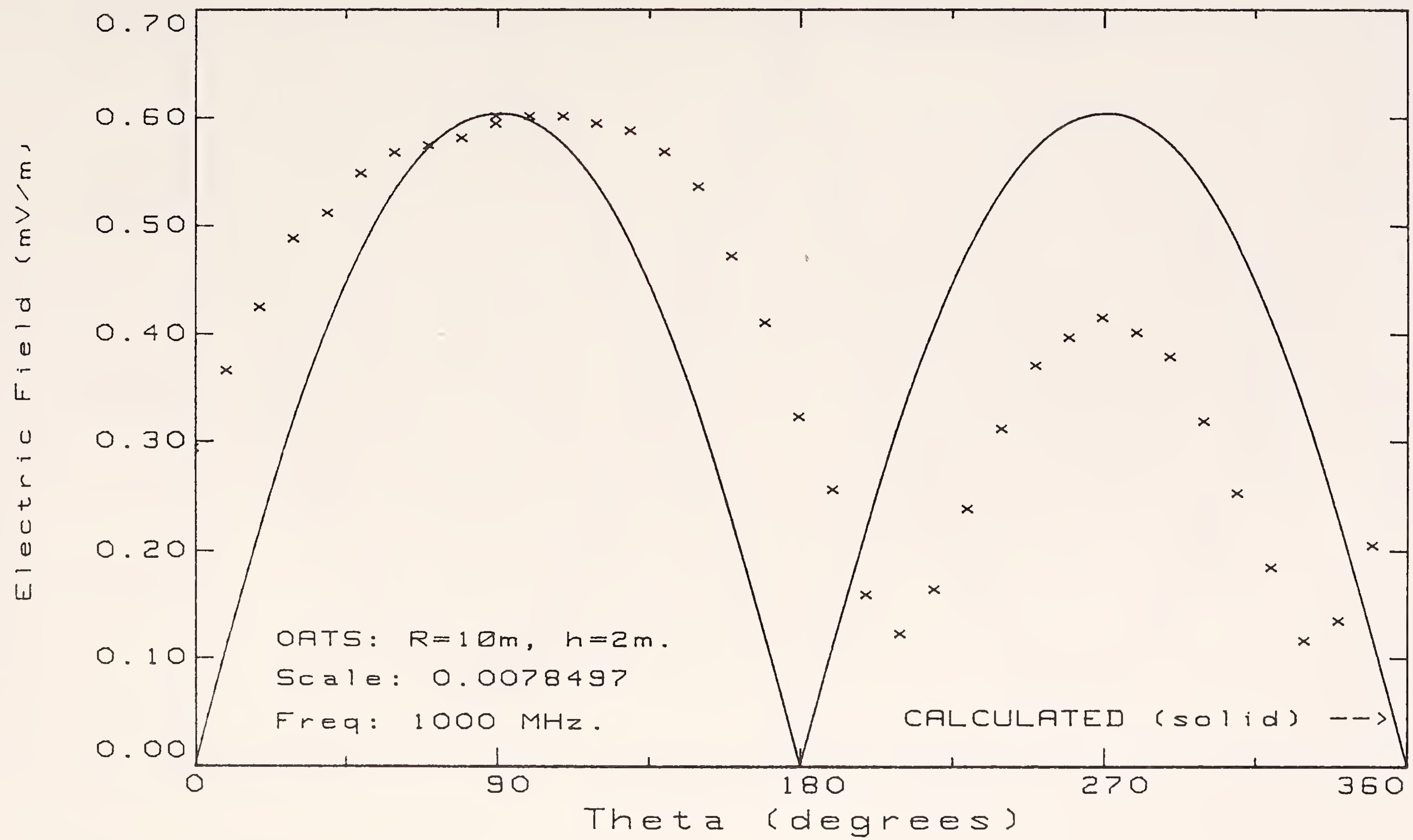

Figure 23. Sphere electric field radiation pattern determined using OATS measurements at 1000 MHz.

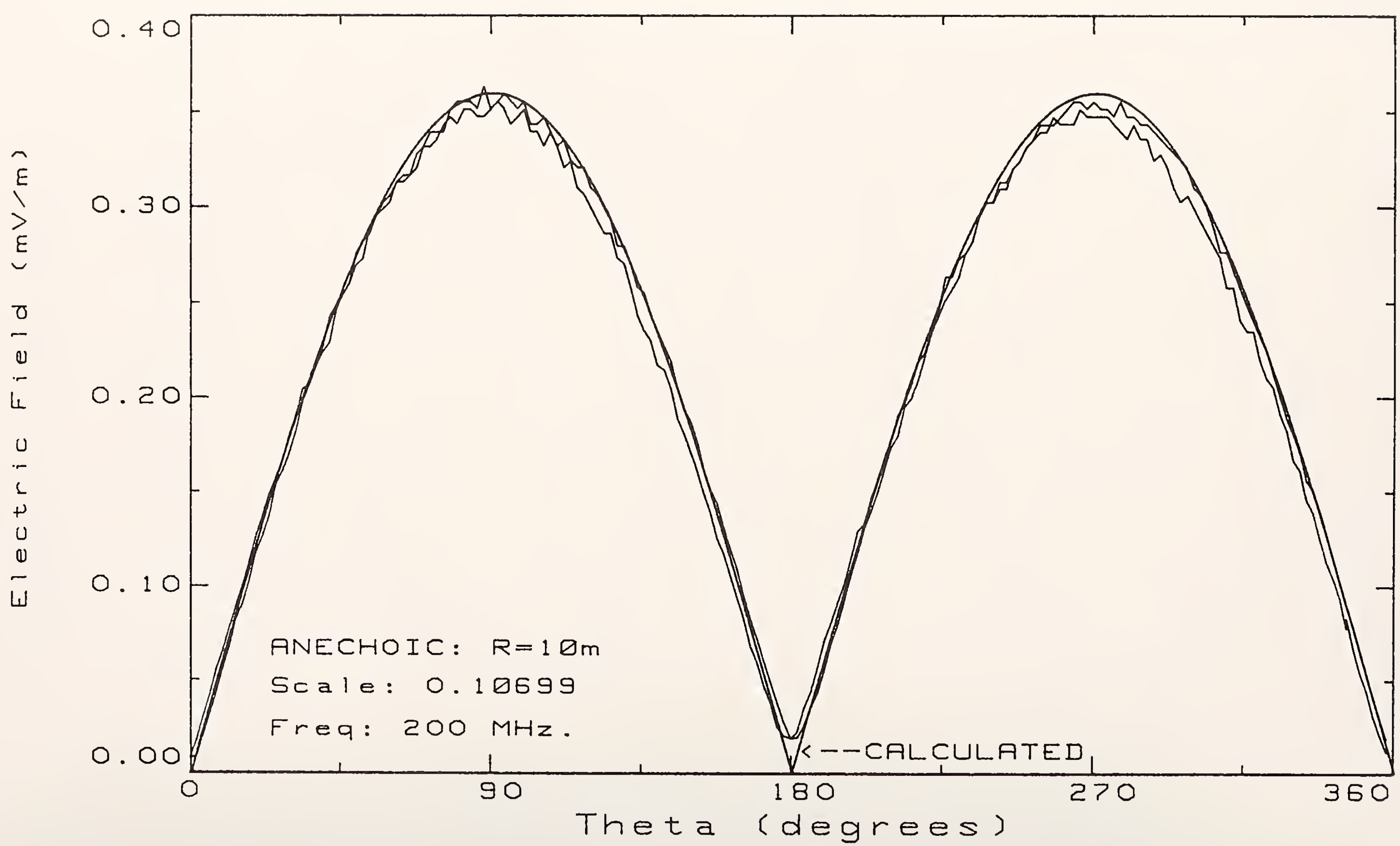

Figure 24. Sphere electric field radiation pattern determined using Anechoic Chamber measurements at 200 MHz.

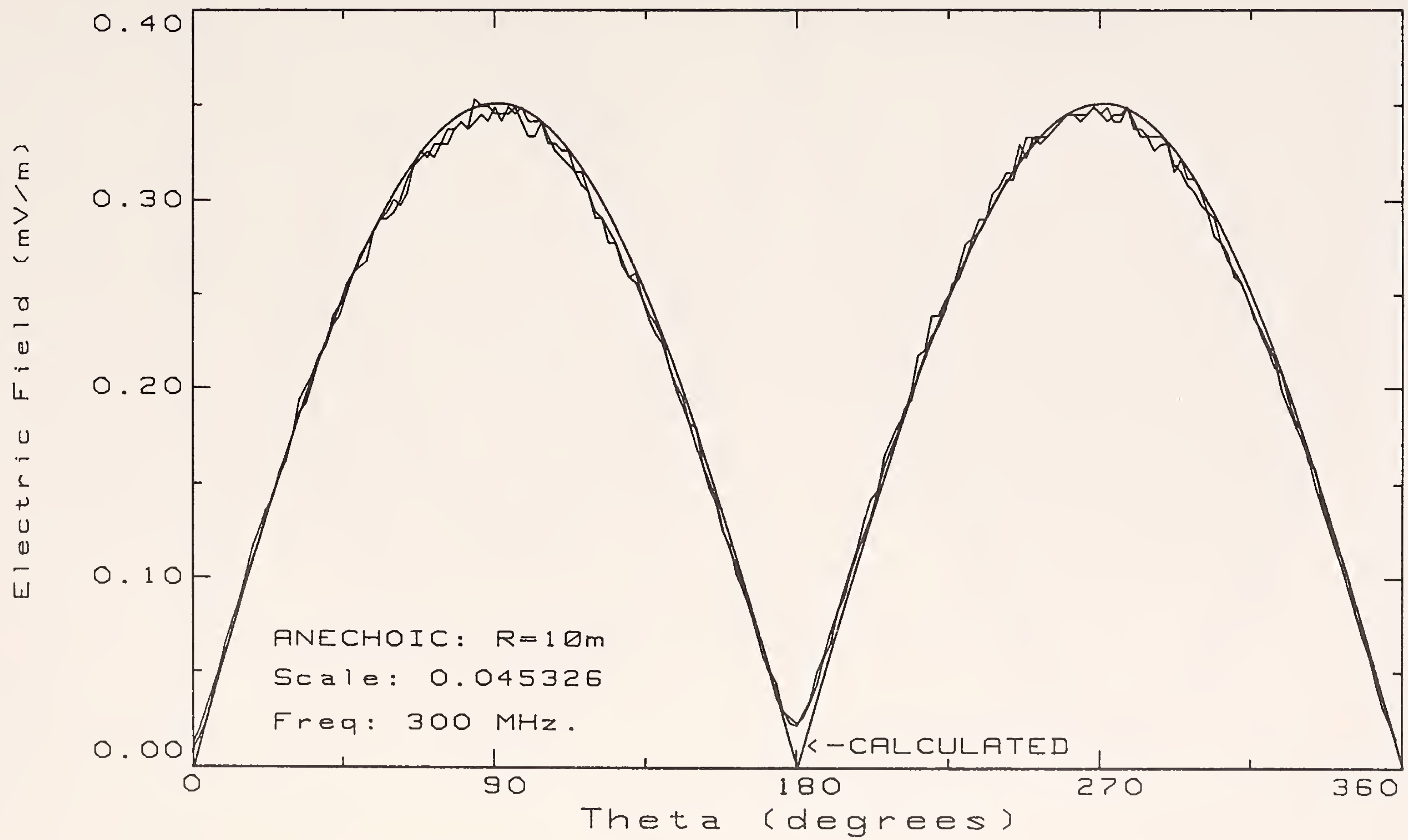

Figure 25. Sphere electric field radiation pattern determined using Anechoic Chamber measurements at 300 MHz.

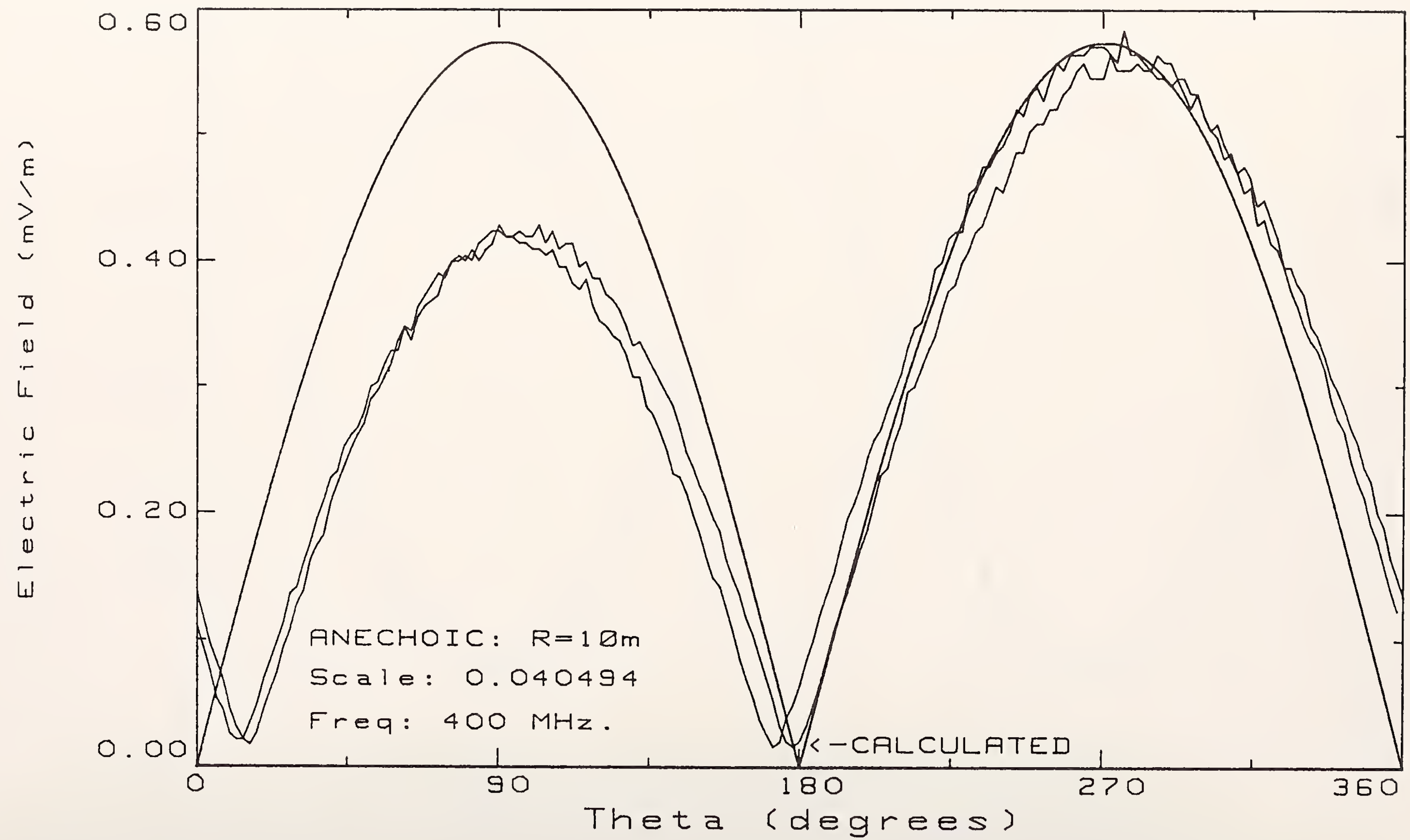

Figure 26. Sphere electric field radiation pattern determined using Anechoic Chamber measurements at 400 MHz.

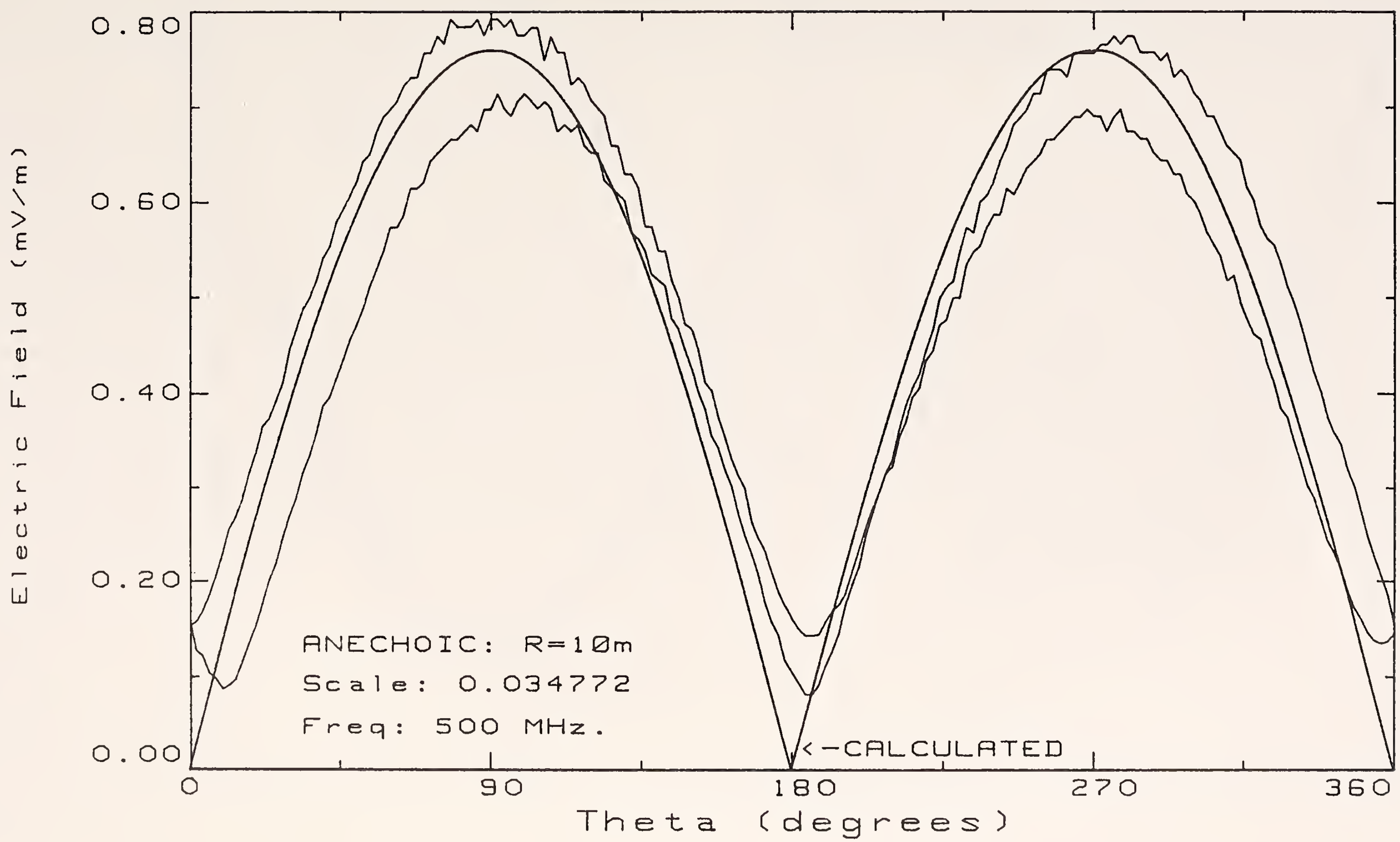

Figure 27. Sphere electric field radiation pattern determined using Anechoic Chamber measurements at 500 MHz.

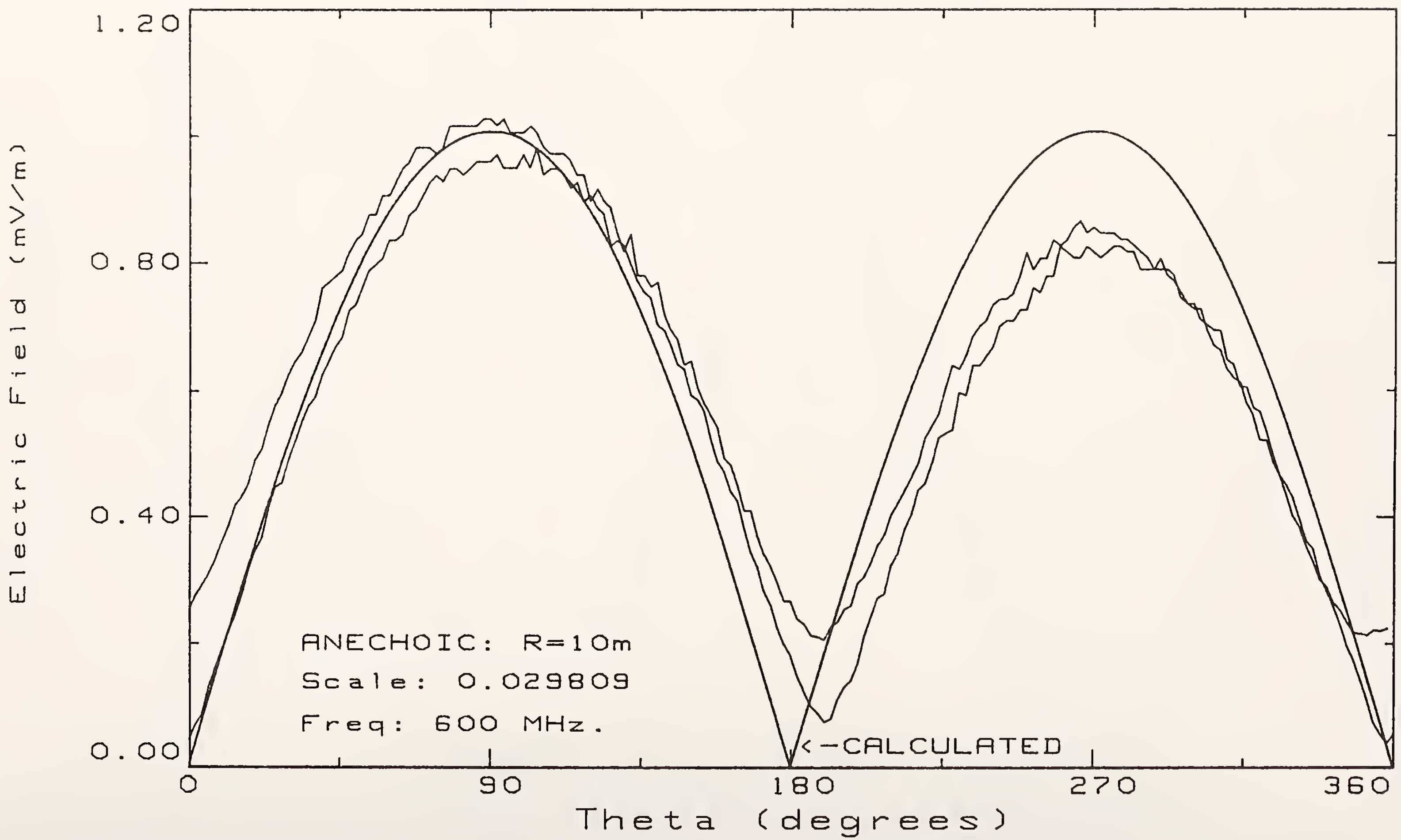

Figure 28. Sphere electric field radiation pattern determined using Anechoic Chamber measurements at 600 MHz.

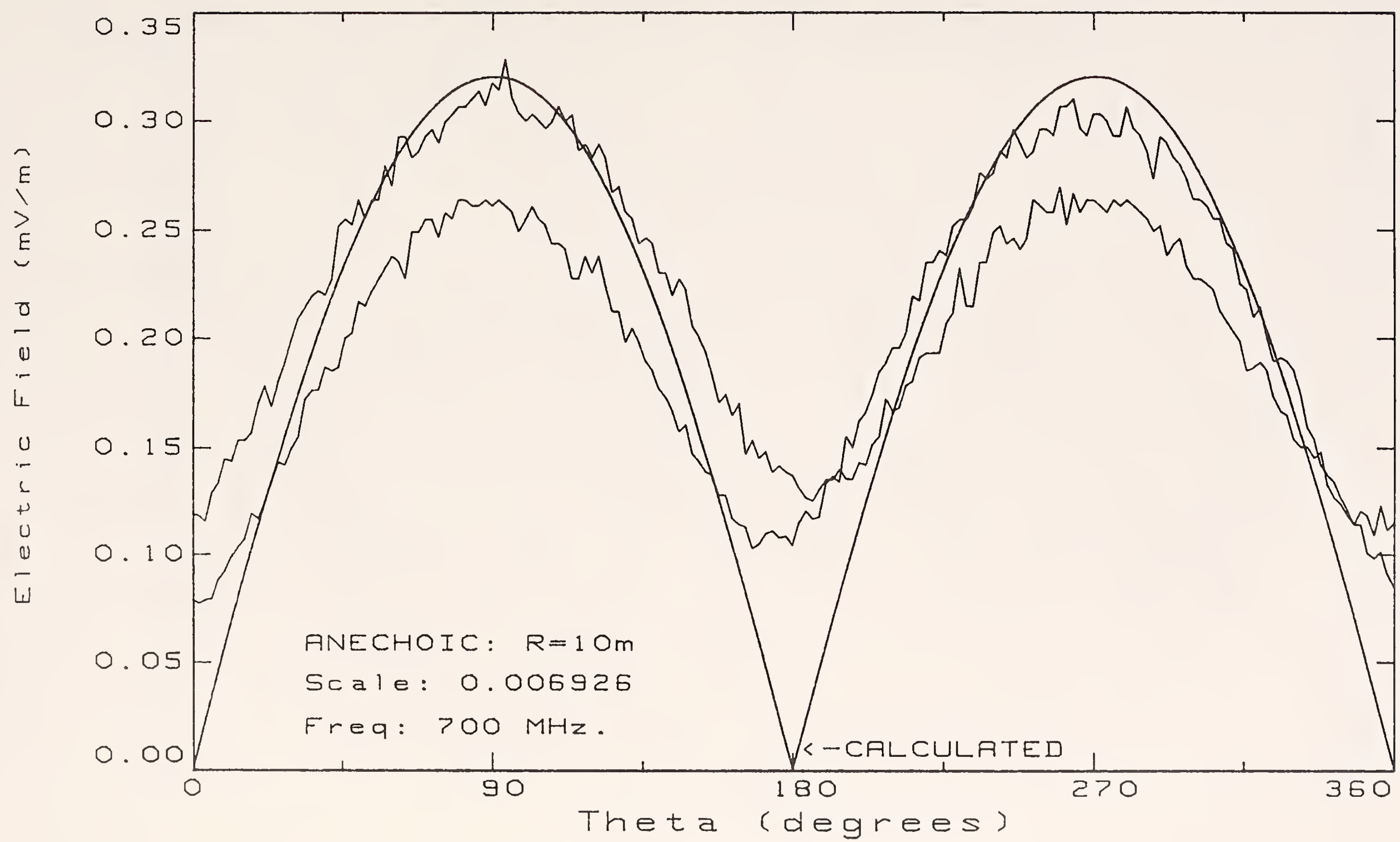

Figure 29. Sphere electric field radiation pattern determined using Anechoic Chamber measurements at 700 MHz.

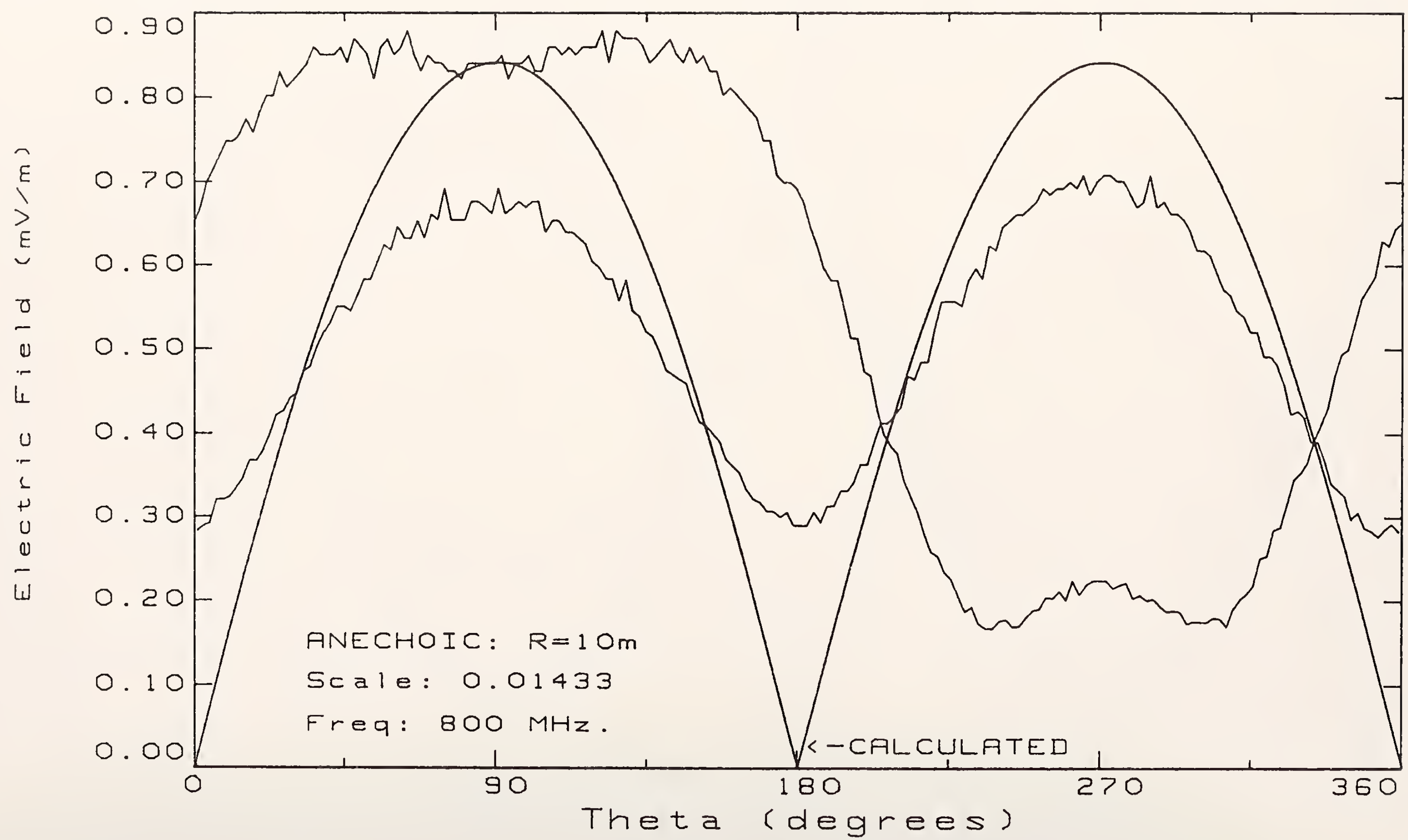

Figure 30. Sphere electric field radiation pattern determined using Anechoic Chamber measurements at 800 MHz.

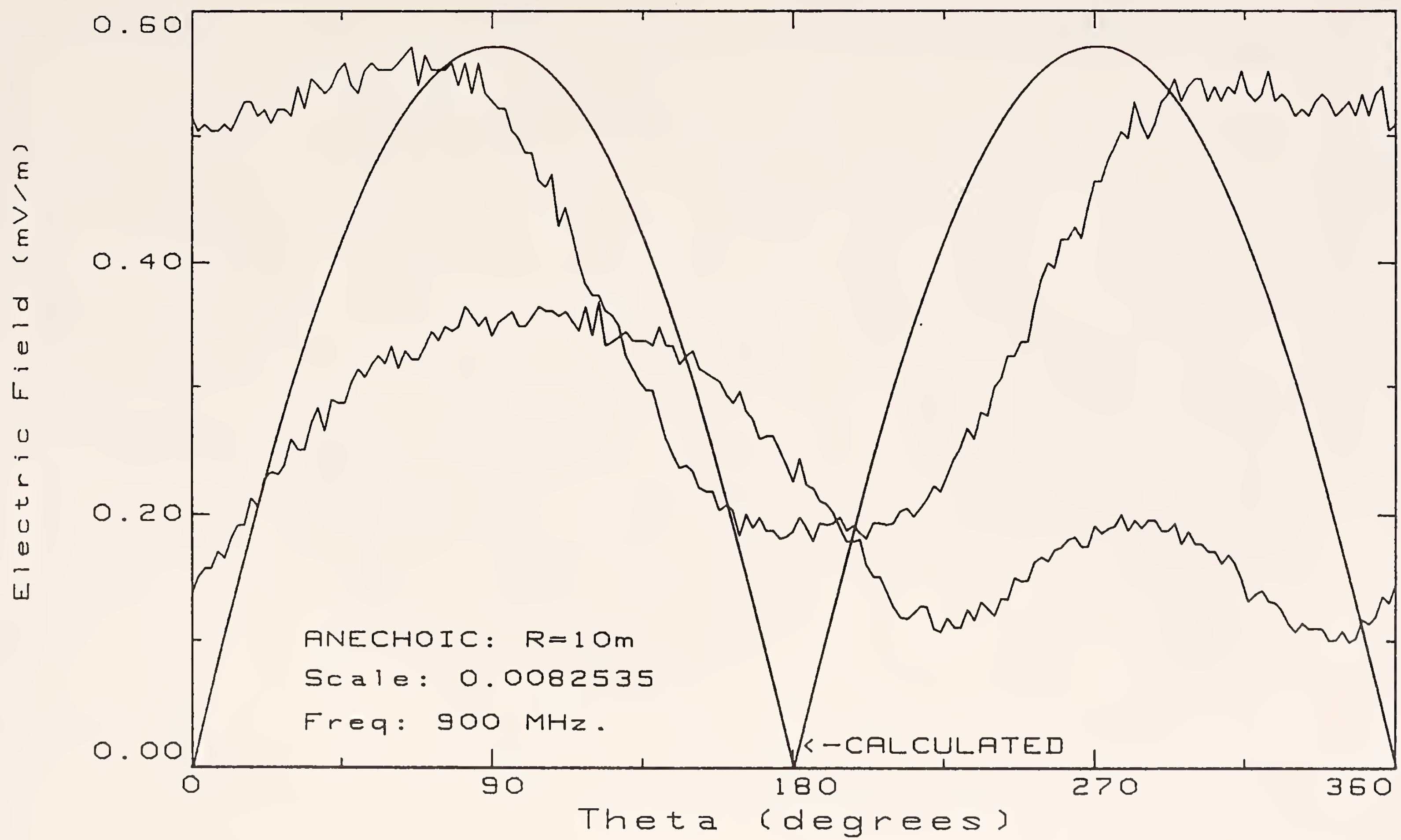

Figure 31. Sphere electric field radiation pattern determined using Anechoic Chamber measurements at 900 MHz.

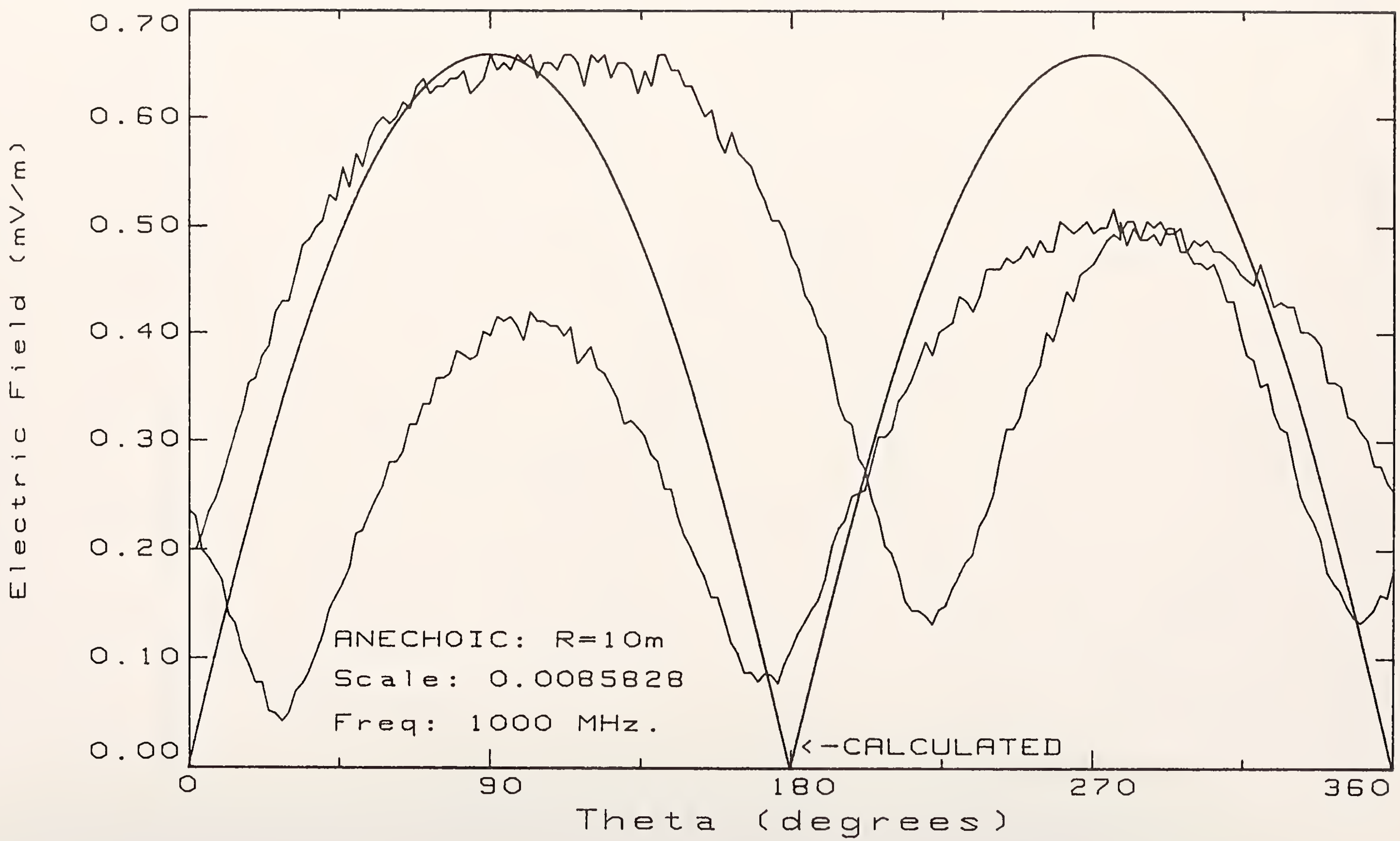

Figure 32. Sphere electric field radiation pattern determined using Anechoic Chamber measurements at 1000 MHz.

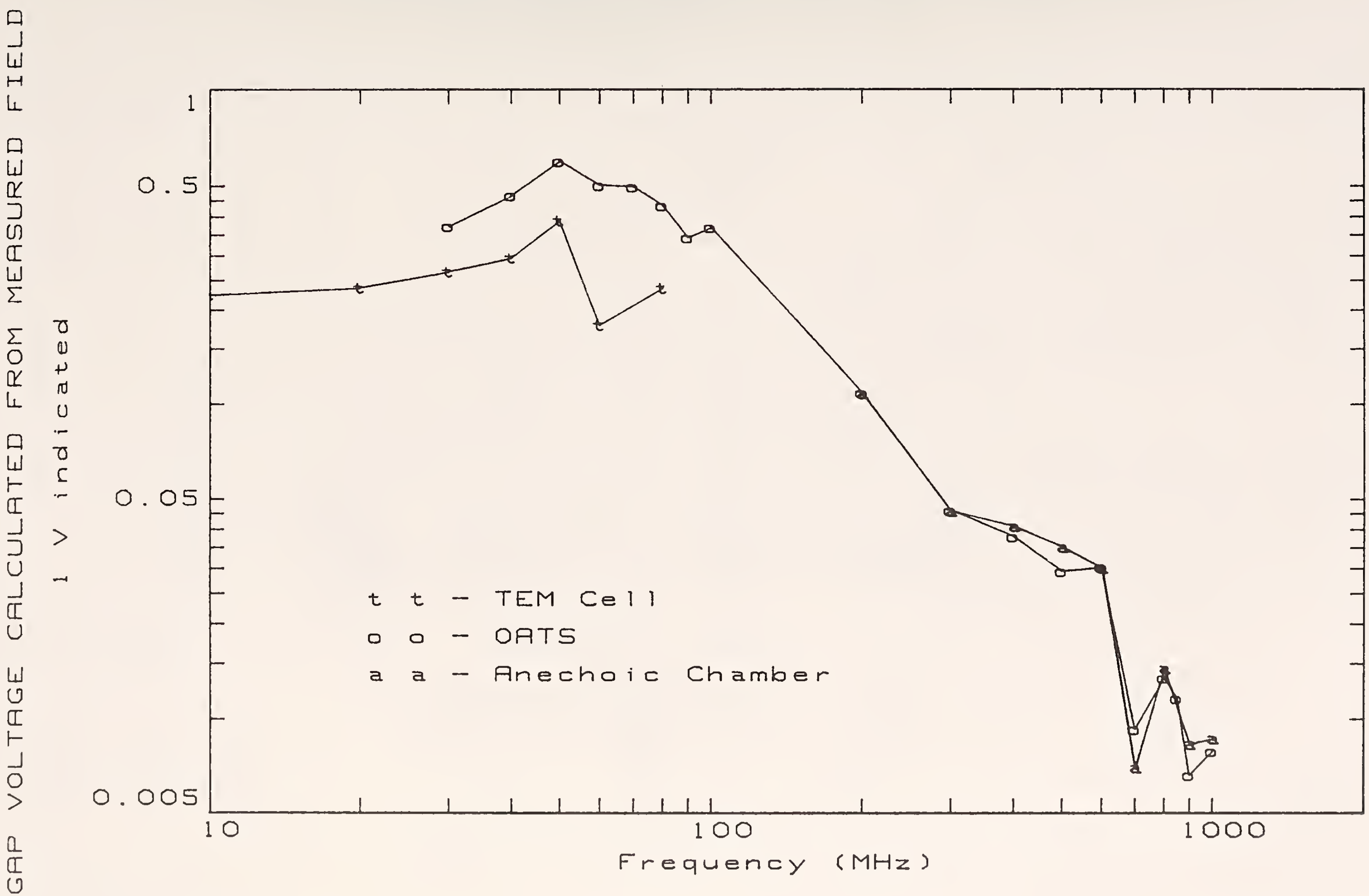

Figure 33. Gap Voltage Scale Factor Summary.

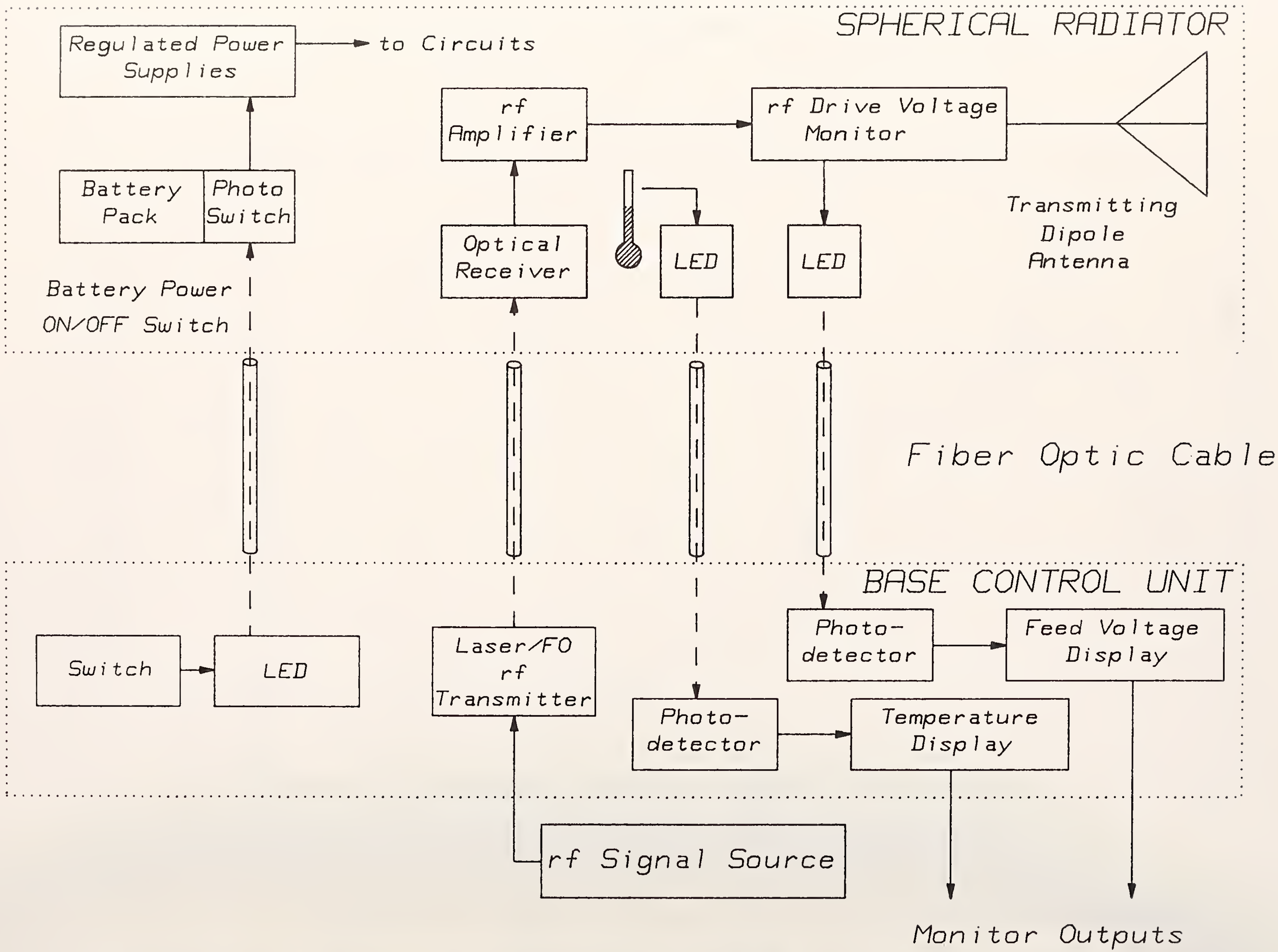

Figure 34. System Block Diagram.

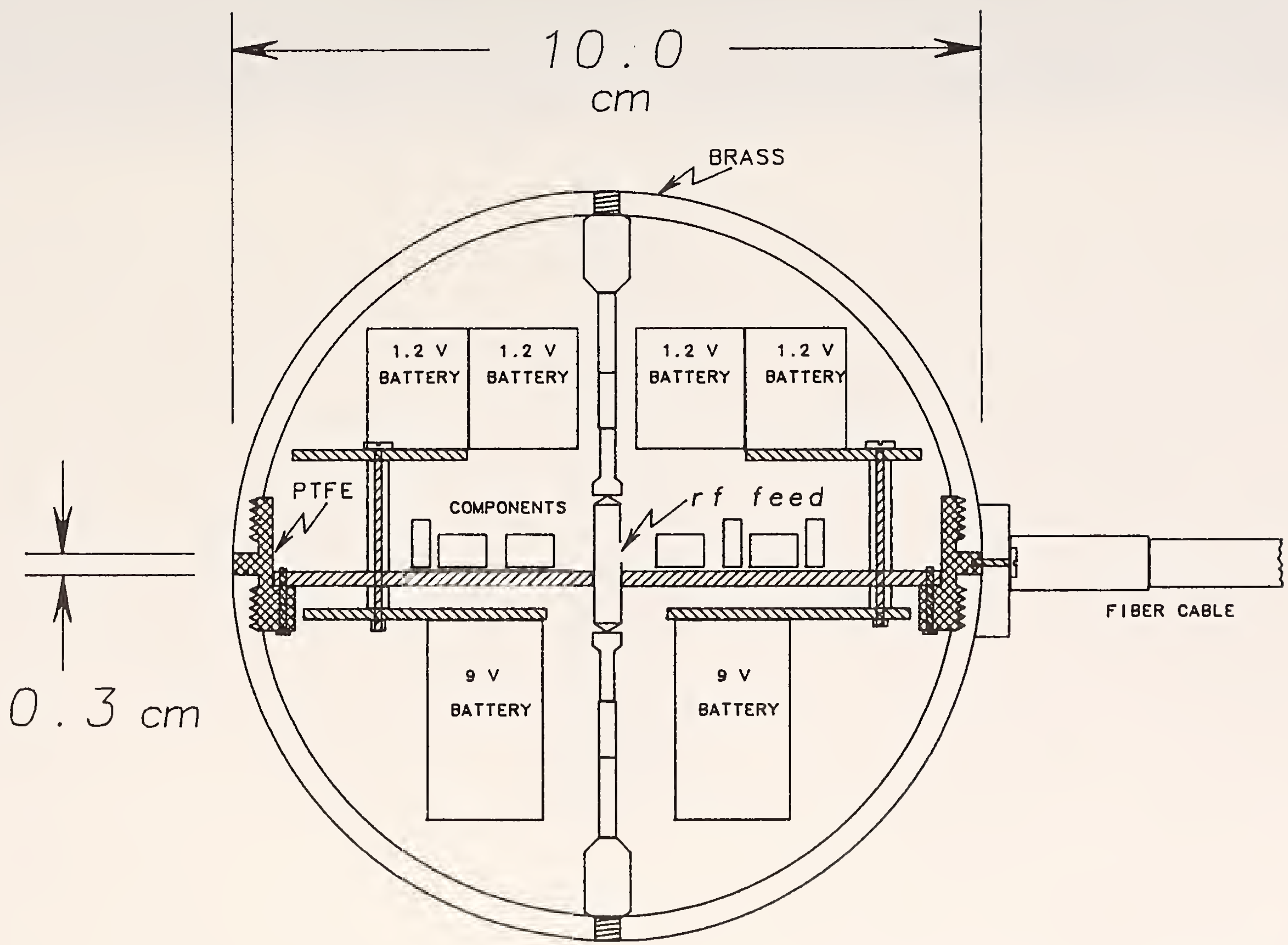

Figure 35. Mechanical drawing of the sphere.

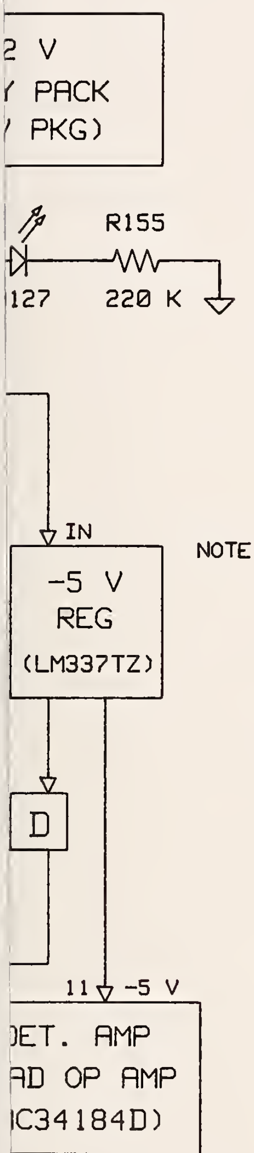

DC POWER DISTRIBUTION
IN THE SPHERE

NOTE: D INDICATES DECOUPLING NETWORK. BATTERIES ARE SWITCHED "ON" WITH SURFACE MOUNTED SWITCHES. DOWNLINKS CONTAIN V/F CONVERTERS, ONE-SHOTS, AMPS, & TRANSMITTING LEDs, BATTERIES ARE NiCADS.

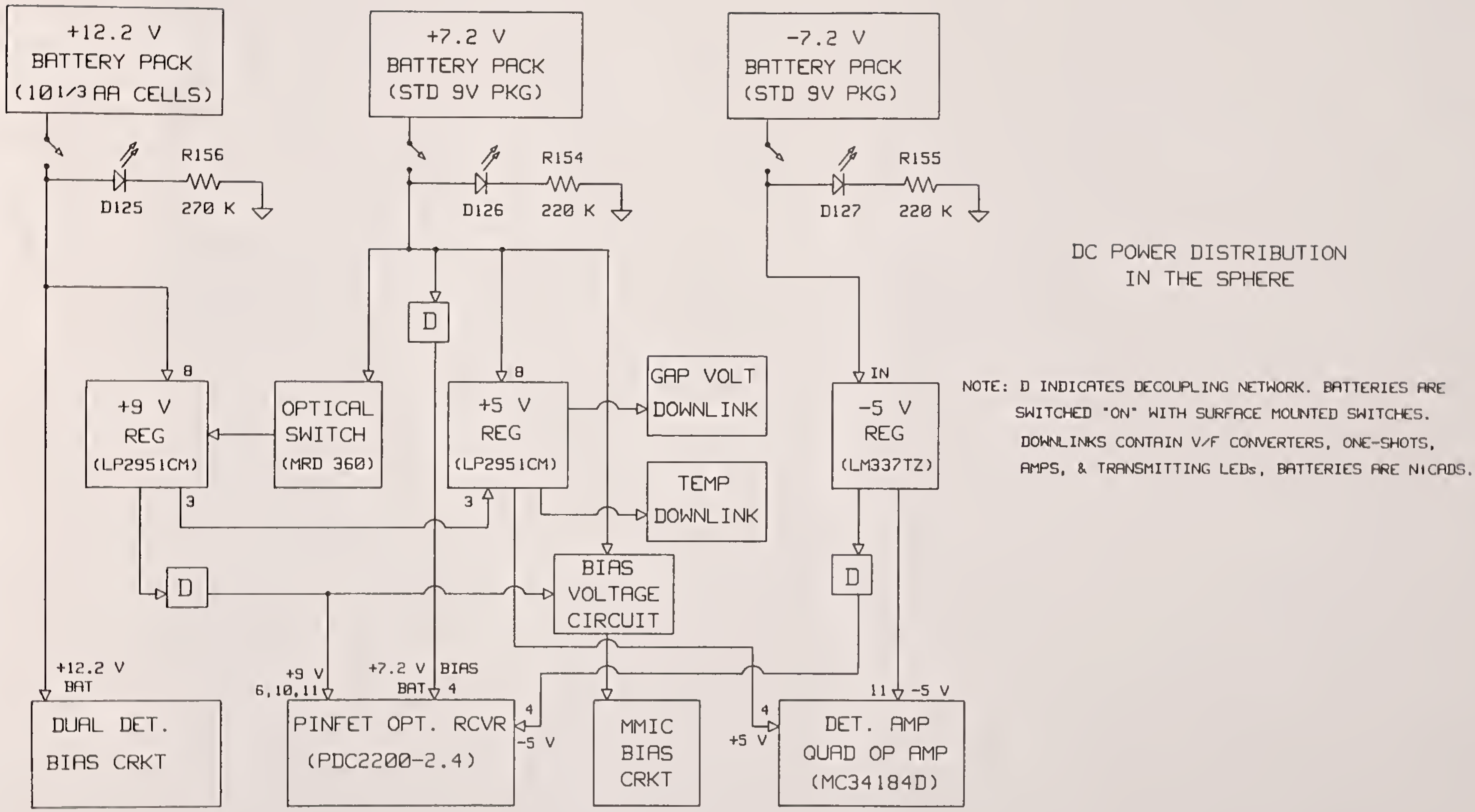

Figure 36. Schematic – DC distribution in the sphere.

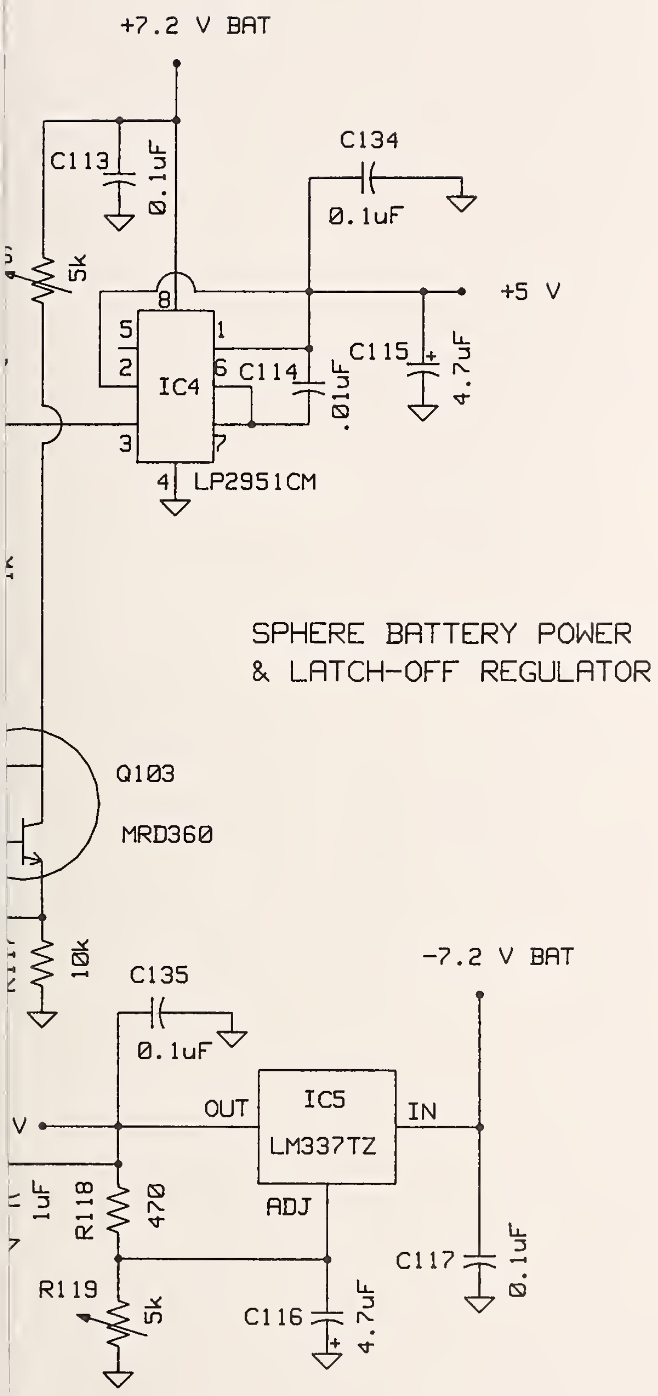

and latch-off regulator.

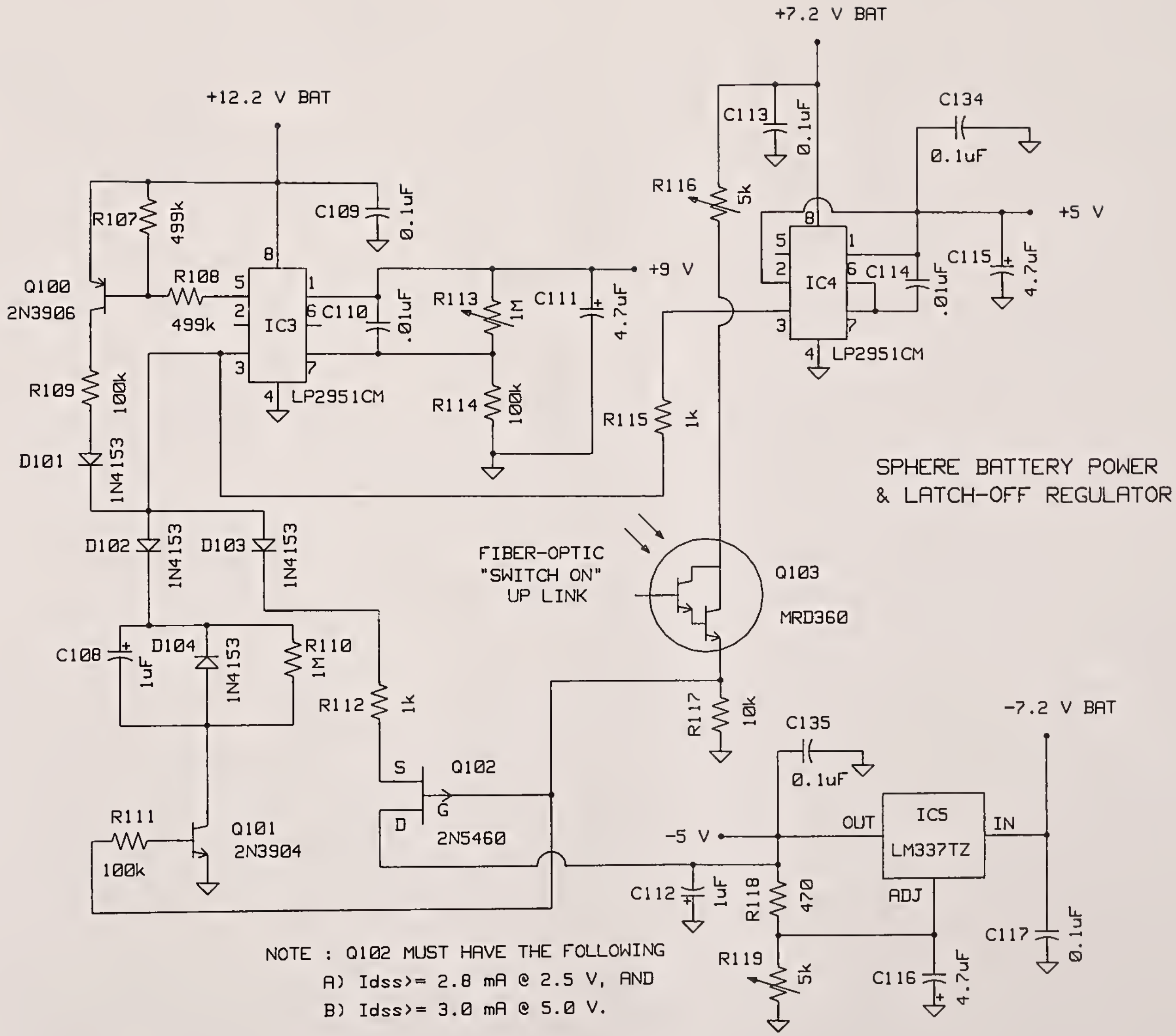

Figure 37. Schematic – Sphere battery power and latch-off regulator.

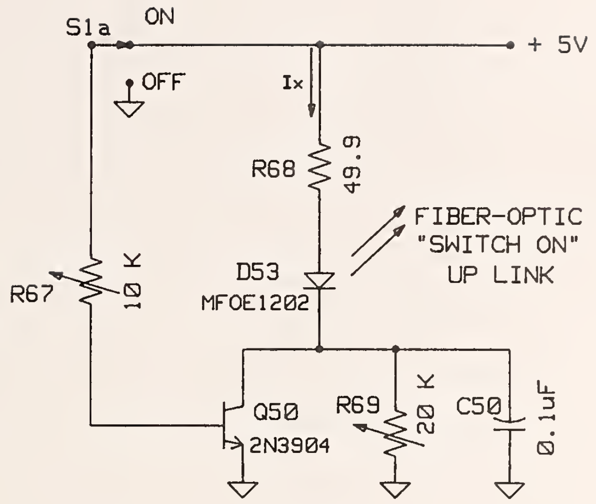

POWER ON/OFF
UPLINK DRIVE

NOTES: WITH S1a "OFF", ADJUST R69 TO OBTAIN Ix=0.2mA.
WITH S1a "ON", ADJUST R67 TO OBTAIN Ix=60 mA.
THE 2nd POLE OF S1(S1b) IS USED WITH IC18 OF
THE ALARM CIRCUITRY.

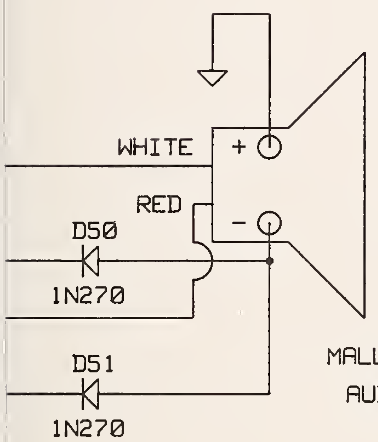

MALLORY SC616WY
AUDIO ALARM

T MONITOR/ALARM CIRCUITS
R & DIPOLE BATTERY STATUS

dipole battery status. Power on/off uplink drive.

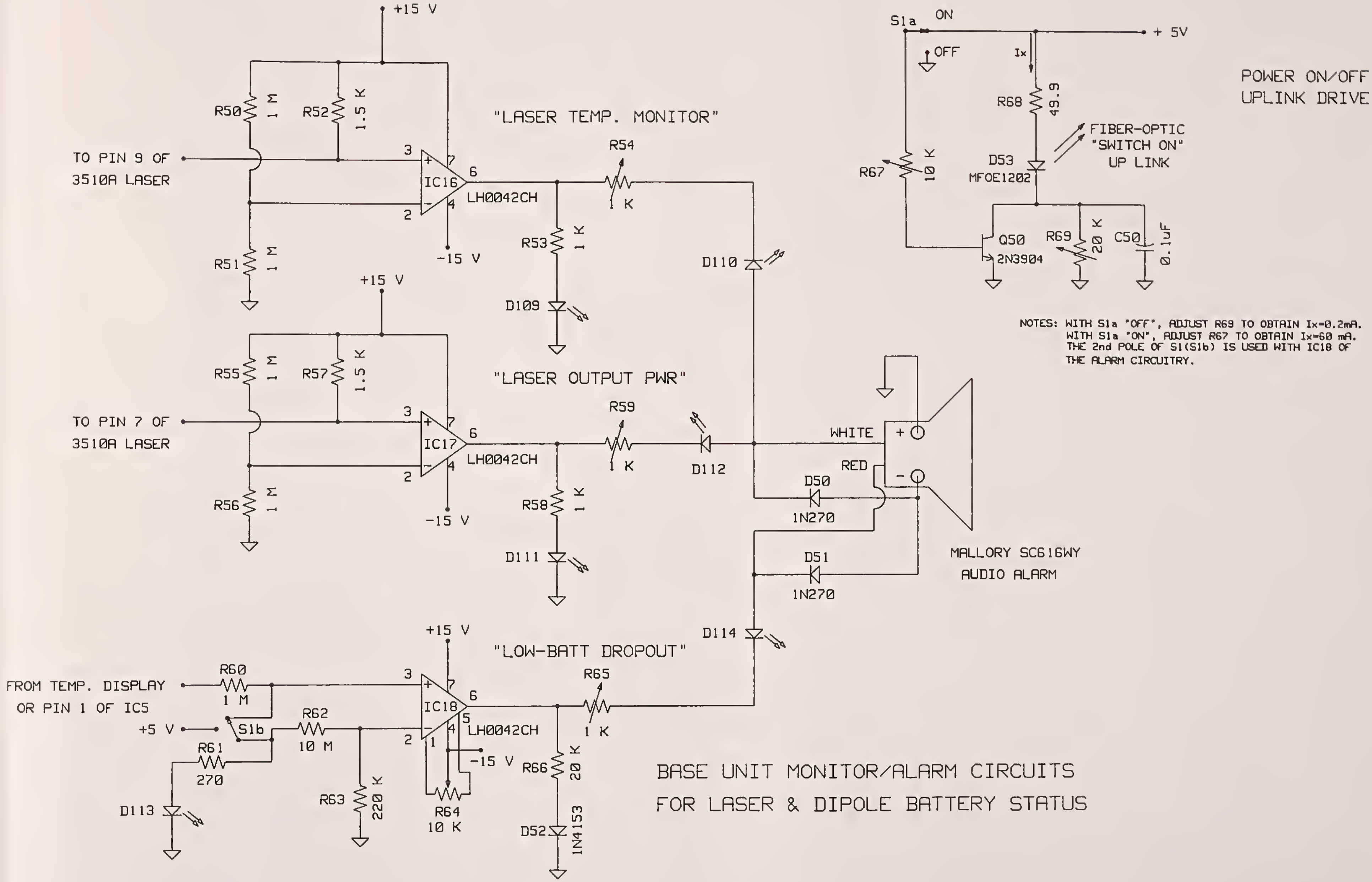

Figure 38. Schematic - Base unit monitor/alarm circuits for laser & dipole battery status. Power on/off uplink drive.

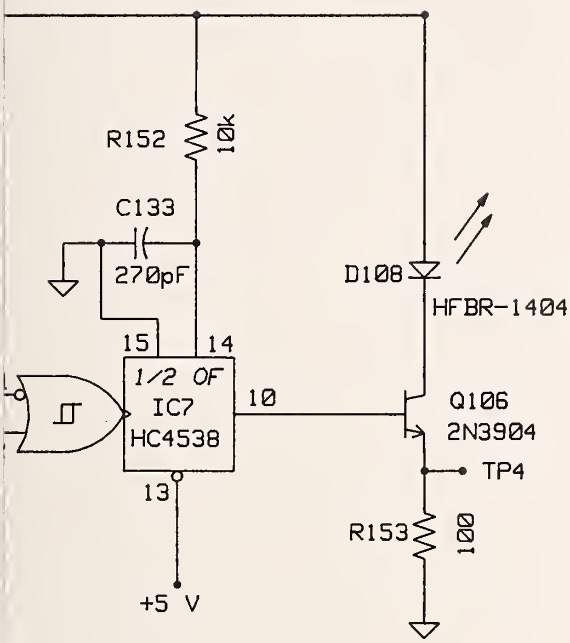

E
LINK

ATE OR POLYSTYRENE.

cal downlink.

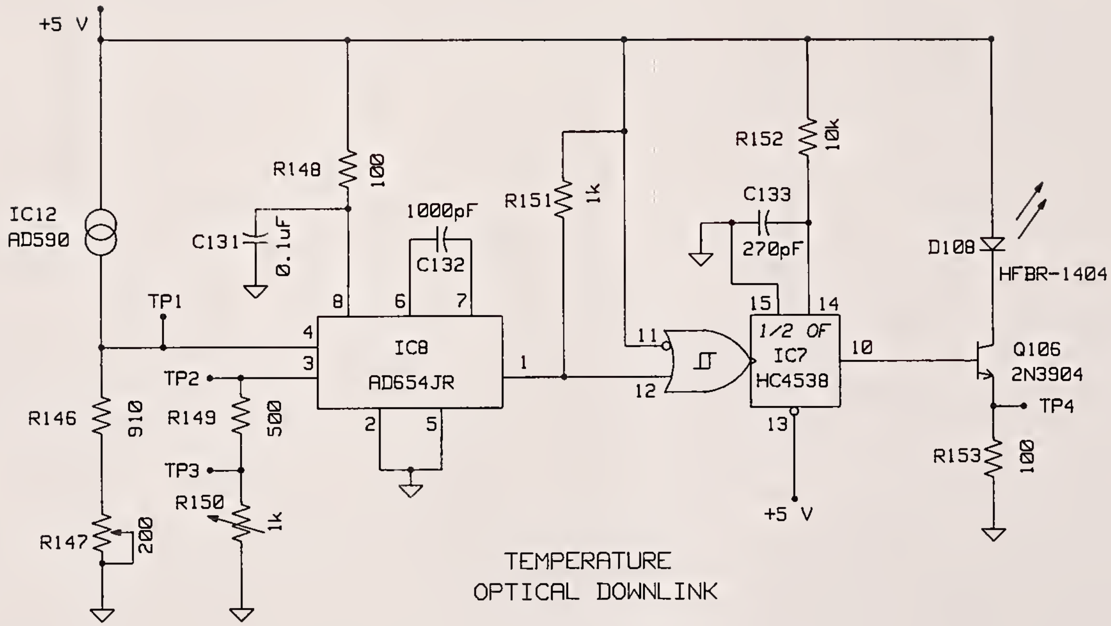

NOTE: C132 MUST BE POLYCARBONATE OR POLYSTYRENE.

Figure 39. Schematic – Temperature optical downlink.

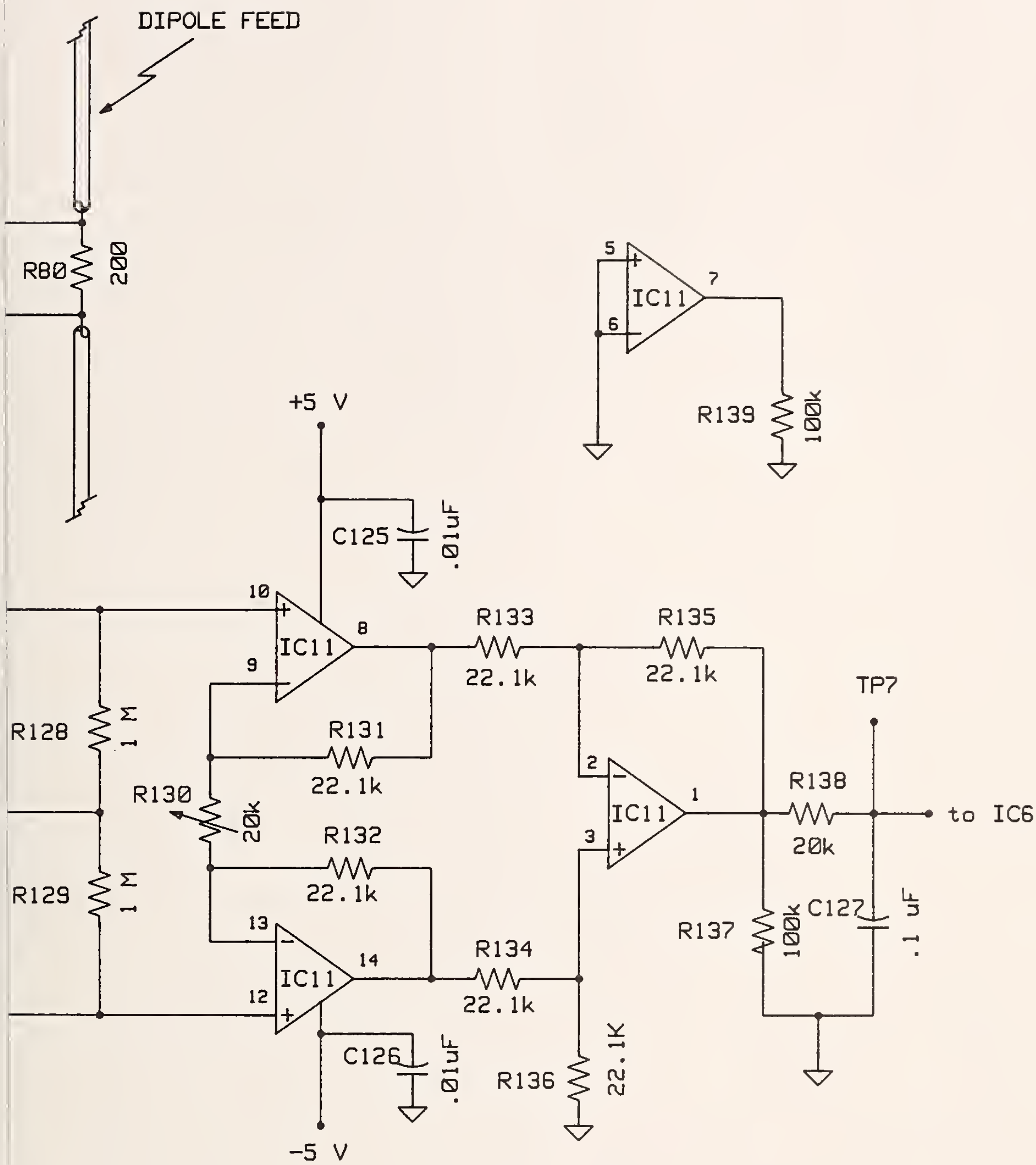
DIPOLE FEED
R80
200
+5 V
C125
.01uF
IC11
5
6
7
R139
100k
10
9
8
R133
22.1k
R135
22.1k
TP7
R128
1 M
R131
22.1k
R130
20k
2
3
1
R138
20k
to IC6
R132
22.1k
R129
1 M
13
14
12
R134
22.1k
R137
100k
C127
.1 uF
C126
.01uF
R136
22.1K
-5 V

WS:

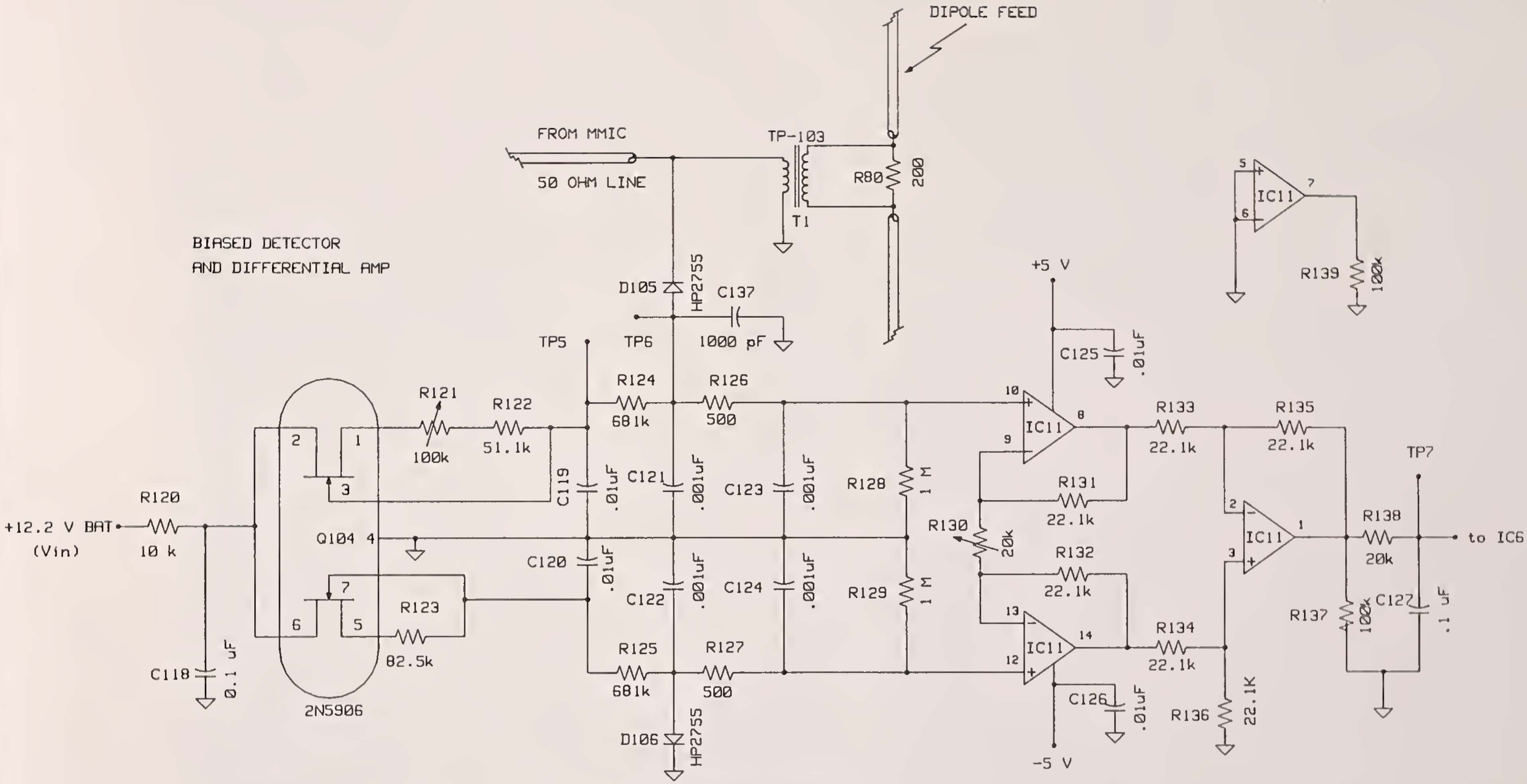

NOTE: Q104 MUST BE CAPABLE OF PROVIDING CONTROL BIAS CURRENTS AS FOLLOWS:

$$\frac{\Delta Id}{Vin} < \frac{10nA}{V}$$

FOR 1) 9V < Vin < 14V

2) 4uA < Id < 8uA

Figure 40. Schematic - Biased detector & differential amplifier.

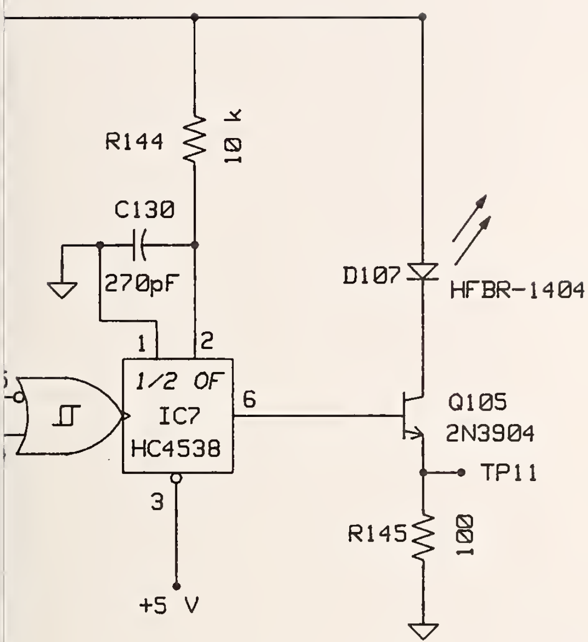

AGE
NK

ATE OR POLYSTYRENE.

ge optical downlink.

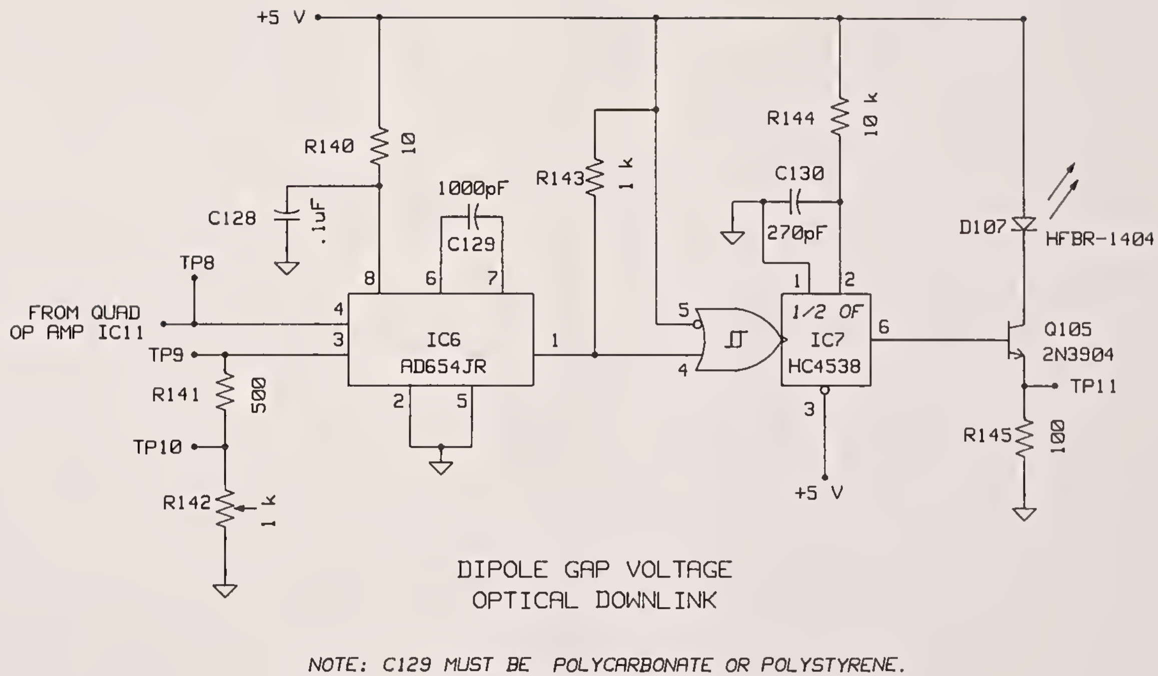

Figure 41. Schematic - Dipole gap voltage optical downlink.

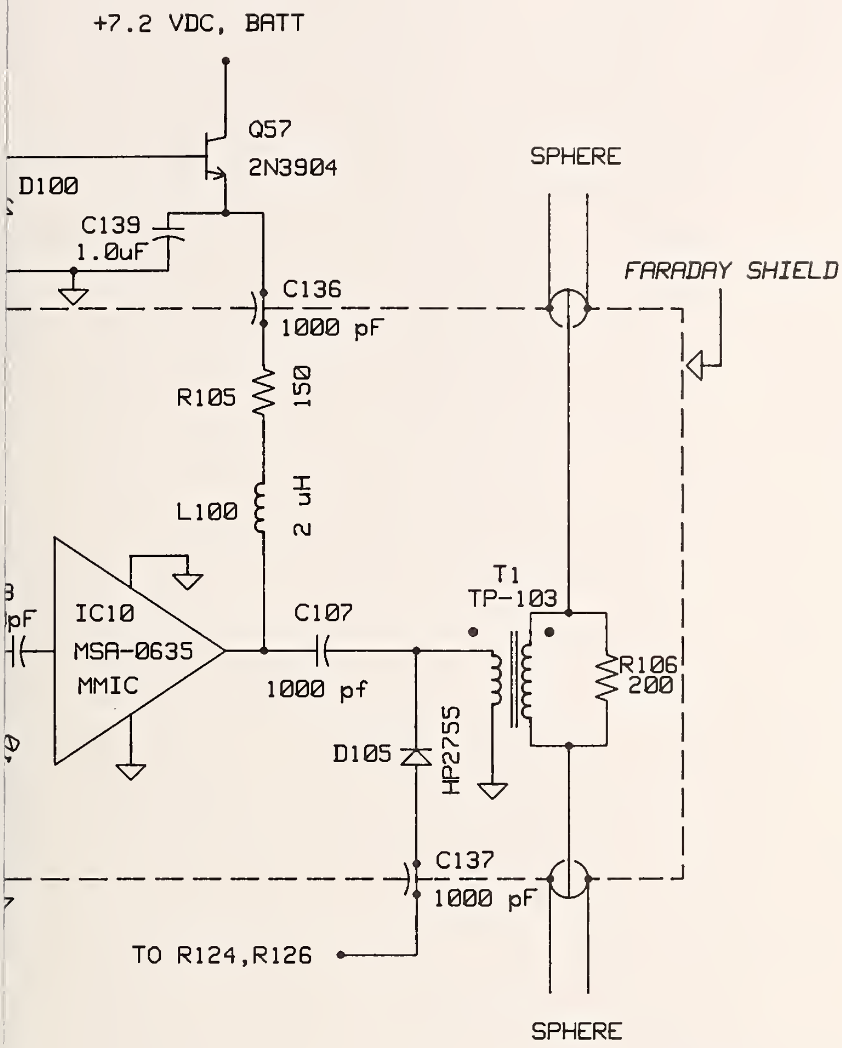

PINFET AND MMIC RF AMPLIFIER

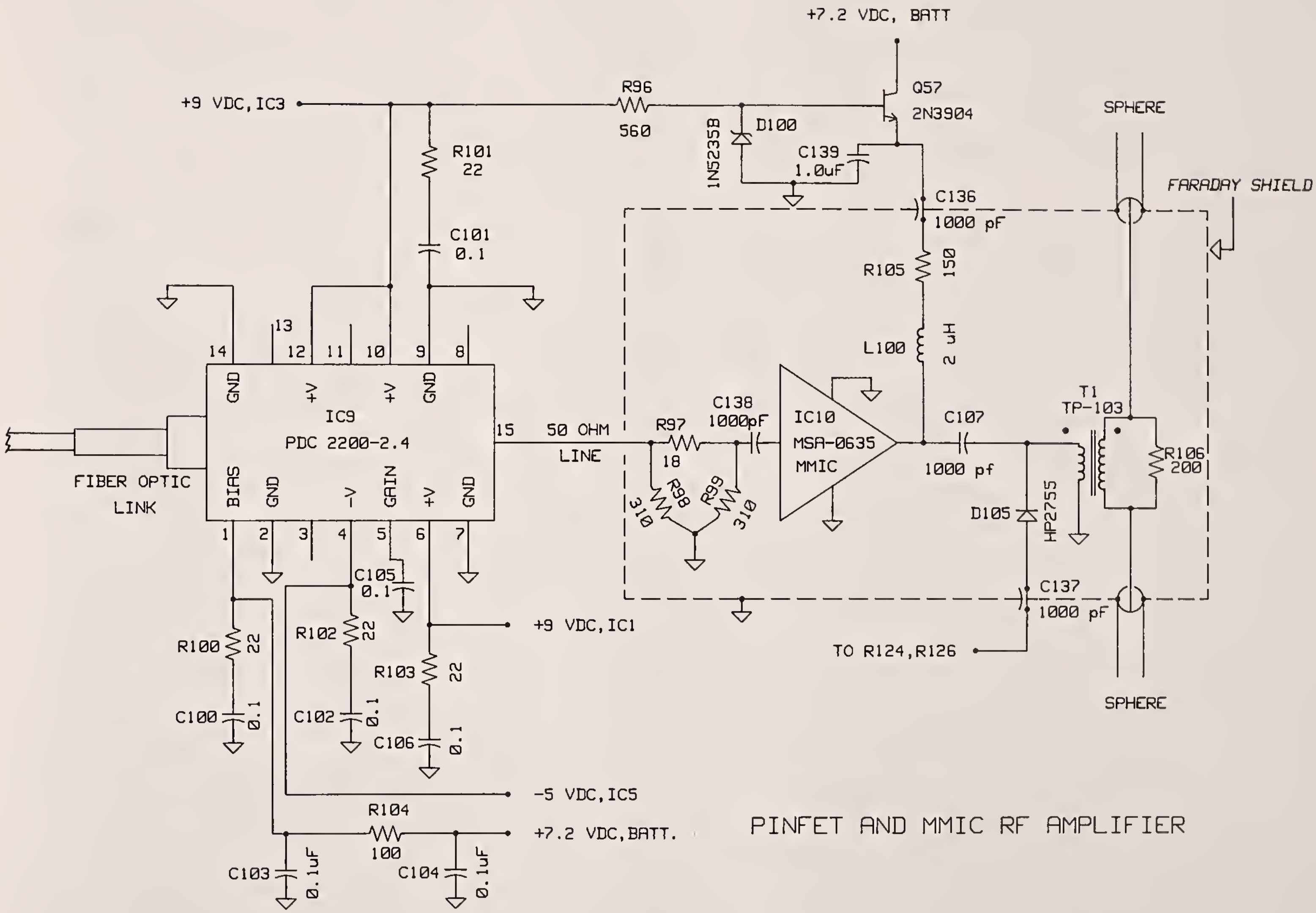

Figure 42. Schematic – PINFET and MMIC rf amplifier.

BLOCK DIAGRAM

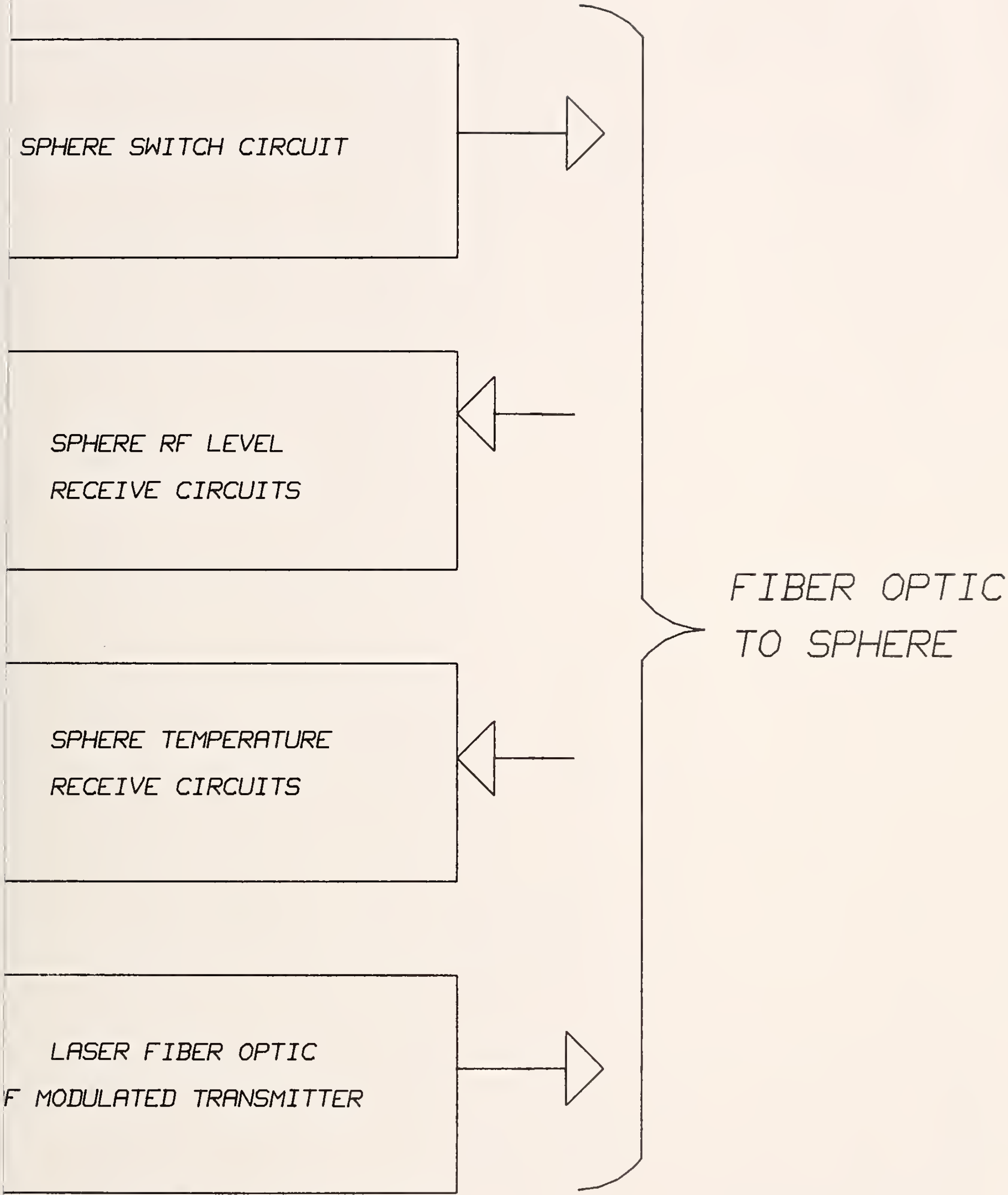

S LASER TEMPERATURE LED, L13 IS LASER OUTPUT POWER LED
S SPHERE LOW BATTERY LED. A IS AN AUDIO ALARM.
A DIGITAL PANEL METER READOUT.

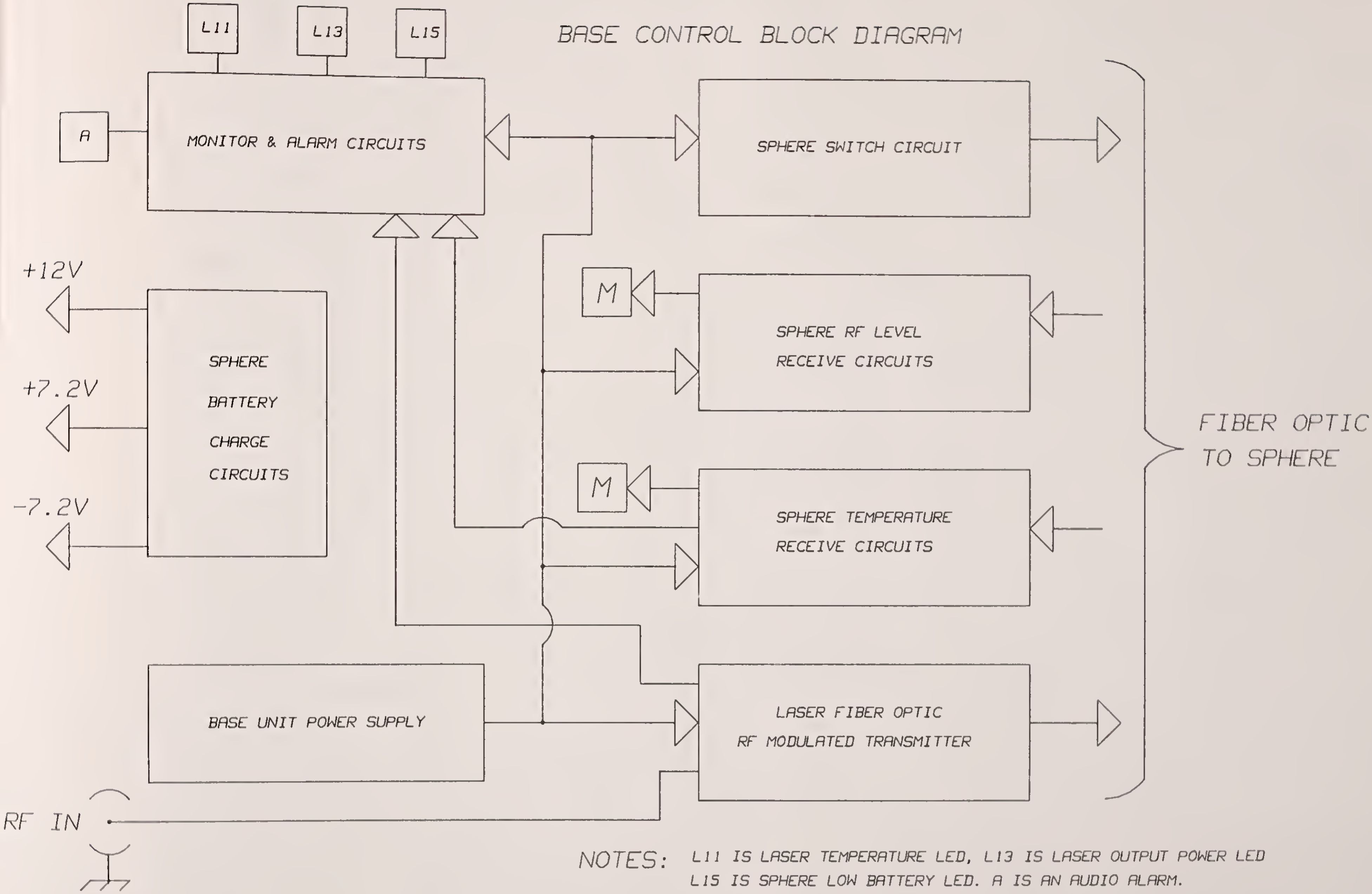

NOTES: L11 IS LASER TEMPERATURE LED, L13 IS LASER OUTPUT POWER LED
L15 IS SPHERE LOW BATTERY LED. A IS AN AUDIO ALARM.
M IS A DIGITAL PANEL METER READOUT.

Figure 43. Base control block diagram.

BASE UNIT CHARGING CIRCUITS
FOR SPHERICAL DIPOLE BATTERIES

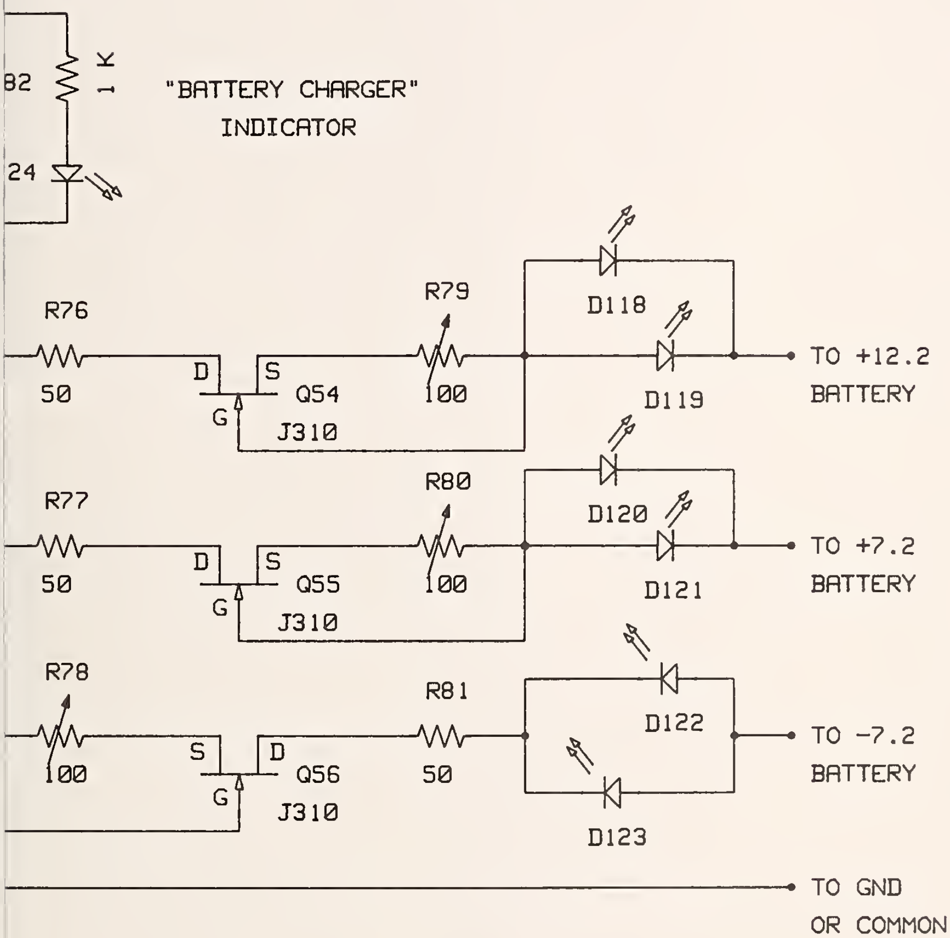

QUICK CHARGE GROUP

al dipole batteries.

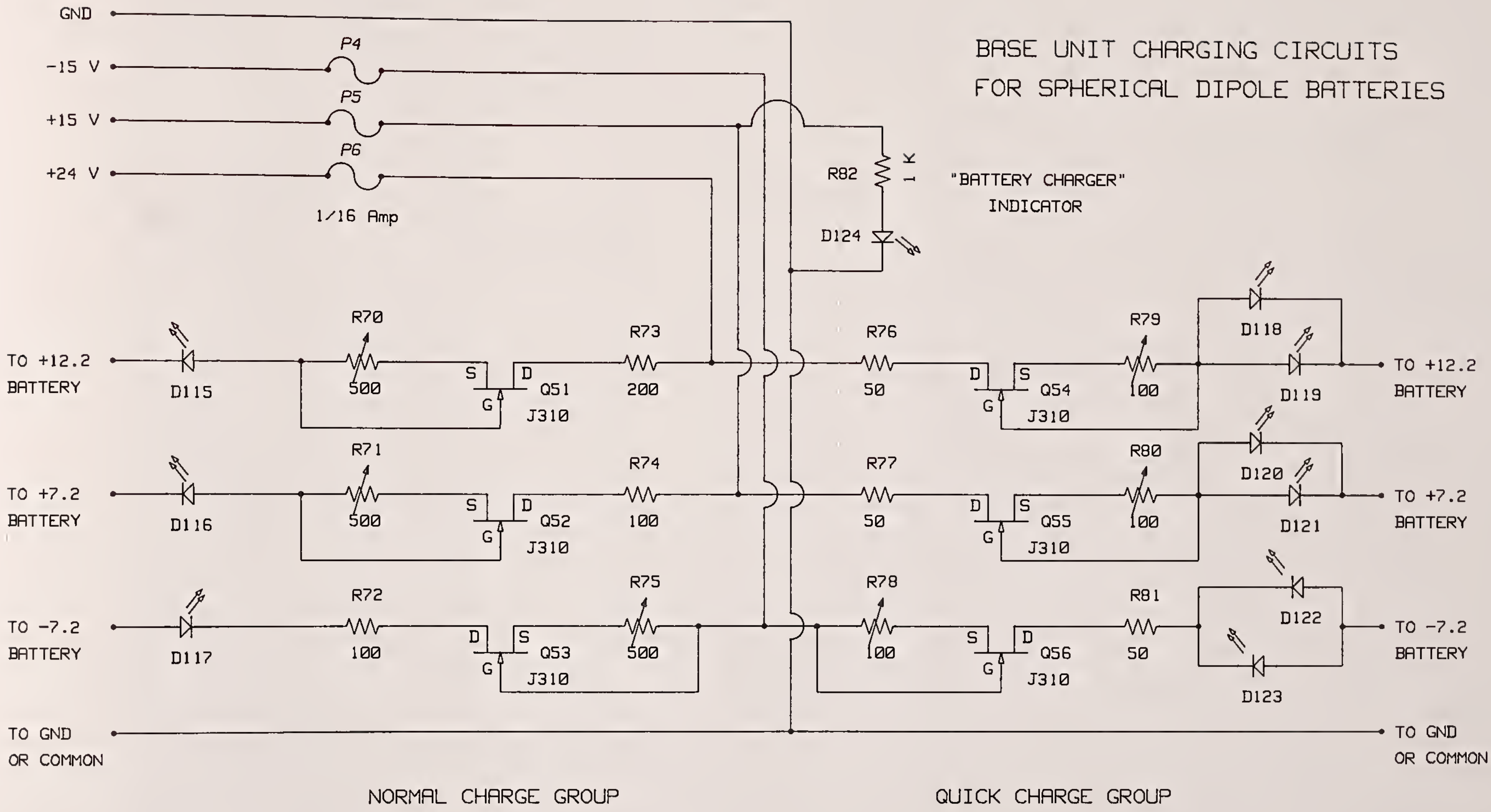

NOTE: FOR J310, Idss IS MATCHED TO REQUIREMENT.

Figure 44. Schematic – Base unit charging circuits for spherical dipole batteries.

OPTICAL DOWN LINK RECEIVER

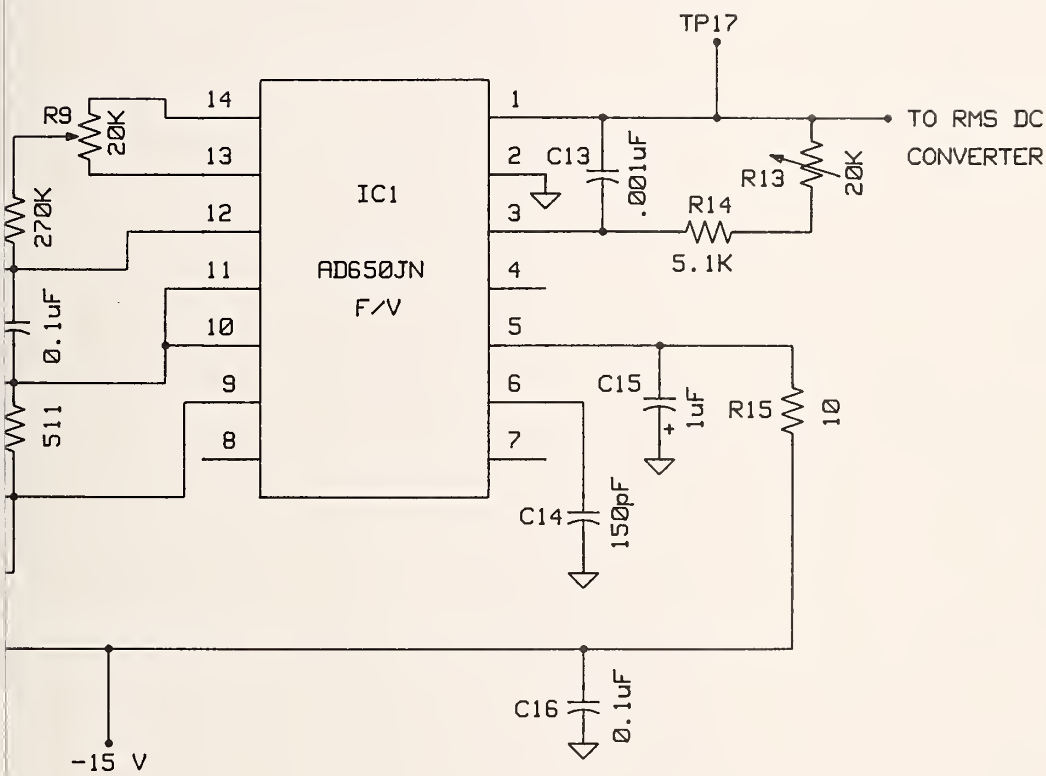

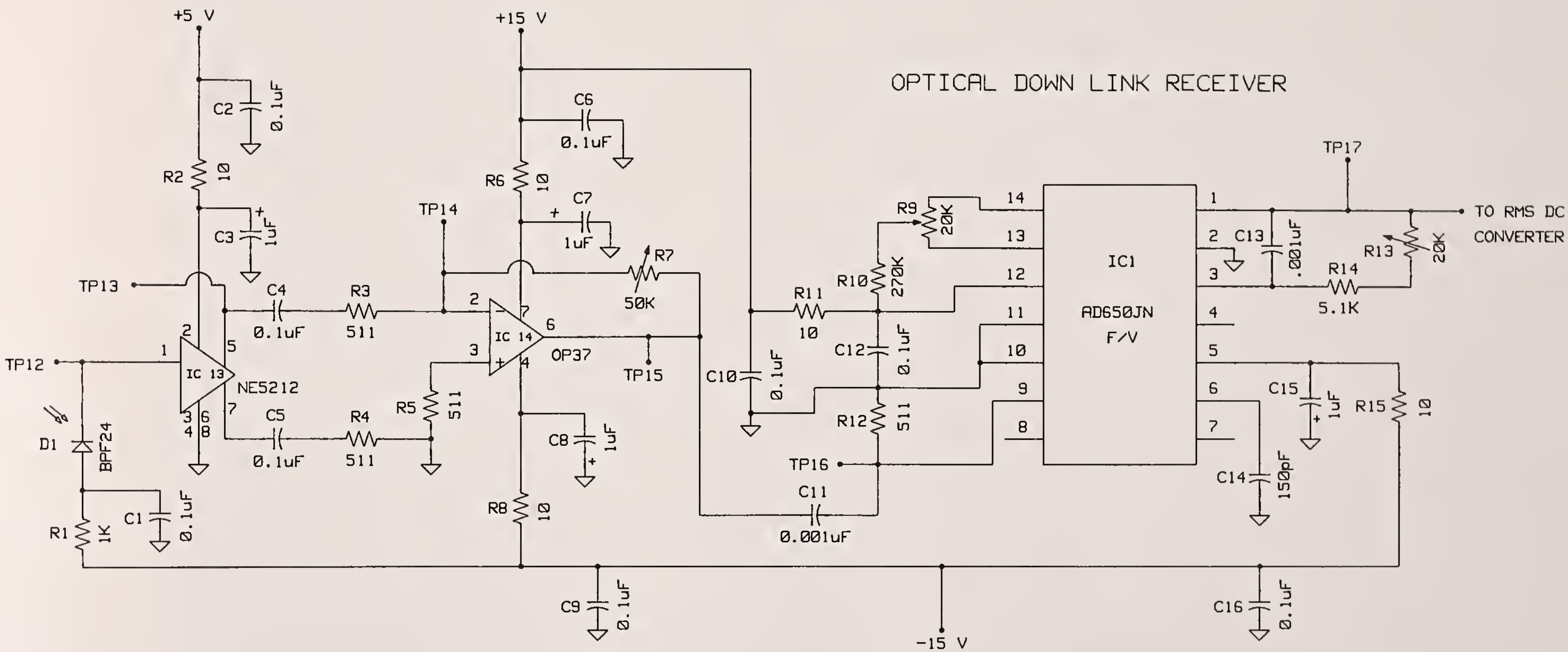

Figure 45. Schematic - Optical downlink receiver.

DOWNLINK SIGNAL PROCESSING CIRCUITRY

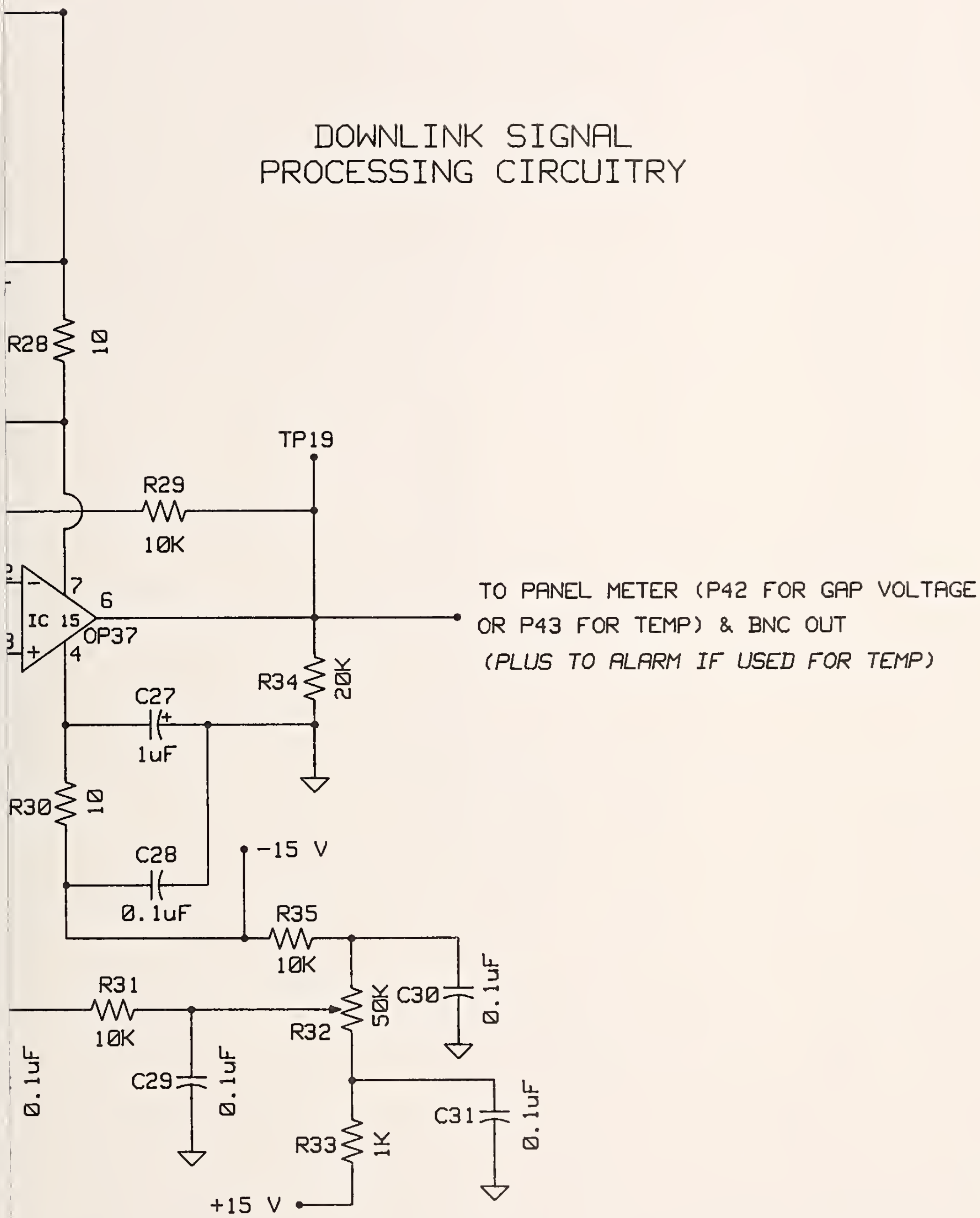

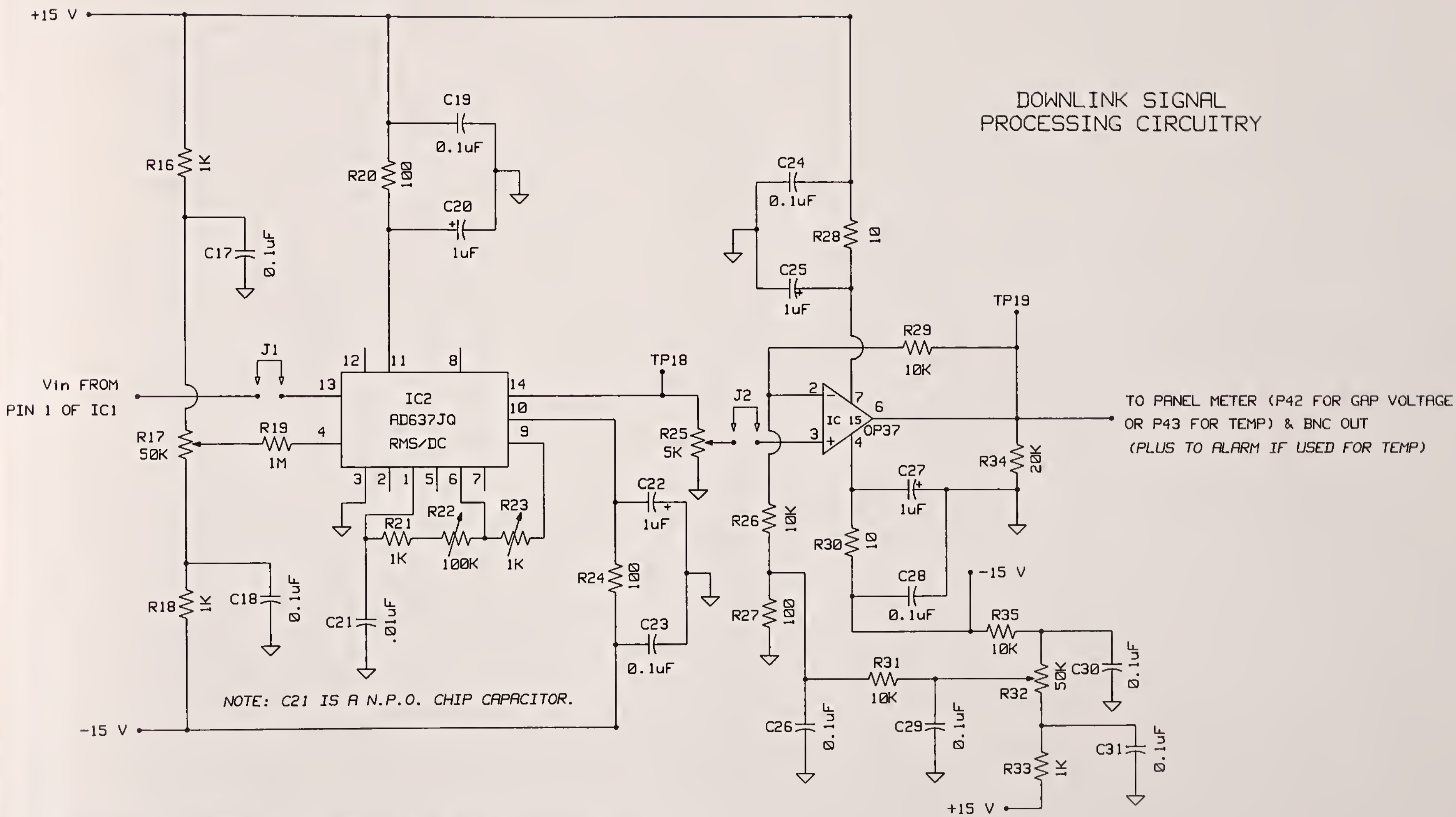

Figure 46. Schematic – Downlink signal processing circuitry.

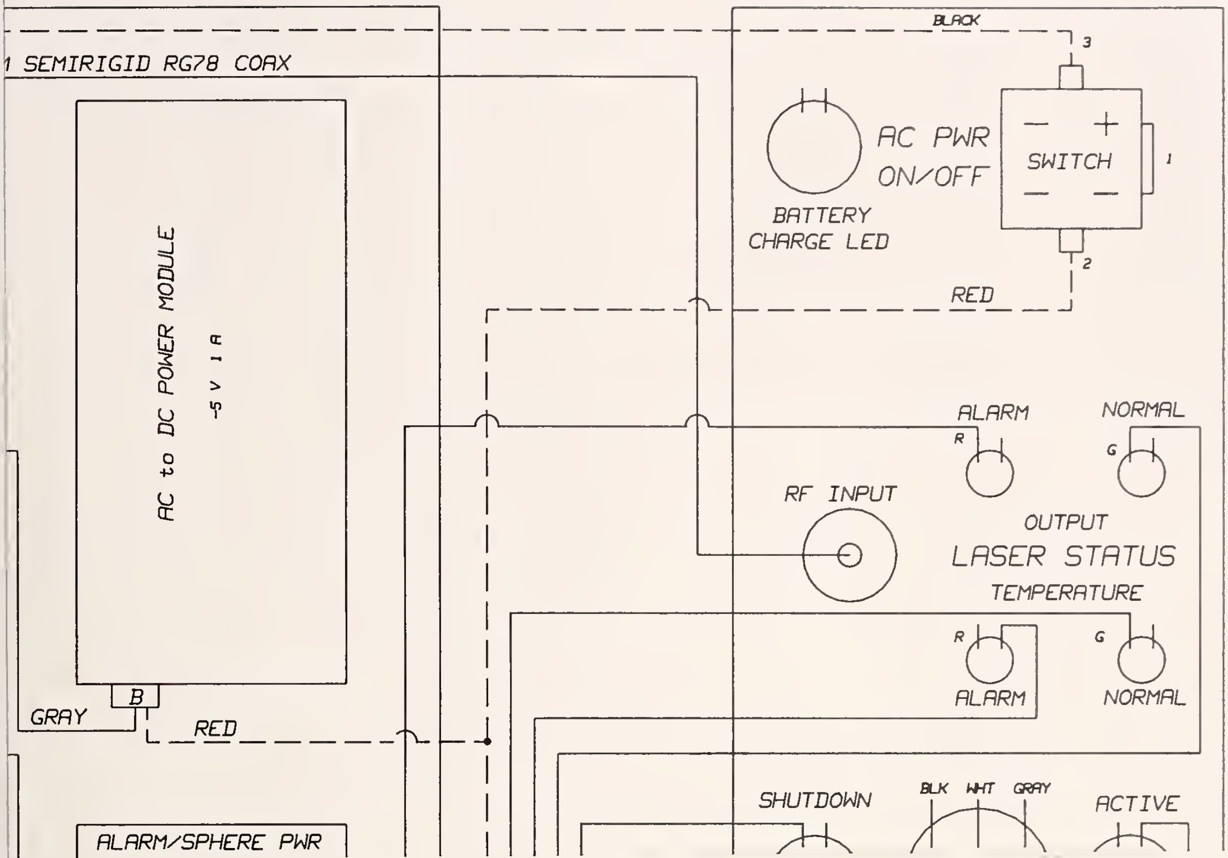

BLACK
3
1 SEMIRIGID RG78 COAX
AC PWR
ON/OFF
SWITCH
1
BATTERY
CHARGE LED
2
RED
AC to DC POWER MODULE
-5 V 1 A
ALARM
NORMAL
R
G
RF INPUT
OUTPUT
LASER STATUS
TEMPERATURE
R
G
ALARM
NORMAL
B
GRAY
RED
SHUTDOWN
BLK
WHT
GRAY
ACTIVE
ALARM/SPHERE PWR

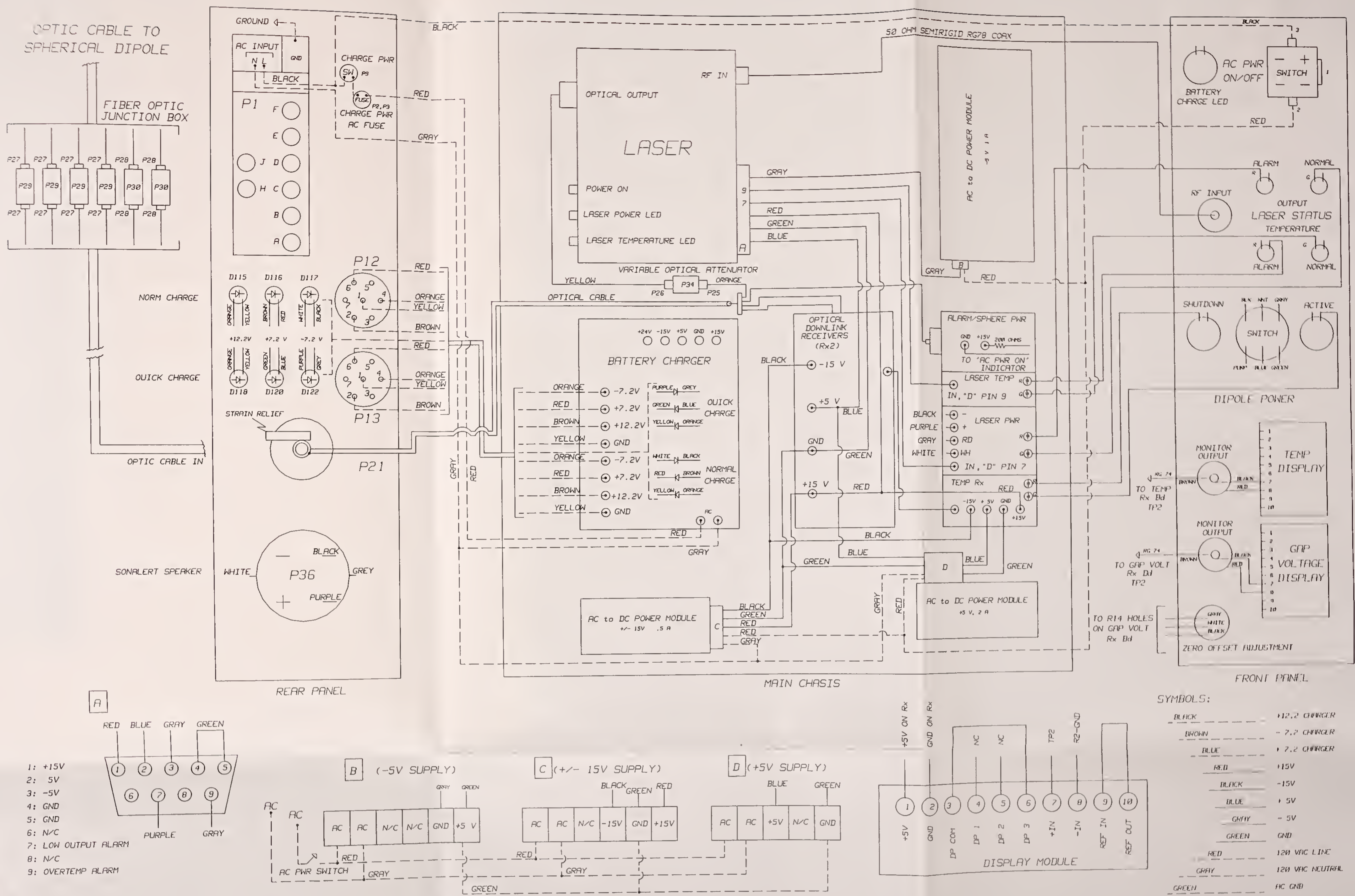

Figure 47. Assembly drawing - Base unit.

RY CHARGING CIRCUIT BOARD

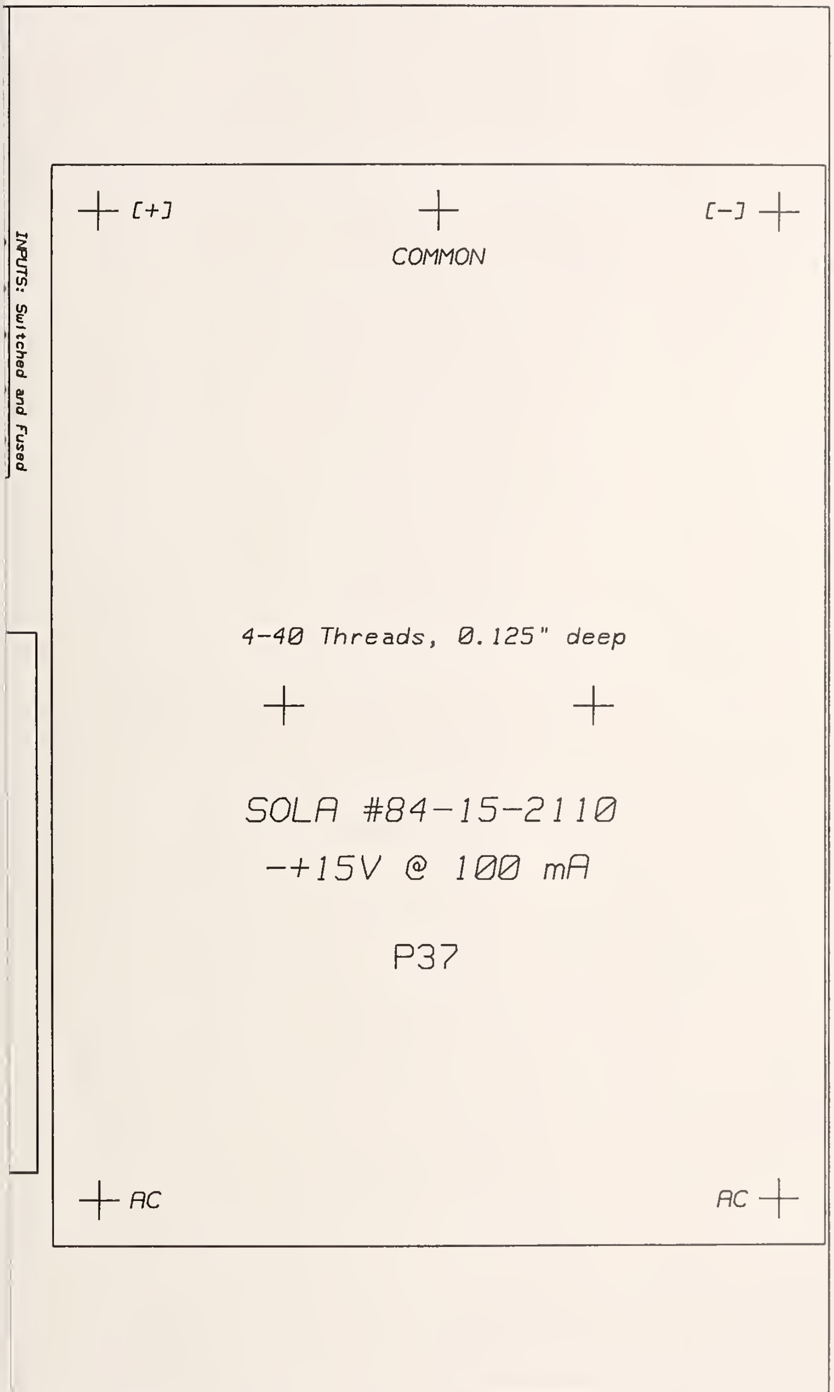

cuit board.

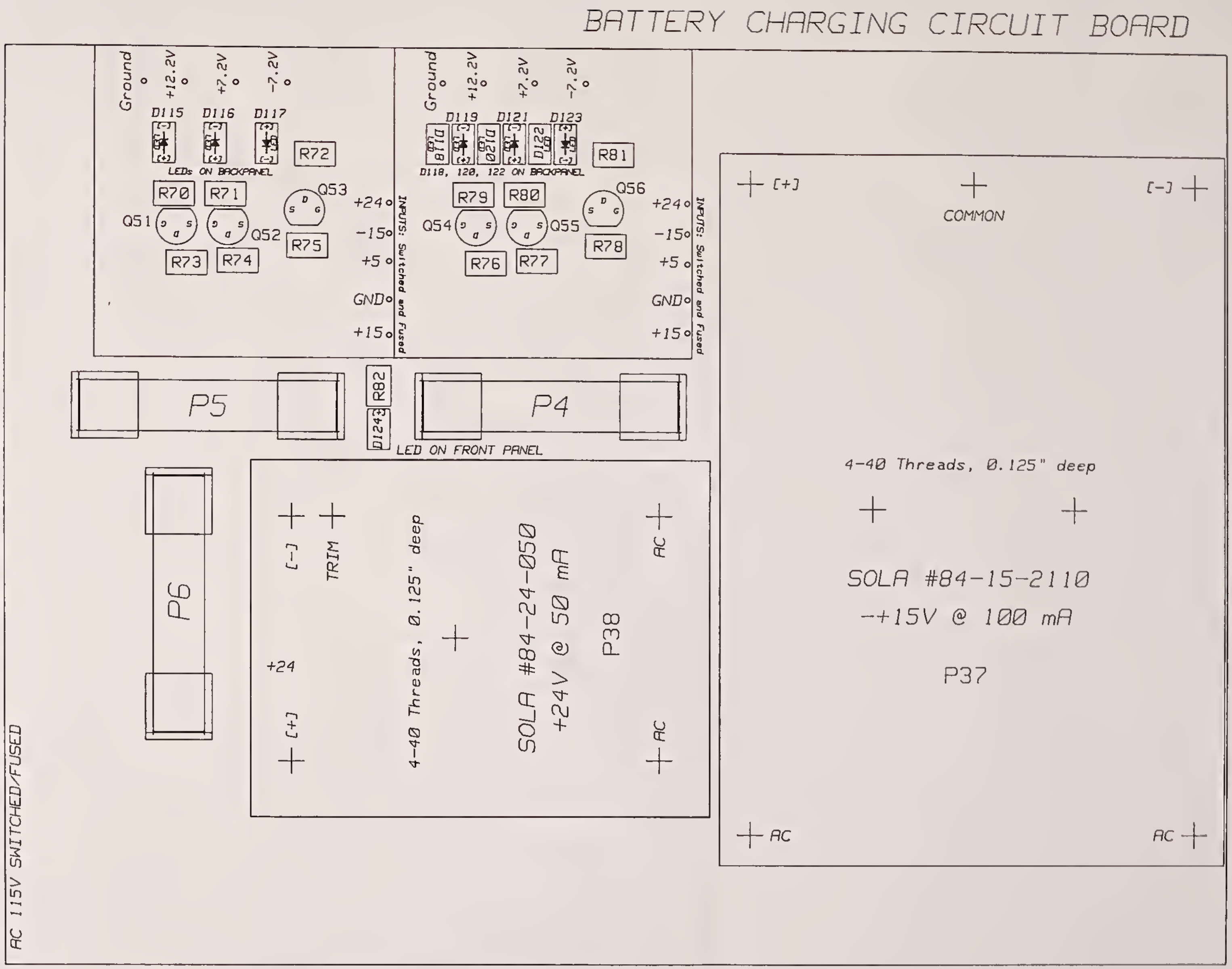

Figure 48. Assembly drawing - Battery charging circuit board.

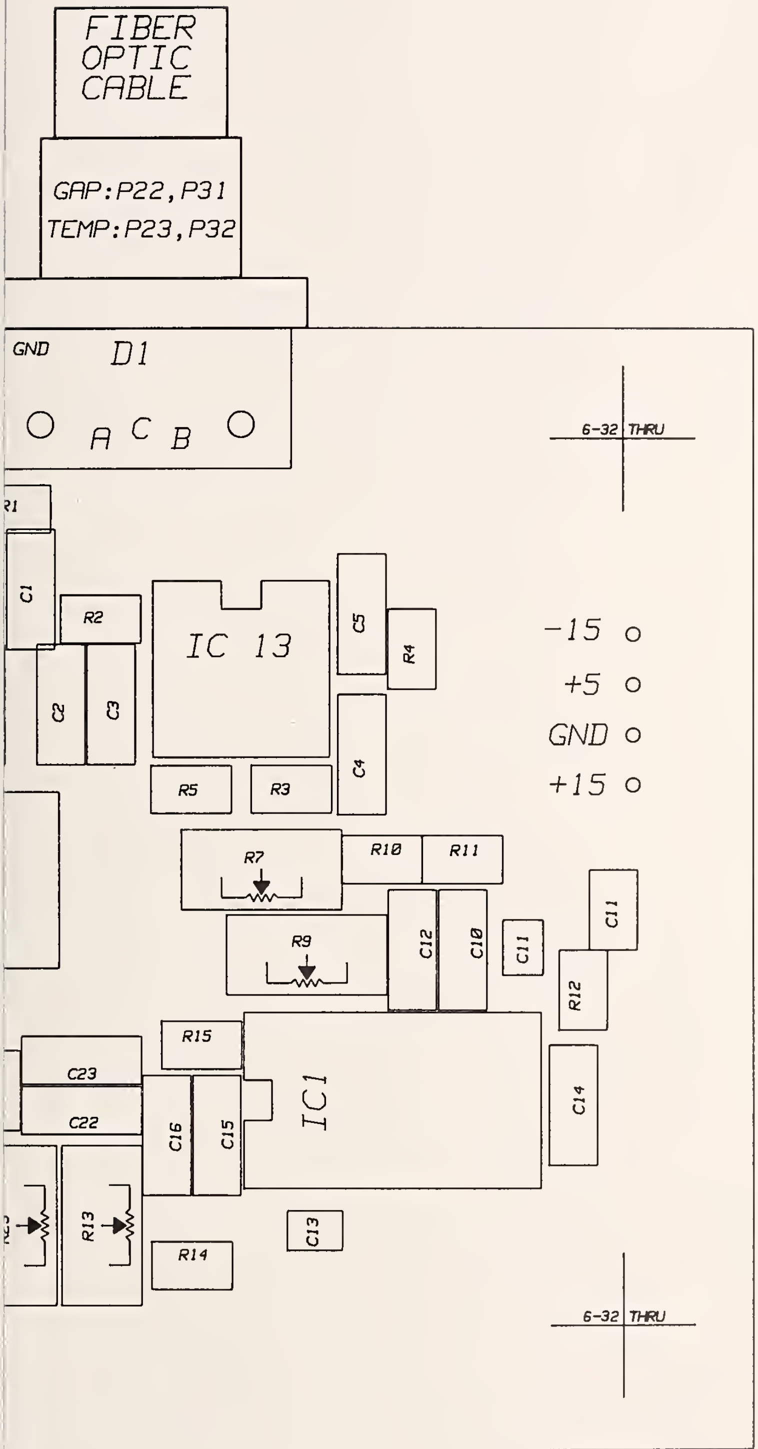

FIBER OPTIC CABLE
GAP:P22,P31
TEMP:P23,P32
GND
D1
A C B
R1
C1
R2
IC 13
C5
R4
C2
C3
C4
R5
R3
6-32 THRU
-15
+5
GND
+15
R7
R10
R11
R9
C12
C10
C11
C11
R12
R15
C23
C22
C16
C15
IC1
C14
R13
R14
C13
6-32 THRU

it board.

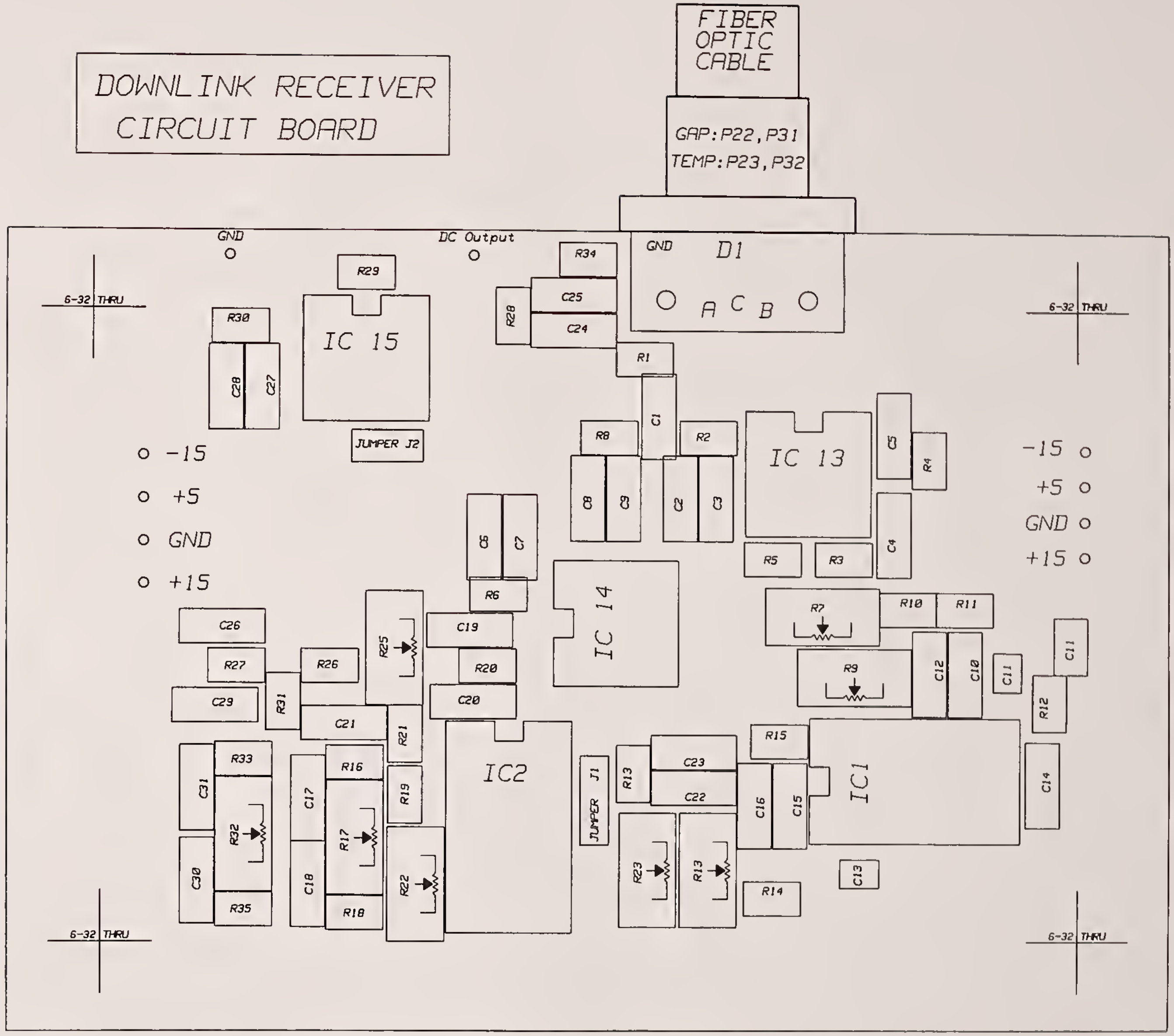

Figure 49. Assembly drawing - Downlink reciever circuit board.

BOARD

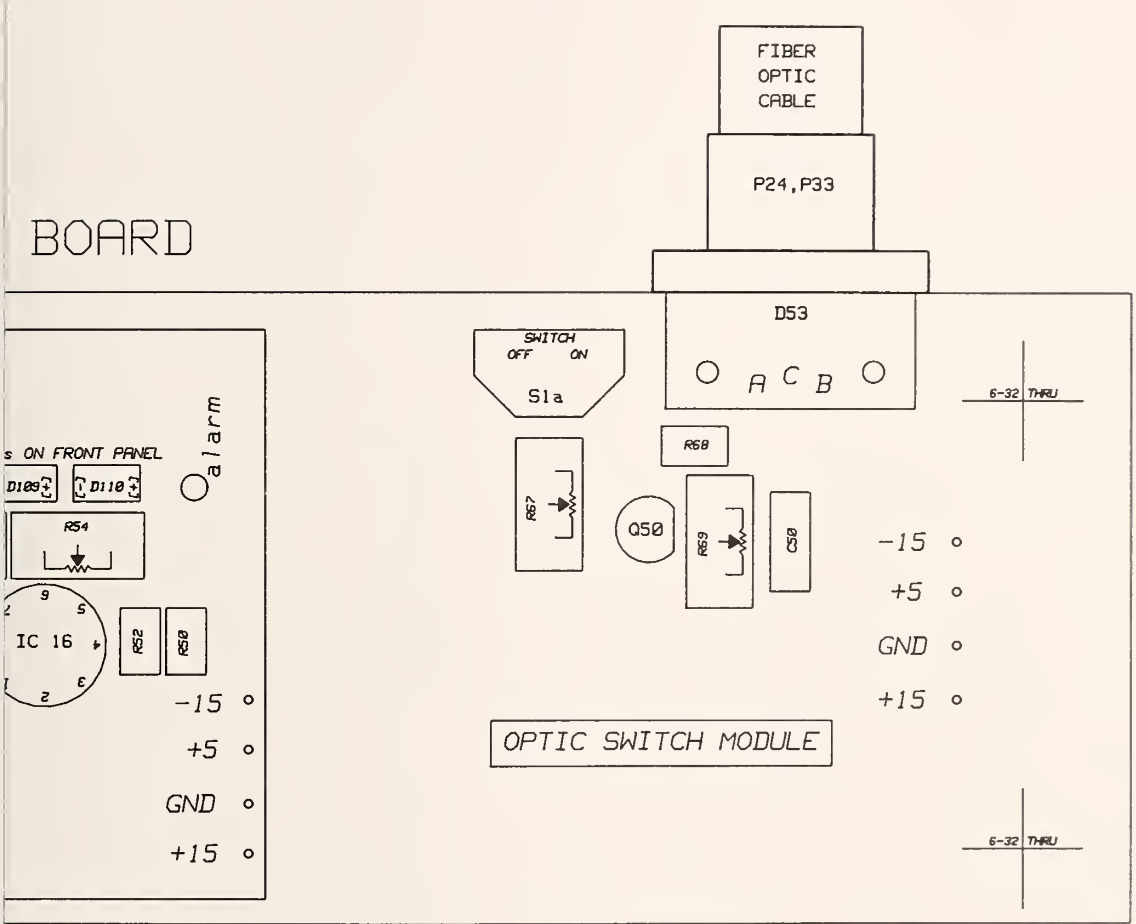

FIBER OPTIC CABLE
P24,P33
D53
A C B
SWITCH
OFF ON
S1a
R68
R67
Q50
R69
C50
6-32 THRU
6-32 THRU
-15
+5
GND
+15
OPTIC SWITCH MODULE
alarm
s ON FRONT PANEL
D109
D110
R54
IC 16
R52
R50
-15
+5
GND
+15

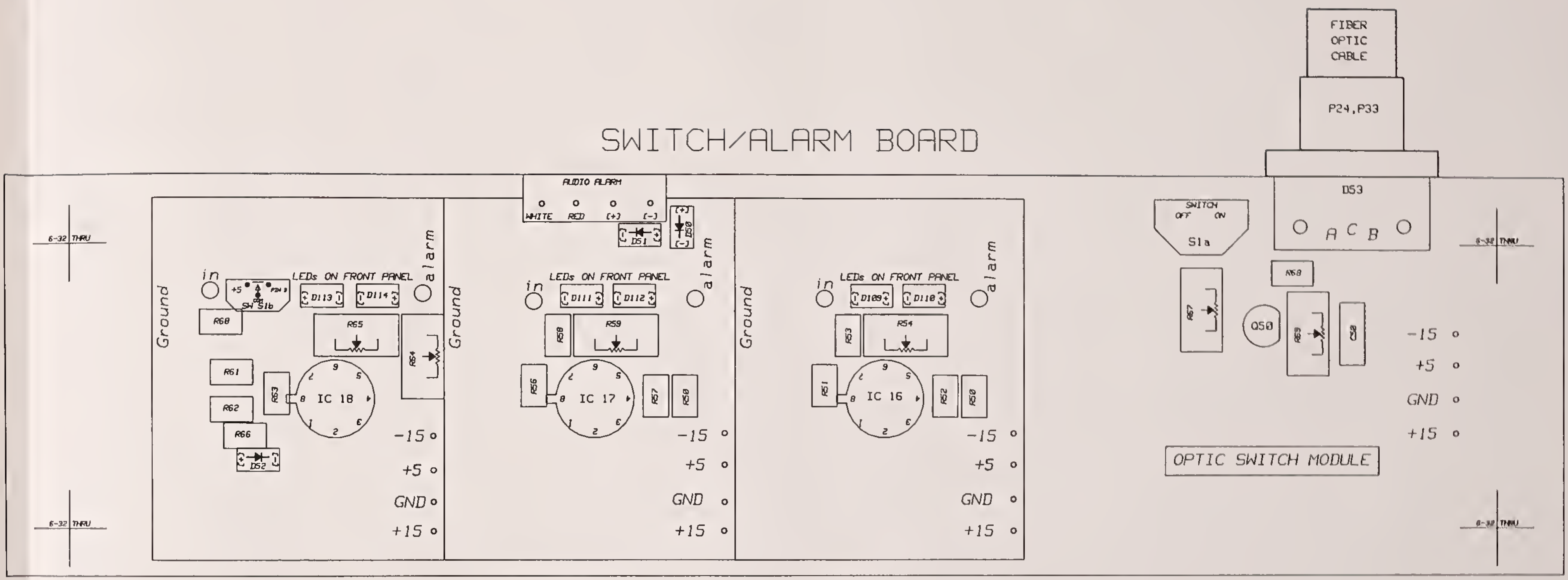

Figure 50. Assembly drawing - Switch alarm circuit board.

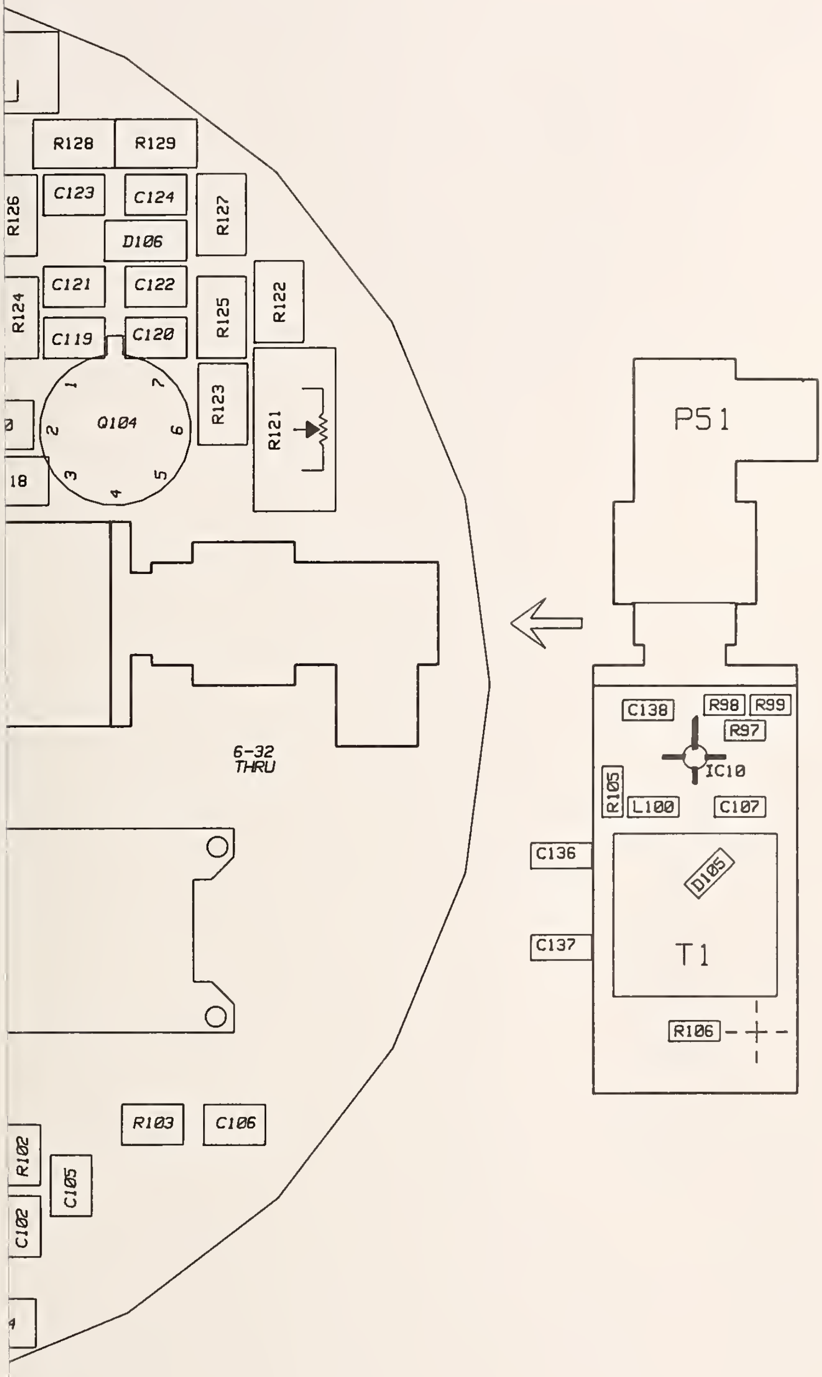

re circuit board.

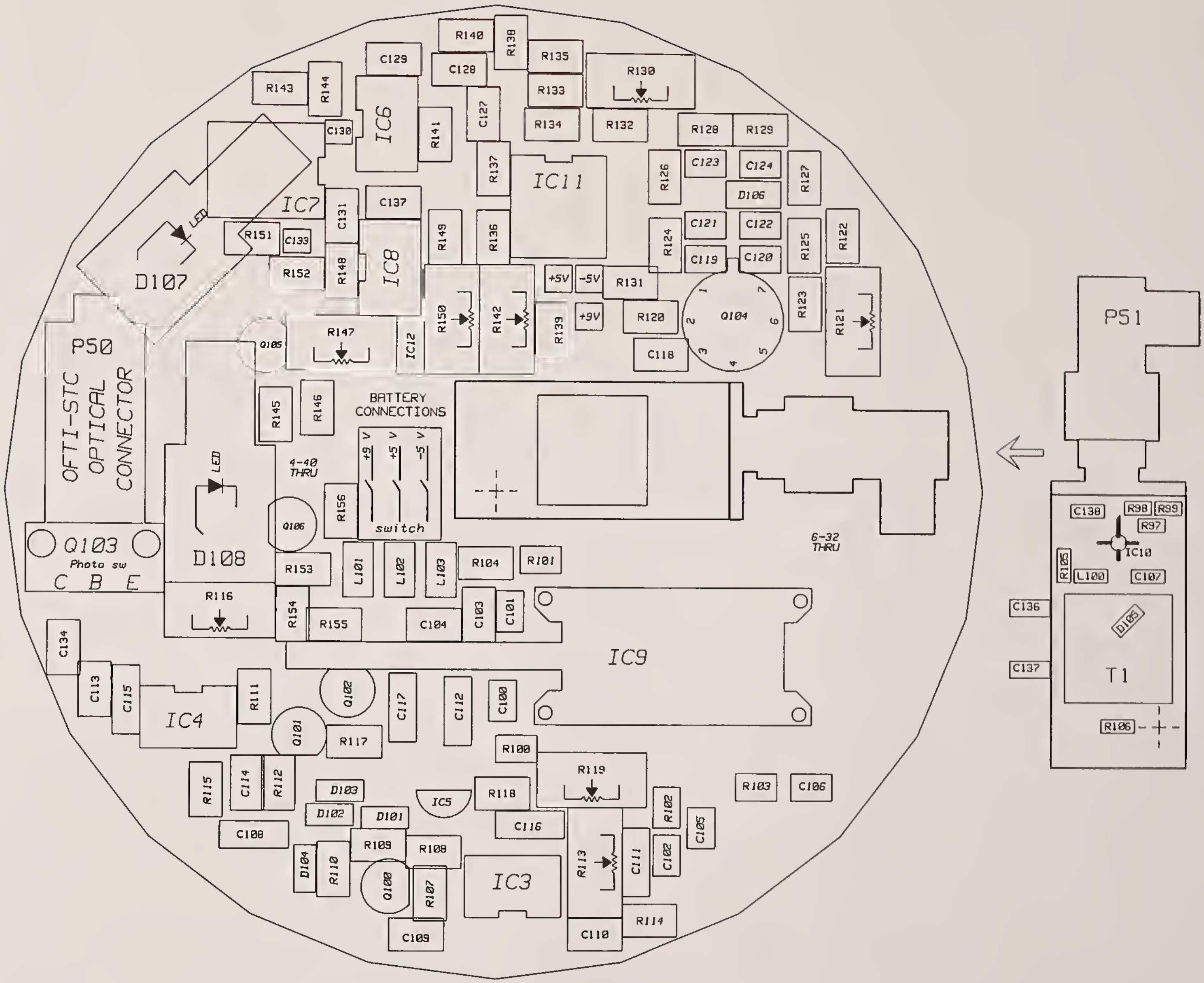

Figure 51. Assembly drawing - Sphere circuit board.

BL-114A (5-90) ADMAN 15.01	U.S. DEPARTMENT OF COMMERCE NATIONAL INSTITUTE OF STANDARDS AND TECHNOLOGY **BIBLIOGRAPHIC DATA SHEET**	1. PUBLICATION OR REPORT NUMBER NIST TN 1351 2. PERFORMING ORGANIZATION REPORT NUMBER B91-0278 3. PUBLICATION DATE December 1991

4. TITLE AND SUBTITLE

Standard Spherical Dipole Source

5. AUTHOR(S)

G. Koepke, L.D. Driver, K. Cavcey, K. Masterson, R. Johnk, M. Kanda

6. PERFORMING ORGANIZATION (IF JOINT OR OTHER THAN NIST, SEE INSTRUCTIONS)

U.S. DEPARTMENT OF COMMERCE
NATIONAL INSTITUTE OF STANDARDS AND TECHNOLOGY
BOULDER, COLORADO 80303-3328

7. CONTRACT/GRANT NUMBER

8. TYPE OF REPORT AND PERIOD COVERED

9. SPONSORING ORGANIZATION NAME AND COMPLETE ADDRESS (STREET, CITY, STATE, ZIP)

10. SUPPLEMENTARY NOTES

11. ABSTRACT (A 200-WORD OR LESS FACTUAL SUMMARY OF MOST SIGNIFICANT INFORMATION. IF DOCUMENT INCLUDES A SIGNIFICANT BIBLIOGRAPHY OR LITERATURE SURVEY, MENTION IT HERE.)

A spherical dipole was developed to provide a source that can be characterized both by theory and experiment and integrated into modern automated test systems. The frequency and amplitude of the radiated electromagnetic field are established remotely using a signal generator. This signal and all other control features are transmitted to and from the sphere using fiber optic cable. The field measurements show good agreement with predictions over much of the frequency band.

12. KEY WORDS (6 TO 12 ENTRIES; ALPHABETICAL ORDER; CAPITALIZE ONLY PROPER NAMES; AND SEPARATE KEY WORDS BY SEMICOLONS)

electromagnetic fields; electronic circuits; fiber optic; remote control; spherical dipole; standard radiator

13. AVAILABILITY

- [ ] UNLIMITED
- [ ] FOR OFFICIAL DISTRIBUTION. DO NOT RELEASE TO NATIONAL TECHNICAL INFORMATION SERVICE (NTIS).
- [ ] ORDER FROM SUPERINTENDENT OF DOCUMENTS, U.S. GOVERNMENT PRINTING OFFICE, WASHINGTON, DC 20402.
- [ ] ORDER FROM NATIONAL TECHNICAL INFORMATION SERVICE (NTIS), SPRINGFIELD, VA 22161.

14. NUMBER OF PRINTED PAGES

15. PRICE

ELECTRONIC FORM

☆U.S. GOVERNMENT PRINTING OFFICE 1992-673-971/65034

NIST *Technical Publications*

Periodical

Journal of Research of the National Institute of Standards and Technology—Reports NIST research and development in those disciplines of the physical and engineering sciences in which the Institute is active. These include physics, chemistry, engineering, mathematics, and computer sciences. Papers cover a broad range of subjects, with major emphasis on measurement methodology and the basic technology underlying standardization. Also included from time to time are survey articles on topics closely related to the Institute's technical and scientific programs. Issued six times a year.

Nonperiodicals

Monographs—Major contributions to the technical literature on various subjects related to the Institute's scientific and technical activities.

Handbooks—Recommended codes of engineering and industrial practice (including safety codes) developed in cooperation with interested industries, professional organizations, and regulatory bodies.

Special Publications—Include proceedings of conferences sponsored by NIST, NIST annual reports, and other special publications appropriate to this grouping such as wall charts, pocket cards, and bibliographies.

Applied Mathematics Series—Mathematical tables, manuals, and studies of special interest to physicists, engineers, chemists, biologists, mathematicians, computer programmers, and others engaged in scientific and technical work.

National Standard Reference Data Series—Provides quantitative data on the physical and chemical properties of materials, compiled from the world's literature and critically evaluated. Developed under a worldwide program coordinated by NIST under the authority of the National Standard Data Act (Public Law 90-396). NOTE: The Journal of Physical and Chemical Reference Data (JPCRD) is published quarterly for NIST by the American Chemical Society (ACS) and the American Institute of Physics (AIP). Subscriptions, reprints, and supplements are available from ACS, 1155 Sixteenth St., NW, Washington, DC 20056.

Building Science Series—Disseminates technical information developed at the Institute on building materials, components, systems, and whole structures. The series presents research results, test methods, and performance criteria related to the structural and environmental functions and the durability and safety characteristics of building elements and systems.

Technical Notes—Studies or reports which are complete in themselves but restrictive in their treatment of a subject. Analogous to monographs but not so comprehensive in scope or definitive in treatment of the subject area. Often serve as a vehicle for final reports of work performed at NIST under the sponsorship of other government agencies.

Voluntary Product Standards—Developed under procedures published by the Department of Commerce in Part 10, Title 15, of the Code of Federal Regulations. The standards establish nationally recognized requirements for products, and provide all concerned interests with a basis for common understanding of the characteristics of the products. NIST administers this program as a supplement to the activities of the private sector standardizing organizations.

Consumer Information Series—Practical information, based on NIST research and experience, covering areas of interest to the consumer. Easily understandable language and illustrations provide useful background knowledge for shopping in today's technological marketplace.

Order the **above** *NIST publications from: Superintendent of Documents, Government Printing Office, Washington, DC 20402.*

Order the **following** *NIST publications—FIPS and NISTIRs—from the National Technical Information Service, Springfield, VA 22161.*

Federal Information Processing Standards Publications (FIPS PUB)—Publications in this series collectively constitute the Federal Information Processing Standards Register. The Register serves as the official source of information in the Federal Government regarding standards issued by NIST pursuant to the Federal Property and Administrative Services Act of 1949 as amended, Public Law 89-306 (79 Stat. 1127), and as implemented by Executive Order 11717 (38 FR 12315, dated May 11, 1973) and Part 6 of Title 15 CFR (Code of Federal Regulations).

NIST Interagency Reports (NISTIR)—A special series of interim or final reports on work performed by NIST for outside sponsors (both government and non-government). In general, initial distribution is handled by the sponsor; public distribution is by the National Technical Information Service, Springfield, VA 22161, in paper copy or microfiche form.

U.S. Department of Commerce
National Institute of Standards and Technology
325 Broadway
Boulder, Colorado 80303-3328